

Development of environmentally friendly Ti alloys by
electronic parameters, and their as-cast applicability

電子パラメータによる環境対応型Ti合金の開発，およ
びそれらの鋳放し使用可能性

Department of Mechanical System Engineering
Graduate School of Engineering
Hiroshima University, Japan

Advisor: Prof. Matsugi Kazuhiro

MA XILONG

March 2020

CONTENTS

Contents	I
List of Figures	IV
List of Tables	X

Chapter 1 Background and objectives

1.1 Introduction.....	2
1.2 Applications of titanium and titanium alloys	5
1.2.1 Applications of α -Ti alloys.....	7
1.2.1.1 Applications of pure titanium and α -Ti alloys	7
1.2.1.2 Applications of near- α Ti alloys.....	9
1.2.2 Applications of β -Ti alloys	9
1.2.3 Preparation methods of titanium alloys	10
1.2.4 Post-treatments of titanium alloys	11
1.2.4.1 Heat treatment.....	12
1.2.4.2 Forging and rolling process.....	12
1.2.4.3 Thermomechanical processing.....	13
1.2.5 As-cast application of titanium alloys.....	13
1.3 Development of alloy design methods.....	14
1.3.1 Semi-empirical mode on the basis of trial and error method.....	15
1.3.2 Phase computation (PHACOMP) method	15
1.3.2.1 Electronic vacancy numbers method	16
1.3.2.2 New Phase computation (PHACOMP) method.....	17
1.3.3 d-Electron alloy design method	18
1.4 Objectives of this study.....	22
References.....	24

Chapter 2 Applicability of as-cast on β type titanium alloys proposed in the compositional region with different tensile deformation types

2.1 Introduction.....	32
-----------------------	----

2.2 Alloy design for the β alloys located on different regions in the Bo_T-Md_t diagram.	35
2.3 Experimental procedures.....	39
2.3.1 Materials and manufacturing process	39
2.3.2 Microstructural characterization and point analysis	43
2.3.3 Tensile test	44
2.4 Results and discussion.....	45
2.4.1 Microstructures and solute segregation in solidification.....	45
2.4.2 Tensile properties and fracture surface	50
2.4.3 Vickers hardness	54
2.4.4 As-cast application possibility of experimental alloys in the view of tension behaviors	55
2.5 Summary	57
References.....	58

Chapter 3 Possibility of as-cast applications on β type titanium alloys proposed in the newly expanded area of Bo_T-Md_t diagram

3.1 Introduction.....	62
3.2 Alloy design for the new β -Ti alloys located in the newly expanded area of Bo_T-Md_t diagram.	62
3.3 Experimental procedures	69
3.3.1 Materials and manufacturing process	69
3.3.2 Microstructural characterization	71
3.3.3 Tensile tests	72
3.4 Results and discussion	73
3.4.1 Microstructures	73
3.4.2 Tensile properties and fracture surface.....	81
3.4.3 Vickers hardness	84
3.4.4 As-cast application possibility of proposed alloys in the newly expanded area in the Bo_T-Md_t diagram.....	85
3.5 Summary	87
References.....	88

Chapter 4 Optimization of both composition and manufacturing process for α -type titanium alloys and their characterizations

4.1 Introduction.....	92
4.2 Alloy design for the α alloys in the Bo_T-Md_I diagram.....	94
4.3 Experimental procedure	98
4.3.1 Materials and manufacturing processes	98
4.3.2 Evaluation of some properties	99
4.4 Results and discussion	103
4.4.1 Microstructures	103
4.4.2 Tensile properties	107
4.4.3 Hot salt corrosion resistance abilities	112
4.4.4 The mechanism of hot salt corrosion test of titanium alloys	118
4.5 Summary	121
References.....	123
Chapter 5 Conclusions.....	125
Acknowledgements	131
Published papers in regard to this thesis	132
Presentations.....	133

List of Figures

- Fig. 1-1 The trends in demand of titanium materials.
- Fig. 1-2 Grouping of commercial titanium alloys classified into the three types of α , $\alpha + \beta$, and β alloys on the Bo_t-Md_t diagram.
- Fig. 1-3 Commercial titanium alloys classified into the three types of α , $\alpha + \beta$, and β alloys and the boundaries between slip, twin and martensite deformations on the Bo_t-Md_t diagram.
- Fig. 1-4 Relation between the Bo_t and ratio of weight loss to initial weight obtained from the immersion test for 21.6 ks in Na₂SO₄-45 mol% NaCl molten salt at 923 K.
- Fig. 1-5 Bo_t-Md_t diagram showing phase boundaries, and other characteristics obtained from reported alloys, and the positions of proposed alloys. Ninety four reported β alloys for these classification showed the compositional range of Ti-(0-55)Ta-(0-41)Nb-(0-30)Zr-(0-8)Fe-(0-13)Cr-(0-22)V-(0-20)Mo-(0-6)Sn-(0-8)Al-(0-8)Mn in mass%.
- Fig. 2-1 Schematic drawing of thermomechanical process for Ti-15V-3Cr-3Sn-3Al alloy. H.W.: hot-working, C.W.: cold-working, and S.T.: solution-treatment.
- Fig. 2-2 MTi₁₄ cluster model in the case of bcc Ti.
- Fig. 2-3 Models of (a) Bo and (b) Md level.
- Fig. 2-4 The positions of three experimental alloys and their compositional scatters in as-cast and solution treated conditions in the Bo_t-Md_t diagram showing phase and deformation type boundaries. The vectors pointing from pure Ti represent the location of Ti-2mass%M. (M is an additional alloying element selected in this study)
- Fig. 2-5 Schematic diagram of vacuum chamber of CCLM.
- Fig. 2-6 Schematic diagram of crucible of CCLM.
- Fig. 2-7 Schematic illustrations of principle of CCLM.
- Fig. 2-8 The images of ingot produced by CCLM, (a) bottom, (b) side and (c) top views.
- Fig. 2-9 Profiles of (a) temperature in molten metal, (b) electric power in upper and

lower coils and (c) pressure in atmosphere of levitation melting and cooling process. Abscissa and ordinate are represented with arbitrary scales.

Fig. 2-10 Cutting procedures of melted ingot prepared by CCLM.

Fig. 2-11 Draft of specimen adopted for tensile test.

Fig. 2-12 OM images of (a) and (d) Ti-5.5Cr-5.4Mn-5.1Zr-2.8Fe, (b) and (e) Ti-4.5Cr-2.5Mn-1.1Al, (c) and (f) Ti-10.8Mo-2.3Sn-1.0Al alloys. (a), (b), (c) and (d), (e), (f) were obtained from as-cast and solution treated conditions, respectively. (1), (2) and (3) showing the paths and directions of point analysis measurement, corresponding to the ones in Fig. 2-14.

Fig. 2-13 X-ray diffraction profiles of (a) and (b) Ti-5.5Cr-5.4Mn-5.1Zr-2.8Fe, (c) and (d) Ti-4.5Cr-2.5Mn-1.1Al, (e) and (f) Ti-10.8Mo-2.3Sn-1.0Al alloys. (a), (c), (e) and (b), (d), (f) were obtained from as-cast and solution treated conditions, and (g) after tensile test for solution treated Ti-4.5Cr-2.5Mn-1.1Al alloy.

Fig. 2-14 The concentration profiles of alloying elements of (a) and (b) Ti-5.5Cr-5.4Mn-5.1Zr-2.8Fe, (c) and (d) Ti-4.5Cr-2.5Mn-1.1Al, (e) and (f) Ti-10.8Mo-2.3Sn-1.0Al alloys. (a), (c), (e) and (b), (d), (f) were obtained from as-cast and solution treated conditions, respectively. And the concentration profiles (a) corresponded to the Vickers hardness values in five positions. (1) to (3) corresponded to the ones in Fig. 2-12.

Fig. 2-15 Solidification paths of (a) Ti, Cr and Mn, (b) Ti, Cr and Zr and (c) Ti, Cr and Fe for Ti-5.5Cr-5.4Mn-5.1Zr-2.8Fe alloy in as-cast condition.

Fig. 2-16 Stress-strain curves of as-cast and solution treated three β -Ti alloys.

Fig. 2-17 Low and high magnified fractographies of tensile specimens for (a), (b) as-cast and (c), (d) solution treated Ti-5.5Cr-5.4Mn-5.1Zr-2.8Fe specimens, respectively.

Fig. 2-18 TEM images of (a) solution treated Ti-5.5Cr-5.4Mn-5.1Zr-2.8Fe alloy in tensile fractured specimen, and solution treated Ti-4.5Cr-2.5Mn-1.1Al alloy in (b), (c) 1 and 5% plastic strained specimens, (d) SAED pattern along with $[\bar{1}11]$ of (c) and (e) tensile fractured specimen.

Fig. 2-19 Vickers hardness of Ti-5.5Cr-5.4Mn-5.1Zr-2.8Fe, Ti-4.5Cr-2.5Mn-1.1Al and Ti-10.8Mo-2.3Sn-1.0Al alloys for as-cast and solution treated specimens.

Fig. 2-20 Deformation bands around the Vickers indentations of (a) and (d) Ti-5.5Cr-5.4Mn-5.1Zr-2.8Fe, (b) and (e) Ti-4.5Cr-2.5Mn-1.1Al and (c) and (f) Ti-10.8Mo-2.3Sn-1.0Al alloys. (a), (b), (c) and (d), (e), (f) were obtained from as-

cast and solution treated specimens, respectively.

Fig. 3-1 The compositional positions of ten proposed alloys (HU-01 to -10) and 93 conventional β -Ti alloys in the Bo_r-Md_t diagram, which represented phase boundaries between β , $\beta + \alpha$ and α alloys, and deformation mode consisting of slip, twin and martensite types. The compositional range of 93 β -Ti alloys were Ti-(0-55)Ta-(0-41)Nb-(0-30)Zr-(0-8)Fe-(0-13)Cr-(0-22)V-(0-20)Mo-(0-6)Sn-(0-8)Al-(0-8)Mn in mass%. The line among the HU-02, HU-03, HU-06 and HU-07 alloys indicated the phase boundary between the mono β phase and dual β plus intermetallic compound phases, which was derived from this study.

Fig. 3-2 The vectors pointing from pure Ti represented the location of Ti-10mass%M. (M were alloying elements). The elements circled by squares showing the positions of alloying elements selected in the present study corresponded to the Cr, Mn, Fe, V, Zr, Mo, Al, Sn and Ta, respectively.

Fig. 3-3 Profiles of (a) temperature in molten metal, (b) electric power in upper and lower coils and (c) pressure in Ar atmosphere of levitation melting and cooling process. Abscissa and ordinate are represented with arbitrary scales.

Fig. 3-4 Schematic illustrations of ingots produced by CCLM and tensile specimens showed the distribution of both equiaxed and columnar grains and cut positions for a tensile specimen with equiaxed grains of approximately 200 μm in ingot. Dimensions of ingot and tensile specimen were given in millimeters (mm). The edge lengths of rectangle blocks were \overline{ab} , \overline{cd} , \overline{ef} and \overline{gh} of 30 mm, \overline{ad} , \overline{bc} , \overline{eh} and \overline{gf} of 10 mm and \overline{ae} , \overline{bf} , \overline{cg} and \overline{dh} of 35 mm, respectively. OM images of equiaxed and columnar grains further showed the different grain size distributions in the ingot.

Fig. 3-5 OM images of (a) and (b) HU-01, (c) and (d) HU-02, (e) and (f) HU-03, (g) and (h) HU-04, (i) and (j) HU-05 alloys. (a), (c), (e), (g), (i) and (b), (d), (f), (h), (j) were obtained from as-cast and solution treated conditions, respectively.

Fig. 3-6 OM images of (a) and (b) HU-06, (c) and (d) HU-07, (e) and (f) HU-08, (g) and (h) HU-09, (i) and (j) HU-10 alloys. (a), (c), (e), (g), (i) and (b), (d), (f), (h), (j) were obtained from as-cast and solution treated conditions, respectively.

Fig. 3-7 Area fraction of intermetallic compounds of (a) in HU-01 to HU-05 alloys, (b) in HU-06 to HU-10 alloys, according to the results of OM images as shown in Figs. 3-5 and 3-6, respectively.

- Fig. 3-8 X-ray diffraction profiles with Cu-K α radiation of (a) and (b) HU-01, (c) and (d) HU-03, (e) and (f) HU-05 alloys, and (g) the higher sensitive condition for identification of TiCrMn and TiCr₂ in the 2 θ value of 43 to 46° for (e). (a), (c), (e) and (b), (d), (f) were obtained from as-cast and solution treated conditions, respectively.
- Fig. 3-9 X-ray diffraction profiles with Cu-K α radiation of (a) and (b) HU-06, (c) and (d) HU-07, (e) and (f) HU-10 alloys, and (g) the higher sensitive condition for identification of TiCrMn and TiCr₂ in the 2 θ value of 43 to 46° for (e). (a), (c), (e) and (b), (d), (f) were obtained from as-cast and solution treated conditions, respectively.
- Fig. 3-10 Relation between the lattice constant calculated by the 2 θ value of (110) plane and Md_t values of (a) HU-01 to HU-05 and (b) HU-06 to HU-10 alloys in as-cast and solution treated conditions.
- Fig. 3-11 Solidification paths of HU-01 (a) and (b), and HU-05 (c) and (d) β -Ti alloys, (a), (c) and (b), (d) were obtained from as-cast and solution treated conditions, respectively.
- Fig. 3-12 Stress-strain curves of (a) HU-02, (b) HU-03, (c) HU-06 and (d) HU-07 alloys at as-cast and solution treated conditions.
- Fig. 3-13 Low and high magnified fractographies of tensile specimens of (a) and (b) for HU-02, (c) and (d) for HU-03, (e) and (f) for HU-06, and (g) and (h) for HU-07 alloys at as-cast condition, respectively.
- Fig. 3-14 Relation between the σ_{UTS} or ϵ_f and Md_t of (a) HU-01 to HU-05 and (b) HU-06 to HU-10 alloys in as-cast and solution treated conditions.
- Fig. 3-15 Vickers hardness of (a) HU-01 to HU-05 and (b) HU-06 to HU-10 alloys in as-cast and solution treated conditions.
- Fig. 4-1 MTi₁₈ cluster model in the case of hcp Ti.
- Fig. 4-2 The Bo_t - Md_t line of Ti-M binary alloys. The vectors represent the location of Ti-10mass%M. (M is alloying element in binary alloy)
- Fig. 4-3 Bo_t - Md_t diagram showing phase boundaries, and contour lines of σ_{UTS} obtained from reported alloys, and the positions of experimental α -Ti alloys.
- Fig. 4-4 Bo_t - Md_t diagram showing phase boundaries, and contour lines of σ_{UTS} obtained from reported alloys, and the positions of experimental near- α Ti alloys.
- Fig. 4-5 Profiles of (a) temperature in molten metal, (b) electric power in upper and lower coils and (c) pressure in atmosphere of levitation melting and cooling

process. Abscissa and ordinate are represented with arbitrary scales.

Fig. 4-6 Coefficient of thermal expansion for α titanium of designed alloy Ti-5Al-4Zr-3.6Sn, modified alloy Ti-6Al-1.7Sn-1.3Zr and reference alloy Ti-5Al-2.5Sn.

Fig. 4-7 Coefficient of thermal expansion for near- α titanium alloy of designed alloy Ti-6Al-4Zr-2Sn-2Mo-0.3Si, modified alloy Ti-6Al-9Zr-3Sn-1Cu-0.2Si and reference alloy Ti-6Al-4Zr-2.75Sn-0.4Mo-0.45Si.

Fig. 4-8 Schematic diagrams of the hot salt corrosion test process.

Fig. 4-9 OM images of (a) and (d) Ti-5Al-4Zr-3.6Sn, (b) and (e) Ti-6Al-1.7Sn-1.3Zr, and (c) and (f) Ti-5Al-2.5Sn α titanium alloys in as-cast and solution treated conditions, respectively.

Fig. 4-10 OM images of (a) and (d) Ti-6Al-2Sn-4Zr-2Mo-0.3Si, (b) and (e) Ti-6Al-3Sn-9Zr-1Cu-0.2Si, and (c) and (f) Ti-6Al-2.75Sn-4Zr-0.4Mo-0.45Si near- α titanium alloys in as-cast and solution treated conditions, respectively.

Fig. 4-11 XRD profiles of (a) and (b) Ti-5Al-4Zr-3.6Sn, (c) and (d) Ti-6Al-1.7Sn-1.3Zr and (e) and (f) Ti-5Al-2.5Sn alloys in as-cast and solution treated conditions.

Fig. 4-12 XRD profiles of (a) and (b) Ti-6Al-2Sn-4Zr-2Mo-0.3Si, (c) and (d) Ti-6Al-3Sn-9Zr-1Cu-0.2Si and (e) and (f) Ti-6Al-2.75Sn-4Zr-0.4Mo-0.45Si alloys in as-cast and solution treated conditions.

Fig. 4-13 Stress-strain curves of experimental α -Ti alloys in (a) as-cast and (b) solution treated conditions.

Fig. 4-14 Stress-strain curves of experimental near- α titanium alloys in (a) as-cast and (b) solution treated conditions.

Fig. 4-15 The concentration profiles of alloying elements of (a) and (b) Ti-5Al-2.5Sn, and (c) and (d) Ti-5Al-4Zr-3.6Sn alloys. (a), (c) and (b), (d) were obtained from as-cast and solution treated conditions, respectively.

Fig. 4-16 Fractographies of tensile specimens of (a) and (b) Ti-5Al-4Zr-3.6Sn, (c) and (d) Ti-6Al-1.7Sn-1.3Zr and (e) and (f) Ti-5Al-2.5Sn alloys in as-cast and solution treated conditions, and their respective corresponded high magnified fractographies of (a') and (b') Ti-5Al-4Zr-3.6Sn, (c') and (d') Ti-6Al-1.7Sn-1.3Zr and (e') and (f') Ti-5Al-2.5Sn alloys in as-cast and solution treated conditions, respectively.

Fig. 4-17 Fractographies of tensile specimens of (a) and (b) Ti-6Al-2Sn-4Zr-2Mo-0.3Si, (c) and (d) Ti-6Al-3Sn-9Zr-1Cu-0.2Si and (e) and (f) Ti-6Al-2.75Sn-4Zr-0.4Mo-0.45Si alloys in as-cast and solution treated conditions, and their

respective corresponded high magnified fractographies of tensile specimens of (a') and (b') Ti-6Al-2Sn-4Zr-2Mo-0.3Si, (c') and (d') Ti-6Al-3Sn-9Zr-1Cu-0.2Si and (e') and (f') Ti-6Al-2.75Sn-4Zr-0.4Mo-0.45Si alloys in as-cast and solution treated conditions, respectively.

Fig. 4-18 Relation between immersion time and ratio of weight loss to initial weight obtained from immersion in Na₂SO₄-45mol%NaCl molten salt in 923K for experimental α -Ti alloys (a) and (d) of Ti-5Al-4Zr-3.6Sn, (b) and (e) of Ti-6Al-1.7Sn-1.3Zr, and (c) and (f) of Ti-5Al-2.5Sn in as-cast and solution treated conditions, and for near- α titanium alloys (g) and (j) of Ti-6Al-2Sn-4Zr-2Mo-0.3Si, (h) and (k) of Ti-6Al-3Sn-9Zr-1Cu-0.2Si and (i) and (l) of Ti-6Al-2.75Sn-4Zr-0.4Mo-0.45Si in as-cast and solution treated conditions, respectively.

Fig. 4-19 Compositional images of (a) Ti-5Al-4Zr-3.6Sn, (b) Ti-6Al-1.7Sn-1.3Zr and (c) Ti-5Al-2.5Sn alloys in as-cast condition, and EPMA mappings showing the distribution of Ti, Zr, Al, Sn, O, and S, respectively.

Fig. 4-20 Compositional images of (a) Ti-6Al-2Sn-5Zr-1Mo-0.3Si, (b) Ti-6Al-3Sn-9Zr-1Cu-0.2Si and (c) Ti-6Al-2.75Sn-4Zr-0.4Mo-0.45Si near- α alloys in solution treated condition, and EPMA mappings showing the distribution of Ti, Zr, Al, Si, Sn, O, S, Mo, and Cu, respectively.

Fig. 4-21 Illustrative schematic of (a) showing corrosion process for specimens and (b) the corrosion surface morphology after hot salt corrosion test.

Fig. 5-1 Candidate area for proposing of as-cast applicable Ti alloys in the Bo_t - Md_t diagram.

List of Tables

- Table 1-1 Target mechanical values of β , α , and near- α titanium alloys.
- Table 2-1 List of Bo and Md values for alloying elements in bcc Ti.
- Table 2-2 The compositions of proposed three β -Ti alloys in both mol.% and mass% and their Bo_t and Md_t values.
- Table 2-3 Chemical composition fractions of impurities in ingot produced by CCLM.
- Table 2-4 The segregation coefficient, K , $Bo_t \max$, $Bo_t \min$, ΔBo_t and $Md_t \max$, $Md_t \min$, ΔMd_t values of three β -Ti alloys in as-cast condition.
- Table 3-1 The compositions of ten proposed β -Ti alloys in both mol.% and mass%, and their Bo_t and Md_t values.
- Table 4-1 List of Bo and Md values for alloying elements in hcp Ti.
- Table 4-2 The nominal composition, Bo_t and Md_t values of each α and near- α titanium alloys.
- Table 4-3 The compositions of α and near- α Ti alloys in mass%, the ratio of weight loss of specimens after immersion in molten salts after 43.2 ks, and their Bo_t and Md_t values.

Chapter 1

Background and objectives

1.1 Introduction.....	2
1.2 Applications of titanium and titanium alloys	5
1.2.1 Applications of α -Ti alloys.....	7
1.2.1.1 Applications of pure titanium and α -Ti alloys.....	7
1.2.1.2 Applications of near- α Ti alloys	9
1.2.2 Applications of β -Ti alloys	9
1.2.3 Preparation methods of titanium alloys.....	10
1.2.4 Post-treatments of titanium alloys	11
1.2.4.1 Heat treatment.....	12
1.2.4.2 Forging and rolling process	12
1.2.4.3 Thermomechanical processing.....	13
1.2.5 As-cast application of titanium alloys.....	13
1.3 Development of alloy design methods.....	14
1.3.1 Semi-empirical mode on the basis of trial and error method	15
1.3.2 Phase computation (PHACOMP) method	15
1.3.2.1 Electronic vacancy numbers method	16
1.3.2.2 New Phase computation (PHACOMP) method	17
1.3.3 d-Electron alloy design method	18
1.4 Objectives of this study	22
References	24

1.1 Introduction

Titanium based alloys have been extensively investigated for a variety of applications owing to their excellent material properties, such as biocompatibility¹⁻³⁾, excellent combination of high-temperature strength and lightweight⁴⁻⁹⁾. Moreover, titanium alloys also stand out due to two properties: high specific strength and excellent corrosion resistance¹⁰⁾. This also explains their preferential use in the aerospace sector^{11,12)}, the chemical industry¹³⁾ and medical engineering^{14,15)}. Since the population ratio of the aged people is rapidly growing, the number of the aged people demanding replacing failed tissue with artificial instruments made of biomaterials is increasing. The titanium alloys composed of non-toxic elements that have been developed of β types titanium alloys¹⁶⁻²⁰⁾. The world's demand for titanium alloy has been increasing since 2004. Although half of the demand is expected to be used for civil aircraft and military demand²¹⁾. Most military use is assumed to be military aircraft, because titanium alloys can be applied to both the fuselage structure and the engine. In contrast, the demand of titanium materials in Japan is significantly decreased 10% in the past several years with the increased import of products such as aircraft frames frame of airplane and sports equipment which are made of pure titanium and titanium alloys. However, if the production of independent aircraft such as MRJ made by Japan is activated, it is possible that the increased demand of titanium and its alloys will be need in several years later²²⁾.

Titanium is not actually a rare substance as it ranks as the ninth most plentiful element and the fourth most abundant structural metal in the Earth's crust exceeded only by aluminum, iron, and magnesium²³⁾. Unfortunately, it is seldom found in high concentrations and never found in a pure state. Remaining drawback for Ti alloys is the higher cost than many other light metals because of the long design cycle time, poor refining efficiency, difficulty of melting and complexity of post treatment process etc²⁴⁾. Whereas the cost is the decisive factor for industrial manufacturers when they choose the materials²⁵⁾. Furthermore, the complex post-treatment processes of materials would produce more consumption, pollution and carbon dioxide emissions than those of as-cast condition, which further increased the burden of environment²⁶⁻

28).

To reduce the cost of Ti alloys, some measurements are taken by researchers as follows. In the past, the alloy design and development of Ti alloys mainly relied on the repeated experiments and some empirical rules, which are high cost and inefficient, until the propose of d-electrons concept based on the theoretical calculation of electronic structures of alloys. The d-electrons concept was first published by Morinaga et al²⁹⁻³¹⁾ and has been accepted by numerous Ti alloy researchers^{32, 33)}. Two calculated parameters were mainly utilized in the d-electrons concept. The one is the d-orbital energy level (*Md*) of alloying transition elements, and the other is the bond order (*Bo*) that is a measure of the covalent bond strength between atoms. Moreover, titanium is very chemically reactive and easy to react with many elements like oxygen^{34, 35)} and hydrogen^{36, 37)} during the manufacturing process, which can greatly influence the properties of Ti alloys. The source of these elements usually derives from the gas environment of furnace and the contaminations of the crucible. Therefore, it is essential to control the vacuum level in furnaces and prevent impurities from contaminating. The cold crucible levitation melting (CCLM) method can suit these requests very well. The CCLM consists of a high frequency induction furnace and two electric coils. The upper electric coil is used for heating and the lower electric coil is utilized for levitation the molten metals^{38, 39)}. The molten material can be levitated by the eddy current in the melting crucible so that the alloys can be melted without any contact between materials and the crucible. Moreover, a uniform composition of Ti alloys can be obtained by the diffusion mixing effect and strong stirring from the electromagnetic force⁴⁰⁾.

According to the previous reports and practical applications, many complex post-processing treatments were needed after casting for producing conventional β -Ti alloys with high strength and toughness⁴¹⁾, which further led to their high final costs. For example, one of the most widely applied β -Ti alloy Ti-15V-3Cr-3Sn-3Al with the ultimate tensile strength (σ_{UTS}) of 800~1400 MPa and fracture strain (ϵ_f) of 6~11% can be obtained after solution treated, aged, hot and cold working process^{42, 43)}. The complex post-processing treatments will lead to the high cost and high energy consumption. In addition, the 15-3-3-3 alloy, which was treated by solution treatment and aging was commonly used as sheet, plate, and airframe materials, and showed the

σ_{UTS} of approximately 1000 MPa and a ϵ_f of 10%. Herein, when considering the final cost of the Ti alloy for aircraft applications, if the raw material cost is set as 1, the casting cost is about 0.5, the post-processing cost is about 1.5 and the secondary processing cost can be estimated to be 2⁴⁴). The post-processing treatment cost is remarkably expensive compared with that of casting, because of the high energy consumption. The development of Ti alloys could be used at as-cast condition is urgent needed to reduce the post-processing and simplified manufacturing process. However, there are almost no precedent for Ti alloys with high alloy using at as-cast condition manufactured just by single casting process. Because the solidification segregation of alloying elements, emergence of non-equilibrium phase and instability of the constituent phases usually appeared in the casting Ti alloys^{45, 46}). In contrast, it is also reported that many light metals are developed to be applied at as-cast condition which may be an effective way to reduce energy consumption and production costs by omitting complex post-processing procedures, such as aluminum and magnesium alloys^{47, 48}). Under the premise of maintaining the excellent properties of Ti material, the trend on cost reduction of Ti alloys are focus on the following methods⁴⁴). The first is the choice of cheaper raw materials instead of the expensive ones. The second is the development of new Ti alloys with improved mechanical properties, which can simplify or omit the post-treatment processes^{49, 50}). The third way is to improve the efficient of equipment of manufacturing and post-treatment. Others including the expand of production scale to reduce the fringe cost.

The research and development of as-cast applicable α , near- α , metastable β and β titanium alloys with high mechanical properties are few reported on the open literatures. According to the d-electrons concept, the new titanium alloys were proposed by using mainly ubiquitous elements in the Bo_i-Md_i diagram, respectively. The variant properties of experimental α , near- α , metastable β and β titanium alloys between as-cast and solution treated conditions as well as their as-cast application possibility were discussed in the present study. Their as-cast application possibility of titanium alloys in industry as low cost and energy saving measures has great practical significance.

1.2 Applications of titanium and titanium alloys

The existence of titanium was first recognized in 1791 by William McGregor, an English priest, mineralogist and chemist, discovered titanium. He examined the magnetic sands of the local river Helford in the Menachan Valley in Cornwall, England, and isolated the "black sand" (now known as "titanium iron ore"). By removing iron from magnets and treating sand with hydrochloric acid, he produces an impure oxide of a new element. After that position, he named it "Mechanical Stone". Four years later, Berlin chemist Martin Heinrich Klaproth independently isolated titanium oxide from Hungarian minerals (now known as "golden red stone"). Greek mythology gave him a new name, from the children of the Tera giants Uranos and Gaia. Titan was completely hated by their father, so he was imprisoned in the earth's crust, similar with his hard-to-minore, so he named it Titanium. Matthew Albert Hunter, from Rensselaer, has spent more than 100 years. The Troy Institute of Technology in New York State separated the metal in 1910 by heating titanium tetrachloride (TiCl_4) and sodium in steel bombs. Eventually, Wilhelm Justin Kroll, from Luxembourg, was recognized as the father of the titanium industry. In 1932, he produced a large amount of titanium by mixing TiCl_4 with calcium. He fled to the United States at the beginning of World War II. At the U.S. Bureau of Mines, he demonstrated that TiCl_4 could be restored by changing the reductintor from calcium to magnesium, and that titanium could be commercially extracted. Today, this is still the most widely used method, known as the "Kroll process". In Luxembourg, reacted TiCl_4 with molten magnesium under an atmosphere of argon. This opened the way to the industrial exploitation of titanium and the essential features of the process are as follows:

1. Briquette TiO_2 with coke and tar and chlorinate at $800\text{ }^\circ\text{C}$ to promote the reaction:



2. Purify TiCl_4 by fractional distillation.
3. Reduce TiCl_4 by molten magnesium or sodium under an argon atmosphere, one reaction being:



After World War II, titanium-based alloys were soon considered a key material for

aircraft engines. In 1948, DuPont was the first company to commercialize titanium production. Today, aerospace remains a major consumer of titanium and its alloys, as shown in Fig. 1-1. But other markets such as construction, chemical processing, medicine, power generation, marine and sea, sports and leisure, and transportation are also becoming increasingly popular.

Depending on the effect on the β -transus temperature, the titanium alloy elements are classified as neutral, α -stabilizer or β -stabilizer. The α stabilization element extends the α phase field to a higher temperature, while the β stabilization element extends the β phase field to a lower temperature. The neutral element has little effect on the β -transus temperature. Titanium alloys are generally classified as α , $\alpha+\beta$, and β alloys, with further subdivision into near- α and metastable β alloys. The α alloys comprise commercially pure (cp) titanium and alloys exclusively alloyed with α -stabilizing and/or neutral elements. If minor fractions of β -stabilizing elements are added, they are referred to as near- α alloys. The $\alpha + \beta$ alloys are the most widely used titanium alloys. At room temperature, these alloys have a β volume fraction ranging from about 5 to 40%. If the proportion of β -stabilizing elements is further increased to a level where β no longer transforms to martensite upon fast quenching, the alloys are still in the two-phase field and the class of metastable β alloys is reached. It should be noted that these alloys can still reveal an equilibrium α volume fraction of more than 50%. Finally, the single-phase β titanium alloys mark the end of the alloying scale of the conventional titanium alloys⁵¹).

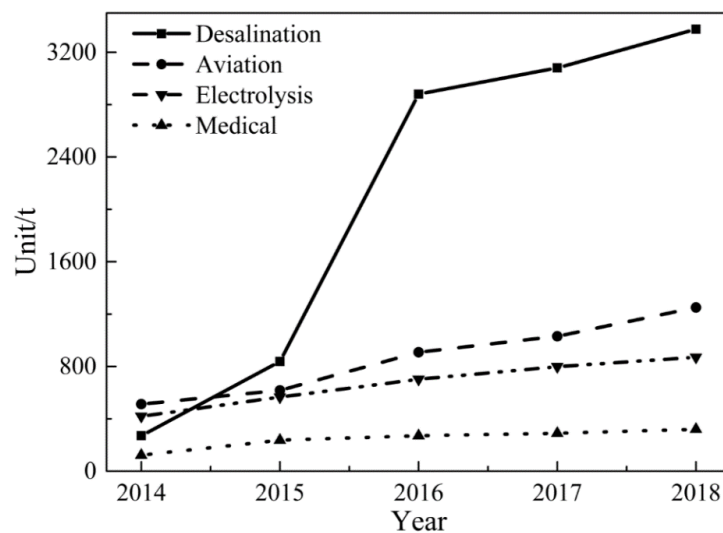


Fig. 1-1 The trends in demand of titanium materials.

1.2.1 Applications of α -Ti alloys

According to statistics, the accumulation of titanium for sports and leisure products is 17%~21%, which is the third largest application of titanium. People often use sports equipment such as golf clubs, ball heads, tennis rackets, badminton rackets, and fencing protection. Masks, swords, sprint studs, climbing tools, snowboards, ski boots, ski poles, ice skates, wetsuits, fishing tackles, tent poles are all made of pure titanium and α -Ti alloy materials. The following are typical applications of titanium and α -Ti alloys in recreational sports.

1.2.1.1 Applications of pure titanium and α -Ti alloys

Due to its excellent physical and mechanical properties, titanium has been used in racing and limited production of sports cars ⁵²⁾. Titanium is used in the automotive industry to significantly reduce vehicle weight, reduce fuel consumption, protect the environment and reduce noise. Metal parts on the car can be made of titanium and titanium alloys, such as: bolts ⁵³⁾, connecting rods ⁵⁴⁾, rockers ⁵⁵⁾, bolt rear brackets, exhaust pipes, return pipes ⁵⁶⁾, titanium can also be used after surface coating to ensure the brake plate is light in weight and long in service life, which also can replace the valves, springs and connecting rods. Titanium golf clubs and ball heads are still a major pillar of titanium in the civilian field ⁵¹⁾. It seems that all the world's manufacturers have produced golf clubs and ball heads. Titanium has a small specific gravity and a high strength, which can make the ball head bigger without increasing the total weight of the club. During the test, the hit rate of the golfer's titanium ball head was increased by 21% on average, and the hitting distance was also improved. Currently larger golf heads require a very thin surface and therefore require a very durable surface material. SP-700 new titanium alloy developed by foreign steel pipe company has high strength and good formability is popular in the golf market ⁵⁷⁾. Bicycle needs to be very light, especially in the racing bicycle, if you reduce the weight of the bicycle by 1 gram, you can reach earlier by a thousandth of a second. Normal bicycles use 36 splines, while a titanium bicycle uses 24, which not only reduces weight but also reduces wind elongation. Titanium and titanium alloys are first used from parts ⁵⁸⁾. Foreign companies

have used titanium and titanium alloys to make various parts of racing bicycles. Lite speed Corporation of the United States uses titanium to produce bicycle frames. The average weight of these frames is 2.5 pounds. The vehicle reaches 2,800 per second including: package quick-distribution pin, left-hand nut, pinless crankshaft, front and rear hub axles, left and right ankle shafts, etc. In the past 4 years, industrial pure titanium tubes have been used for non-aviation Ti-3Al-2.5V (sports grade)⁵⁹. The titanium frame is lighter and more comfortable than the chrome-molybdenum alloy frame. Titanium-made frames are quite popular, with prices ranging from \$1600 to \$3500 per pair and total bikes ranging from \$2,400 to \$6,000. At present, nearly 50 companies produce titanium bicycles. Bicycle sports are now being carried out around the world, so the sales of titanium bicycles are gradually increasing.

The application of titanium on tennis rackets is mainly to embed a net made of pure titanium into the racket frame⁶⁰. It completely improves the instantaneous inertia force of the tennis racket hitting the ball, and even when the ball does not hit the center of the racket, it is easy to hit the ball, which enhances the hitting power of the racket and is highly praised by the user. The demand for foreign titanium tennis rackets is on the rise. Today, tennis racquet manufacturers are selling titanium racquets, which account for about half of the racquet market. In order to divide the grades, each manufacturer produces a racket according to the characteristics of titanium, the titanium nickel super-elastic alloy material and the coating processing method are used in the handle portion of the tennis racket to develop a new use of titanium. The company develops and applies new titanium fiber materials to tennis rackets⁶¹. The alloy is a shape memory alloy with super-elastic function and the external force is eliminated, even deformed under loading, which will restore the original shape immediately. When hitting the ball, the rebound force can be significantly increased and tennis racket-like. The pure titanium developed as frame and long handle and badminton racket been commercialized by titanium alloy (Ti-3Al-2.5V)⁵⁹.

Mountaineering and skiing are moving towards lighter weight and miniaturization. Titanium has the characteristics of light specific gravity, high strength, and low impact value at low temperatures. It is used as a superior mountaineering and skiing material, such as titanium alloy climbing sticks, hiking soles, climbing fasteners, ski poles, and

ice skates. Titanium sporting goods: including fencing protective masks, swords, fishing rods, fishing reels, rowing parts and injection-molded Ti-Fe series soles for track and field running shoes.

The commonly used titanium materials in this group are the several grades of CP titanium, which are in effect Ti-O alloys, and the ternary composition Ti-5Al-2.5Sn. As the alloys are single phase, tensile strengths are relatively low although their high thermal stability leads to reasonable creep strengths in the elevated temperature range. They display good ductility down to very low temperatures and are readily weldable. Sn and Zr are considered neutral elements since they have almost no influence on the α/β phase boundary. As far as strength is concerned, they are not neutral since they primarily strengthen the α phase ⁶²).

1.2.1.2 Applications of near- α Ti alloys

Materials with excellent high temperature properties, low densities and high reliability can make a significant contribution to performance improvements of modern gas turbines. Near- α alloys have the above characteristics and have been used as gas turbine engine compressor components, such as rotors, discs and stator blades ⁶³⁻⁶⁵). The usage of titanium alloys was limited to about 600°C due to severe oxidation problems associated with degradation of mechanical properties ⁶⁶). However, with the development of aero-engines, it is required to have better performance at high temperature, to widely used in jet engines as compressor discs and blades. To solve this problem, the researchers tried to design new near-alpha titanium alloys. Recently, many countries have developed different high-temperature titanium alloys with their own brands, such as Ti1100 in the America ^{67, 68}), IMI834 in the Britain ⁶⁶), BT36 in Russia, Ti60 ⁶⁹) and Ti600 in China ⁷⁰). These alloys have been successfully used in variety of aircraft engines at elevated temperatures up to 600 °C with good lightweight, superior fatigue and creep properties.

1.2.2 Applications of β -Ti alloys

Unique combination of high strength weight ratio, high hardenability ⁷¹), excellent

hot and cold-working ability and high resistance to the bio-fluidic environment make β titanium alloys an attractive material for aerospace and biomedical applications ⁷²). For the high cost material such as titanium, casting is a choice in the fabrication of components with complex geometry without incurring much wastage ⁷³). Significant weight savings (35%) can be achieved by replacing stainless steel castings with titanium castings in B-777 aircraft ⁷⁴). Ti-5Al-5V-5Mo-3Cr castings treated by hot isostatic pressing show a superior strength compared to hiped Ti-6Al-4V castings with no sacrifice ductility.

In order to extend the braking life of the fighter aircraft (F-18 EF), the Ti-15V-3Cr-3Sn is used instead of the Ti-6Al-4V casting. Ti-13V-11Cr-3Al (B120VCA) as the first beta alloy developed for SR-71 (surveillance aircraft) ⁷⁵). Its inherent properties include significant elongation due to the crystal structure (bcc), including cold-Ti, heat-treatable and excellent cold-resistant rolling, making it an effective alternative to the traditional $\alpha + \beta$ alloys. In particular, β alloys have lower transus temperature than the $\alpha + \beta$ alloys. In this case, β alloys are considered an economical option when the post treatments are necessary. For the $\alpha + \beta$ alloys, the thinner specification (2 mm thick) of the Ti-15V-3Cr-3Sn alloy is approximately one-tenth of that of the Ti-6Al-4V, despite the high formulation cost ⁷⁶).

1.2.3 Preparation methods of titanium alloys

The first step is to prepare ingots from sponges to convert them into abrasive products. The preparation methods for the production of titanium alloy ingots can be roughly divided into vacuum arc re-melting (VAR) ⁷⁷) and cold furnace melting ^{38-40, 78}). The conventional method for melting titanium alloys is vacuum arc re-melting (VAR) in a self-consuming arc furnace. In the VAR, the furnace is first drained to achieve the required vacuum, and then an arc is generated between the two electrodes. Here, the consumable electrode (material to be melted) is used as a cathode and raw materials such as titanium-based scraps or machine turning are used as anodes. Consumable electrodes can be manufactured from either of the two strategies. (1) The compacted sponge and/or scrap. (2) From plasma/electron beam hearth melting

The first method of pre-compacting by using hydraulic compaction is widely used to manufacture electrodes. The pressed electrodes with a nominal alloy component are made by pressing the mixed clean uniform size of titanium sponges and alloy elements that do not contain any harmful inclusions. These cladding (called clumps) are then assembled with large pieces of waste by appropriate welding methods to form the first molten electrode (called the welding rod). Finally, these manufactured electrodes are placed in a vacuum furnace. After the arc is established, the associated heat generation will cause the molten metal to drip into the water-cooled copper crucible, forming ingots.

A layer of solid titanium sheet or particles will be formed on the surface of the cooled copper crucible, which will hold the molten metal that will subsequently fall. To ensure chemical uniformity, the ingots are inverted and re-melted. Ingots produced during the first stage of melting are again used as consuming electrodes during two or three re-melting processes. In addition, in most VAR furnaces there are coils to produce electromagnetic fields that stir the molten metal to further improve uniformity.

CCLM is another developing technique which uses either plasma arc (PAM) or electron beam (EBM) melting furnace. Proper monitoring should be ensured to observe the solidification of Ti-based ingots. The CCLM consists of a high frequency induction furnace and two electric coils. The two electric coils are used for heating and levitation of the metals in the crucible, respectively. The materials will be melted and suspended by the induction current without contact between materials and the copper crucible during the melting process. Furthermore, a uniform composition and high purity of Ti alloys can be obtained by the effect of electromagnetic stirring force and the higher vacuum performance of the furnace³⁸⁻⁴⁰.

1.2.4 Post-treatments of titanium alloys

1.2.4.1 Heat treatment

Solution treatment is a broad term in heat treating used to refer to the heating of a material to temperatures enough for the dissolution of its soluble phases. It is then held for a time until it is quenched, causing the material to retain the properties of the solution.

The ageing process usually applied after the solution treatment of titanium alloys. Alloys must be kept at elevated temperature for hours to allow precipitation to take place. This time delay is called "aging". Solution treatment and aging is sometimes abbreviated "STA" in specifications and certificates for metals. Heat treatment is a basic metallurgical process optimized for hardness, tensile strength, fatigue strength and fracture toughness. Compared with the single aging of Ti-15V-3Al-3Cr-3Sn-3Zr and Ti-3Al-8V-6Cr-4Mo-4Zr ⁷⁹⁾, duplex aging treatment has excellent mechanical properties, no precipitation free zone and fine α precipitation. The heating rate to the aging temperature has been found have effect on the evolution of microstructure and mechanical properties ⁸⁰⁾. The choice of solution treatment condition is very important. For Ti-1Al-8V-5Fe (Ti185) alloy, solution treatment near the β transus temperature produces the highest tensile and yield strength ⁸¹⁾. The aging of the decomposable β alloy after solution treatment will result in a microstructure consisting of soft α phase within the beta grain boundary. For example, it was also reported the adverse effects of α -phase layers on the tensile and fatigue behavior of Ti-5Al-2Sn-4Zr-2Cr-1Fe, which may lead to the decreasing of tensile strength ⁸²⁾.

1.2.4.2 Forging and rolling process

For α and $\alpha + \beta$ titanium alloys, ingot decomposition forging is done above the β transus temperature ⁸³⁾. In general, titanium alloys are pre-heat before forging at high temperatures. Forging to produce the titanium blanks and rods, obtaining the combination of strength and ductility ⁸⁴⁾. Titanium reactivity requires inert or vacuum treatment to prevent contamination during high-temperature processing. Compared to other titanium alloys, β titanium alloys can withstand high pressure before cracking. Ti-13V-11Cr-3Al can withstand the pressure of 690 MPa without cracking ⁸⁵⁾. This effect is caused by enough sliding systems to accommodate deformation. Cylindrical rollers are used to produce strips and plates. In contrast, slotted rollers are used to produce circular and other structural shapes. Cross-rolling during sheet rolling anisotropy that reduces mechanical properties ⁸⁶⁾.

1.2.4.3 Thermomechanical processing

Material processing with both mechanical forces and heat treatment can be called thermal machining. The main goal of this process is to obtain components in the functional design with predetermined microstructure and corresponding mechanical properties. Thermal machining of β Ti alloys can be carried out above and below transus temperature processing. In the process of thermal machining, it has a significant impact on the machinery of the final product. The Ti-15V-3Al-3Cr-3Sn alloy show the usefulness of thermal machinery to obtain a wide range of tensile strength (from 1000 to 1610 MPa).

1.2.5 As-cast application of titanium alloys

When calculating the cost of the Ti alloy for aircraft applications, if the raw material cost is set as unit 1, the cost of casting process is approximately 0.5, the post-treatment cost is approximately 1.5 and the cost of secondary processing is approximately 2. The post-treatment cost is remarkably expensive compared with that of casting, because of the higher energy consumption is necessary. The trend on cost reduction of Ti alloys are focus on the following methods. The first is the choice of cheaper raw materials instead of the expensive ones. The second is the development of new Ti alloys with improved mechanical properties, which can simplify or omit the post-treatment processes. The third way is to improve the efficient of equipment of manufacturing and post-treatment. Others including the expand of production scale to reduce the fringe cost. The high performance of titanium alloys with the σ_{UTS} of 1000 MPa and ϵ_f of 10% just at as cast condition is a landmark alloy-development for energy-saving measures, compared with conventional alloys such as 15-3-3-3 with high performance manufactured by complex post processing. The pure titanium developed as frame and long handle and badminton racket been commercialized by titanium alloy (Ti-3Al-2.5V) with the σ_{UTS} of more than 900 MPa ⁵⁹⁾. The development of light alloys applied in as-cast condition have been proved to be an effective way to reduce their cost and energy consumption. A significant weight (35%) saving can be achieved by employing the titanium casting instead of stainless-steel casting in B-777 aircraft ⁷⁴⁾. Investment casting is preferred to obtain thin sections and better surface finish. Ti-5Al-5V-5Mo-3Cr castings followed by hot

isostatic pressing possess a superior strength compared to hipped Ti-6Al-4V castings with almost same ductility. One of the most widely used commercial 15-3-3-3 β -Tic alloys can achieve the σ_{UTS} of 1000 MPa and fracture strain (ϵ_f) of 7~ 10% after the solution treated and ageing treatment. Even further post-treatments, the hot and cold-working can improve its σ_{UTS} to about 1200~1300 MPa, but the ϵ_f will decrease to approximately lower than 7% as a trade-off.^{35, 36)} It was reported that the 15-3-3-3 used as springs, sheet, plate and airframe materials with complex geometric shapes were usually applied in as-cast condition or after solution treated and ageing treatment.⁶⁾ The high performance of titanium alloys with the σ_{UTS} of 1000 MPa and ϵ_f of 10% just at as cast condition is a landmark alloy development for energy-saving measures.

1.3 Development of alloy design methods

To development of alloys for industry applications, the optimization of performances and components were carried out by numbers of researchers by using various methods. In the past, the development of titanium alloys mainly relied on experimental methods of trial and error tests. Although some tests use orthogonal testing to reduce the number of tests, this “tentative” test is not only time-consuming and laborious, but also needs significant economic losses. This method still takes the essential aspect among alloys design methods.

The alloy design with specific target properties under the guidance of theory or empirical to determine the kinds and content of elements need to be added to the base metal. Based on the scientific, efficient, economical and predictable requirements for development of material design, it will be the trend to design material through calculation method. The development of metal materials on theory of microstructure, phase structure, atomic/electronic structure, band energy theory, chemical bond theory, electronic theory and the continuous development of computer technology, the material scientific design gradually become mature, and begins to move toward practical stage. The following contents will introduce some major methods on alloy design.

1.3.1 Semi-empirical mode on the basis of trial and error method

The semi-empirical mode is a method to predict the microstructure and property of material by existing experimental data. Japan engineering manufacturing center has established Linus Pauling File database. This database covers structure, diffraction, composition, intrinsic properties and other information of alloys, intermetallic compounds, ceramics, minerals and so on ⁸⁷⁾. At least 200,000 data items related to structure, diffraction, intrinsic properties, and 35 thousand data items recorded since 1900 are stored in this knowledge information system. The laws, principles can be obtained by this powerful material database with an accuracy beyond 95% only by entering the atomic number with considering of possible compound compositions in alloys ⁸⁷⁾.

1.3.2 Phase computation (PHACOMP) method

In 1964, the phase computation (PHACOMP) method was mainly used to predict the formation of harmful and brittle phases in Ni-based alloys. PHACOMP is a computerized calculation technique can predict the tendency of precipitation of intermetallic compounds in an austenitic alloy, which usually identified as topologically close-packed phases. The PHACOMP are founded on atomic electron vacancy (electron hole) theory. Thus, the system is limited to these specific phases where electron bonding plays a strong role^{88, 89)}. Such phases are characterized by a narrow, rather specific, range of electron-atom ratios^{88, 90)}.

The PHACOMP is a vehicle prompted by the experience that the formation of σ , μ , Laves and the commercial high strength and temperature alloys which usually produces embrittlement and loss of ductility, a significant reduction in fracture strength, or some combination of properties which seriously degrade performance. These specific effects, and the properties of the topologically close-packed phases themselves are of considerable practical and scientific importance. The PHACOMP calculation itself is at early stage of the alloy design development. It is also importance to describe meaningful ways of applying the tool to alloy systems which appeared to be exceptions to the general case. The sufficient detail on the alloy design method on the basis of alloy design method are list in the follow.

1.3.2.1 Electronic vacancy numbers method

In 1968, Woodyatt et al. published a specific procedure to calculate an average N_v for commercial alloys of each element. The equation to calculate the average electron vacancy number of an alloy is given as:

$$N_v = \sum_i (X_i) (N_{vi}) \quad (1-3)$$

where X_i is the atomic fraction of element i and N_{vi} is the electron hole number for this element. As early as 1952, Das et al⁹¹⁾, had found a correlation between the electron vacancy number (N_v)⁹²⁾ and phase stability in Mo-Fe-Co, Mo-Fe Ni, and Mo-Ni-Co ternary systems. Greenfield and Beck^{93, 94)} checked the formation of σ phase in systems that contain transition elements. Only elements in the solid solution were considered,

which need a method of reducing the alloy content of the compound-forming elements. Although the electron vacancy method ignores the difference between relative electrical negative and atomic dimensions, there is a correlation between the calculated N_v value higher than the critical N value and the appearance of the topologically close-packed phases in a lot of alloy systems⁹¹⁾. This analysis method was used to define phase boundaries. Some nickel-base alloy mismatches where a significant amount of σ phase is formed within the predicted safe region, or where the σ phase is not formed with a composition in the region where σ phase is likely to occur⁹⁰⁾, Barrows and Newkirk⁹⁵⁾ developed a temperature-dependent critical vacancy number (N_{vi}). The algebraic coefficients used to determine the N_v are based on solid solubility data from existing phase diagrams. Since this method is an extension of the original PHACOMP method, its accuracy is limited to the availability of phase diagrams and the electron vacancy concept.

1.3.2.2 New Phase computation (PHACOMP) method

As an extension of the electron vacancy approach New PHACOMP as described by Morinaga^{96, 97)} is based on a theoretical approach to the solubility problem in alloys containing transition elements. Similar with PHACOMP, New PHACOMP does not predict the forms of TCP, only the likelihood of a given composition to contain such phases. To predict the type of phase forming on solidification, ternary phase diagrams closely representing the given alloy are used⁹⁷⁾. In the new PHACOMP model, the parameter M_d is defined as the average energy level above the Fermi level of the "d" orbit in the transition element. The average energy in the alloy metal d-level (M_d) is calculated by multiplying the contribution of each alloying element by its atomic fraction like N . The equation is shown as follow:

$$M_d = \sum M_{di} X_i \quad (1-4)$$

A critical M_d (in eV) value is measured by fitting the solid solubility line in phase diagrams by a constant M_d line. By plotting the σ phase safe boundary at different temperatures for various alloys the following equation was developed⁹⁶⁾:

$$M_{dc} = 6.25 \times 10^5 T + 0.834 \quad (1-5)$$

Where temperature T is in absolute Kelvin. As the average M_d exceeds a critical value, M_{dc} , the energy associated with the solid solution becomes favorable for a TCP to form. In theory, the M_{dc} should depend on the type of phase forming. While σ phase is chemically and structurally similar to other TCP phases and historically their critical values have been expressed by the same value.

1.3.3 d-Electron alloy design method

Molecular orbital theory refers to research electronic motion status based on quantum chemistry calculation. This method can design and predict the material structure and performance. The molecular orbital theory is based on non-relativistic approximation, Born-Oppenheimer approximation and orbital approximation, its basic concepts are: regard molecule as a whole; atomic orbitals corresponding to each atomic in molecule consist several molecule orbitals; then arrange atomics in a series of molecular orbits, and atomics belong to whole molecule. The Discrete Variational (DV)- $X\alpha$ cluster method are adopted in the field of material design more frequently. DV- $X\alpha$ cluster method was put forward firstly by Slater in 1951. This method takes electronic exchange function as statistical average value, and substitutes into Hartree-Fock function to achieve $X\alpha$ equation. DV- $X\alpha$ cluster method is based on Hartree-Fock-Slater approximation and can provide rather accurate electronic structure even for larger size cluster system. In this method, the potential energy of Slater's local electronic exchange involves the interaction between electrons. $V\alpha$ is given by equation below:

$$V\alpha = -3\alpha [3\rho(r)/8\pi]^{1/3} \quad (1-6)$$

Where $\rho(r)$ is the local electron density, the parameter α is fixed value 0.7. The calculation adopts self-consistent electronic approximation and uses discrete sampling method to integrate matrix elements. Hamiltonian function matrix elements and overlapping integrals are calculated by the method of random sampling⁹⁸⁾. The molecular orbital is consisted by linear combination of atomic orbit. The DV- $X\alpha$ cluster method doesn't have unique physical model, but only is an improvement in computational methods. Its accuracy is generally slightly lower than the ab initio method. But because it has adopted the localized density functional approximation of

exchange potential, so that it doesn't need to calculate a large number of multi-center integrals. This method is one of the common methods of calculating heavy atom-containing molecules and solid atom clusters.

In 1984, M. Morinaga et al. adopted DV- $X\alpha$ cluster method to research the electronic structure of elements of Zn, Ni and Ti system alloys⁹⁹⁻¹⁰¹), and obtained Fermi level parameters of 20 alloy elements, and put forward the d-electrons concept for evaluation of alloy phase stability and various properties¹⁰²). The two parameters, Bo and Md were used in this approach. The mean Bo_t and Md_t values of each alloy were calculated by the following equations:

$$Bo_t = \sum X_i (Bo)_i \quad (1-7)$$

$$Md_t = \sum X_i (Md)_i \quad (1-8)$$

Where X_i is the molar fraction of component i in Ti alloy, $(Md)_i$ and $(Bo)_i$ were the numerical values of Bo_t and Md_t for each component i , respectively. In the present, this method is widely used and accepted by titanium researchers. Simultaneously, the predicted regions showed the slip, twin and martensite deformation behaviors in the Bo_t - Md_t diagram, on the basis of d-electrons concept, providing guidance to propose β -Ti alloys with specific deformation type^{103, 104}). Compositions of forty commercial alloys were plotted on the Bo and Md coordinates, three types of titanium alloys were clearly separated in the Bo_t - Md_t diagram¹⁰³) as shown in Fig. 1-2. In addition, titanium alloys are classified into the α , $\alpha + \beta$ and β types according to the phases existing in alloys as shown in Fig. 1-3. A region showing high ultimate tensile strength for β Ti alloy design can be specified concretely adjusting the Bo and Md values on the Bo_t - Md_t diagram. For Ti alloys the values of Bo and Md are defined by taking the compositional average, which is easy to use in practical application, compared with other alloy design methods such as phase-field method and thermodynamic modeling of ordered phases^{105, 106}). The value of the weight loss was null in the NaNO_3 - NaCl immersion tests for 252.9 ks, regardless of the kinds of alloys¹⁰⁷). It has been found that various physical properties could be interpreted in term of Bo . For example, Bo correlated well with activation energies for impurity-diffusion of transition elements in β -Ti¹⁰⁸). Figure 1-4 shows the results of the Na_2SO_4 - NaCl immersion tests. The ratio of weight loss to the initial weight of titanium alloys increased as immersion period increased in all

specimens. There were not remarkable different values in this ratio throughout the immersion period of 0.3 to 3.3 ks, for Ti-5.5Al-2Fe and Ti-6Al-4V of $\alpha + \beta$ type alloys. The relation between Bo_t of alloys and the ratio of weight loss to the initial weight after

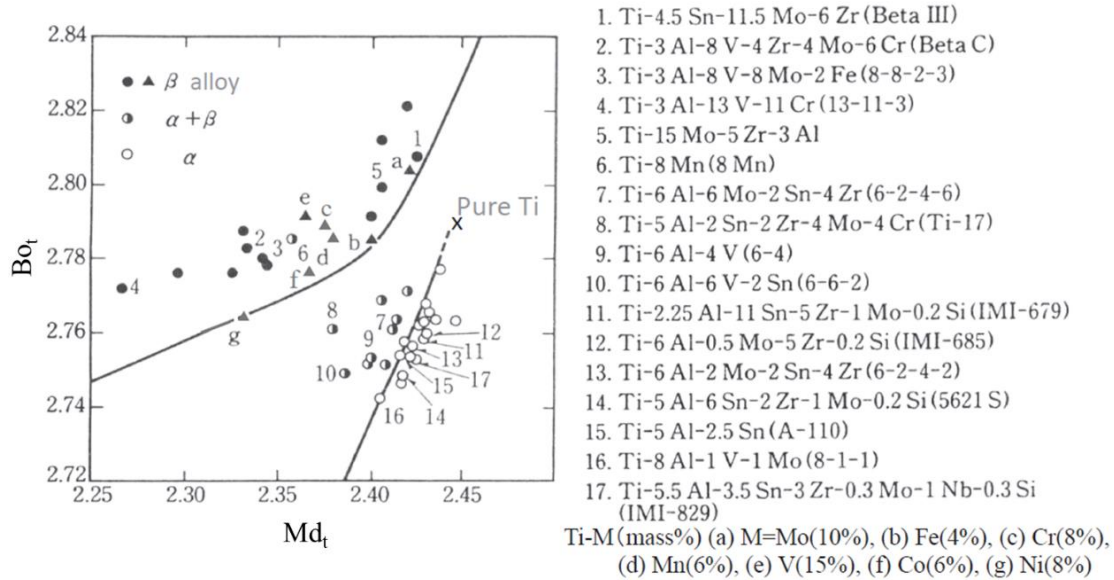


Fig. 1-2 Grouping of commercial titanium alloys classified into the three types of α , $\alpha + \beta$, and β alloys on the Bo_t - Md_t diagram.

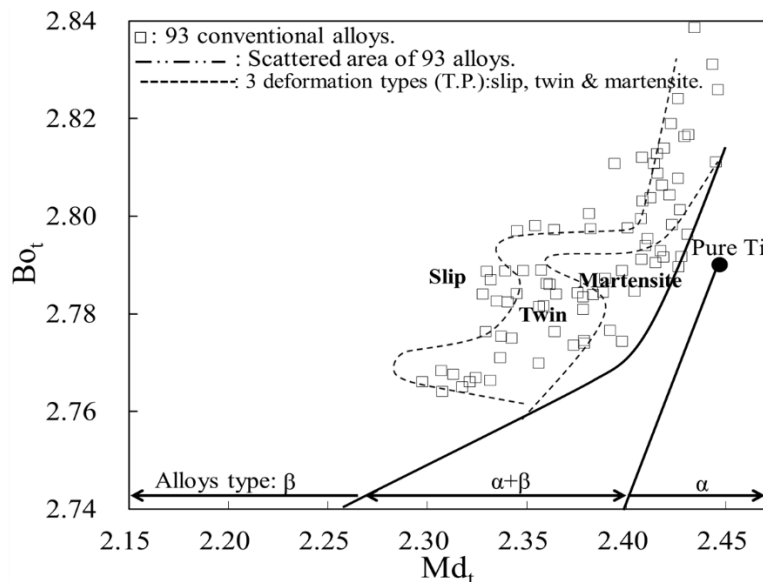


Fig. 1-3 Commercial titanium alloys classified into the three types of α , $\alpha + \beta$, and β alloys and the boundaries between slip, twin and martensite deformations on the Bo_t - Md_t diagram.

the immersion period of 21.6 ks. There was a good correlation between this ratio and Bo_t . As Bo_t increased in alloys, this ratio of weight loss decreased linearly, although there were a few data. In addition, there was report discussed the position of Ms temperature line in the Bo_t - Md_t diagram, as shown in Fig. 1-5¹⁰³⁾. The near or metastable β alloys with Ms temperature higher than room temperature (25 °C) is easy to process the phase transition behavior.

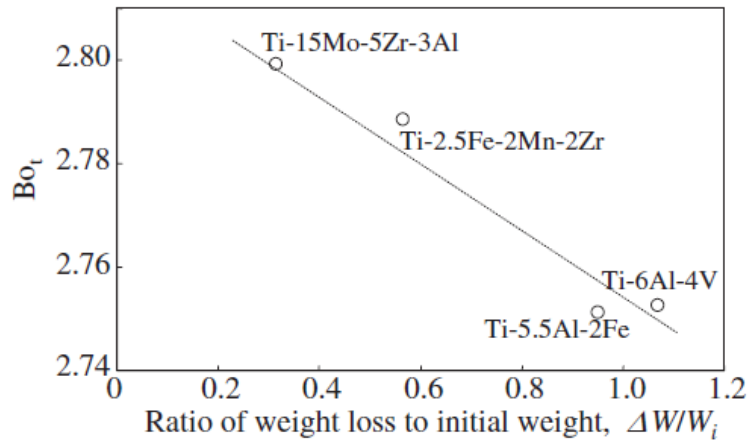


Fig. 1-4 Relation between the Bo_t and ratio of weight loss to initial weight obtained from the immersion test for 21.6 ks in Na_2SO_4 -45 mol% NaCl molten salt at 923 K.

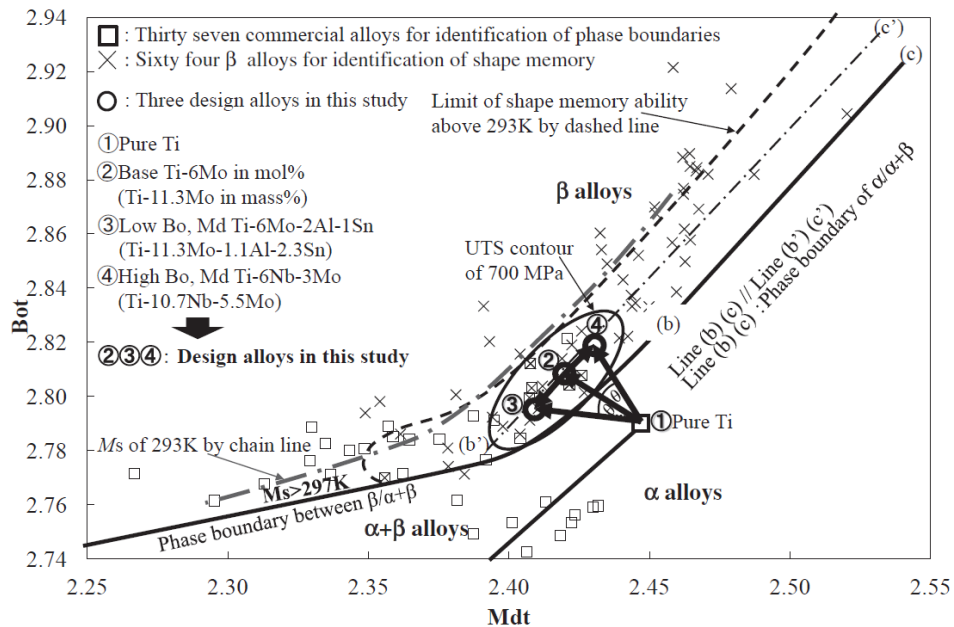


Fig. 1-5 Bo_t - Md_t diagram showing phase boundaries, and other characteristics obtained from reported alloys, and the positions of proposed alloys. Ninety four reported β alloys for these classification showed the compositional range of Ti-(0-55)Ta-(0-41)Nb-(0-30)Zr-(0-8)Fe-(0-13)Cr-(0-22)V-(0-20)Mo-(0-6)Sn-(0-8)Al-(0-8)Mn in mass%.

1.4 Objectives of this study

The commercial Ti alloys are commonly subjected to the complex post-treatments which will cause additional cost and energy consumption. In the present study, the electric parameters (Bo and Md) were used to design Ti alloys for as-cast applications. The proposed Ti alloys with comparable mechanical properties to those of commercial alloys which were treated by complex post-treatments is chosen as the cost and energy consumption saving measures. Undoubtedly, global warming has become a serious problem and the application of titanium alloys without complex post-treatments will help to develop the environmentally friendly society, which is the responsibility of every industry and individual. The ingots of experimental Ti alloys were produced by the CCLM technique as the single manufacturing process for saving energy. The extra low interstitial (ELI) level composition Ti alloys were obtained and their microstructural and mechanical properties were guaranteed by adjusting its cooling process parameters. The as-cast application possibility of proposed titanium alloys was evaluated by comparing their mechanical properties in both as-cast and solution treated conditions. The target values of β , α and near- α titanium alloys are shown in Table 1-1.

Table 1-1 Target mechanical values of β , α , and near- α titanium alloys.

Properties	Target values	References commercial Ti alloys
Ultimate tensile strength (MPa)	>1000	β titanium alloys (Ti-15V-3Cr-3Sn-3Al)
Fracture strain (%)	>10	
Ultimate tensile strength (MPa)	>800	α titanium alloys (Ti-5Al-2.5Sn)
Fracture strain (%)	>15	
Ultimate tensile strength (MPa)	>1000	Near- α titanium alloys (Ti-6Al-4Zr-2.75Sn-0.4Mo-0.45Si)
Fracture strain (%)	>10	

Chapter 1 reviews the scientific background of this research, points out the objective

and illustrates the overall content of the thesis.

Chapter 2 discusses the mechanical properties of three new β -Ti alloys with different tensile deformation types. The new composition of three β -Ti alloys were proposed to develop β -Ti alloys for as-cast application. According to the d-electrons concept, the new three alloys were proposed using mainly ubiquitous elements in the predicted regions showing the slip, twin and martensite dominant deformation behaviors in the Bo_t - Md_t diagram, respectively. The segregation of solute elements, microstructural and tensile properties had been investigated in both as-cast and solution treated conditions. The variant properties of three β -Ti alloys between as-cast and solution treated conditions as well as their as-cast application possibility were discussed in this chapter.

Chapter 3 shows ten β -Ti alloys with controllable slip dominant deformation were proposed on the basis of the d-electrons concept, by using the Bo_t - Md_t diagram, according to the results of chapter 3. To develop β -type Ti alloys with σ_{UTS} value of 1000 MPa and ε_f value of 10% in as-cast condition, the new compositions of ten types of β -Ti alloys were proposed in the newly expanded area greatly differing from conventional alloys. The increase of additional solute elements contents was used as a method to improve the strength of β -Ti alloys for as-cast applications, by choosing cheap and easy disposal ubiquitous elements. The microstructure and mechanical properties of ten types of β -Ti alloys were discussed in as-cast and solution treated conditions, and their as-cast application possibility was also discussed in the present chapter. In addition, the phase boundary between the mono β phase and dual β plus intermetallic compound phases were successfully identified in the newly expanded area of Bo_t - Md_t diagram for the first time.

Chapter 4 introduces the applications and limitations of α and near- α titanium alloys, the development of α and near- α Ti alloys with improved mechanical properties by using the prediction counter lines in the Bo_t - Md_t diagram, which were proposed for the first time to predict the tensile strength of α and near- α Ti alloys by considering their Bo_t and Md_t values. The dependability of the prediction counter lines was also proved by comparing the newly proposed α and near- α Ti alloys. The higher corrosion resistance ability of designed near- α Ti alloy compared to those of the commercial reference near- α Ti alloy were obtained with the help of considering their Bo_t values.

References

- 1) M. Niinomi: *J. Mechan. Behav. Biomed.* **1** (2008) 30–42.
- 2) X.L. Zhao, M. Niinomi, M. Nakai, G. Miyamoto and T. Furuhashi: *Acta. Biomater.* **7** (2011) 3230–3236.
- 3) H. Attara, M.J. Bermingham, S. Ehtemam-Haghighi, A. Dehghan-Manshadi, D. Kent, and M.S. Dargusch: *Mater. Sci. Eng. A.* **760** (2019) 339–345.
- 4) R. Hosseini, M. Morakabati, S.M. Abbasi and A. Hajari: *Mater. Sci. Eng. A.* **696** (2017) 155–165.
- 5) J.J. Dai, J.Y. Zhu, C.Z. Chen and F. Weng: *J. Alloy. Compd.* **685** (2016) 784–798.
- 6) C. Cai, B. Song, P.J. Xue, Q.S. Wei, C.Z. Yan and Y.S. Shi: *Mater. Design.* **106** (2016) 371–379.
- 7) S. Shekhar, R. Sarkar, S.K. Kar and A. Bhattacharjee: *Mater. Design.* **66** (2015) 596–610.
- 8) K. Shekhar, R. Sarkar, J. Zhao, J.L. Wang and S.J. Yuan: *Mater. Design.* **91** (2016) 269–277.
- 9) Z.Y. Yang, X.H. Zheng, Y. Wu and W. Cai: *J. Alloy. Compd.* **680** (2016) 462–466.
- 10) I.Y. Yang, H. Wendrock, A.S. Volegov, H. Attar, U. Kühn, W. Skrotzki and J. Eckert: *Mater. Sci. Eng. A.* **628** (2015) 297–302.
- 11) S. Pervaiz, S. Anwar, I. Qureshi and N. Ahmed: *Int. J. Precis. Eng. Man.* **6** (2019) 133–145.
- 12) P. Pervaiz, Pungotra and N.S. Kalsi: *ICAAMM.* **4** (2017) 8971–8982.
- 13) R. Goyal and A.K. Dubey: *J. Mech. Sci. Technol.* **30** (2016) 1281–1293.
- 14) K. Wang: *Mater. Sci. Eng. A.* **213** (1996) 134–137.
- 15) H. Shahali, A. Jaggessar and P.K.D.V. Yarlagadda: *Proce. Eng.* **174** (2017) 1067–1076.
- 16) H.M. Khanlou, B.C. Ang, M.M. Barzani, M. Silakhori and S. Talebian: *Neural. Comput. Applic.* **26** (2015) 1751–1761.
- 17) M. Geetha, A.K. Singh, R. Asokamani and A.K. Gogia: *Prog. Mater. Sci.* **54**

- (2009) 397-425.
- 18) Eren Yılmaz, A. Gokce. F. Findik and H.O. Gulsoy: *J. Therm. Anal. Calorim.* **134** (2018) 7–14.
 - 19) H.M. Li, K.M.T. Lei, J.C. Zhao, Q.L. Shang and Z. Lin: *Mater. Manuf. Process.* **31**(2016) 719-724.
 - 20) M.A. Hussein, C. Suryanarayana and N. Al-Aqeeli: *Mater. Design.* **87** (2015) 693–700.
 - 21) Y. Liu, K. Matsugi, Z.F. Xu and Y.B. Choi. Master thesis. (2018) Hiroshima university.
 - 22) N. Mitsuo: *Basic Mater. Sci.* (2009) 144.
 - 23) C. Leyens and M. Peters: *Wiley Vch Verlag GmbH and Co. KGaA*, (2003) 1–36.
 - 24) E.O. Ezugwu and Z.M. Wang: *J. Mater. Proc. Technol.* **68** (1997) 262–274.
 - 25) F.H. Froes, H. Friedrich, J. Kiese and D. Bergoint: *JOM* (2004) February.
 - 26) A.K. Sachdev, K. Kulkarni, Z.Z. Fang, R. Yang, V. Girshov and J. Miner. *Met. Mater. Soc.* **64** (2012) 553–565.
 - 27) G. Crowli: *Adv. Mater. Process.* **161** (2003) 25–27.
 - 28) T. Morita, K. Hatsuoka, T. Iizuka and K. Kawasaki: *Mater. Trans.* **46** (2005) pp. 1681–1686.
 - 29) M. Morinaga, N. Yukawa, T. Maya, K. Sone and H. Adachi: *Proc. 6th World Conf. on Ti, TMS*, (1988) 1601–1606.
 - 30) M. Morinaga, N. Yukawa and H. Adachi: *Tetsu-to-Hagané.* **72** (1986) 555–562.
 - 31) M. Morinaga, J. Saito and M. Morishita: *J. JILM* **42** (1992) 614–621.
 - 32) P. Laheurte, F. Prima, A. Eberhardt, T. Gloriant, M. Wary and E. Patoor: *JMBBM.* **3** (2010) 565–573.
 - 33) X.J. Jiang, Y.K. Zhou, Z.H. Feng, C.Q. Xia, C.L. Tan, S.X. Liang, X.Y. Zhang, M.Z. Ma and R.P. Liu: *Mater. Sci. Eng. A.* **639** (2015) 407–411.
 - 34) J.R.S. Martins, R.O. Araújo, T.A.G. Donato, V.E. Arana-Chavez, M.A.R. Buzalaf and C.R. Grandini: *Mater.* **7** (2014) 232–243.
 - 35) W.J. Joost, S. Ankem and M.M. Kuklja: *Acta. Mater.* **105** (2016) 44–51.
 - 36) Y.Y. Zong, S.H. Huang, Y.J. Feng and D.B. Shan: *Alloy. Compd.* **541** (2012)

- 60–64.
- 37) C.P. Liang and H.R. Gong: *Int. J. Hydrogen. Energ.* **35** (2010) 3812–3816.
- 38) A. Gagnoud, J. Etay and M. Garnier: *ISIJ.* **28** (1988) 36–40.
- 39) A. Morita, H. Fukui, H. Tadano, S. Hayashi, J. Hasegawa and M. Niinomi: *Mater. Sci. Eng. A.* **280** (2000) 208–213.
- 40) K. Matsugi, H. Mamiya, Y.B. Choi, G. Sasaki, O. Yanagisawa and H. Kuramoto: *Int. J. Cast. Metal. Res.* **21** (2008) 156–161.
- 41) C. Brozek, F. Sun, P. Vermaut, Y. Millet, A. Lenain, D. Embury, P. J. Jacques and F. Prima: *Scr. Mater.* **114** (2016) 60–64.
- 42) M. Morinaga, M. Kato, T. Kamimura, M. Fukumoto, I. Harada and K. Kubo: *Proc. 7th World Conf. on Ti, TMS,* (1992) 217–224.
- 43) M.A.H. Gepreel and M. Niinomi: *J. Mech. Behav. Biomed. Mater.* **20** (2013) 407–415.
- 44) K. Ikeda: *JJILM,* **55** (2005) 97–102.
- 45) I.V. Okulov, H. Wendrock, A.S. Volegov, H. Attar, U. Kühn, W. Skrotzki and J. Eckert: *Mater. Sci. Eng. A.* **628** (2015) 297–302.
- 46) B. Cantor, I.T.H. Chang, P. Knight and A.J.B. Vincent: *Mater. Sci. Eng. A.* **375–377** (2004) 213–218.
- 47) V.B. Deev, V.A. Degtyar, A.I. Kutsenko, I.F. Selyanin, and A.P. Voitkov: *Steel. Transl.* **12** (2007) 33–36.
- 48) A.K. Dahle, Y.C. Lee, M.D. Nave, P.L. Schaffer and D.H. StJohn: *JLM.* **1** (2001) 61–72.
- 49) C. Liang, M.X. Ma, M.T. Jia, S.Ratnova, J.Q. Yan and D.L. Zhang, *Metall. Mater. Trans. A.* **46** (2015) 5095–5102.
- 50) Y.F. Zheng, X. Yao, J.M. Liang and Deliang. Zhang: *Mater. Trans. A.* **47A** (2016) 1842–1853.
- 51) T. Hoshi and N. Kamimura: Patent number: 5464216. (1995).
- 52) K. Rüdinger and A. Ismer: *Ti. Sci. Technol.* (1973) 185–199.
- 53) K. G. Budinski: *Wear.* **151** (1991) 203–217.
- 54) T. Kubota, K. Doi, T. Murakami, Y. Kojima and T. Miura: *SAE Int. J. Engines* **9** (2016) 483–490.

- 55) E.B. Clark and B. Roebuck: *Refractory. Metab. Hard. Mater.* **11** (1992) 23–33.
- 56) I.V. Gorynin: *Mater. Sci. Eng. A.* **263** (1999) 112–116.
- 57) T. Fujita, A. Ogawa, C. Ouchi and Hidenori Tajima: *Mater. Sci. Eng. A.* **213** (1996) 148–153.
- 58) Renishaw: *MPR.* (2014) 38-40.
- 59) H. Li, H. Yang, F.F. Song, M. Zhan and G.J. Li: *J. Mater. Proc. Technol.* **212** (2012) 1973–1987.
- 60) S.R. Seagle: *Mater. Sci. Eng. A.* **213** (1996) 1–7.
- 61) P. Ducheyne, G. Willems, M. Martens and J. Helsen: *J. Biomed. Mater. Res.* **18** (1984) 293–308.
- 62) P.D. Ewart: *ISEA. Proceedings.* 2-254 (2018) 1–6.
- 63) P. Wanjara, M. Jahazia, H. Monajatib, S. Yue and J. P. Immarigeon: *Mater. Sci. Eng. A.* **396** (2005) 50–60.
- 64) M.C. Somani, R. Sundaresan, O.A. Kaibyshev and A.G. Ermachenko: *Mater. Sci. Eng. A.* **243** (1998) 134–139.
- 65) Y.G. Zhou, W.D. Zeng and H.Q. Yu: *Mater. Sci. Eng. A.* **393** (2005) 204–212.
- 66) S. Hardt, H.J. Maier and H.J. Christ: *Int. J. Fatigue.* **21** (1999) 779–789.
- 67) H. Ghonem and R. Foerch: *Mater. Sci. Eng. A.* **138** (1991) 69–81.
- 68) A. Zhang, D. Liu and H.M.Wang: *Mater. Sci. Eng. A.* **562** (2013) 61–68.
- 69) L.N. Yang, J.R. Liu, J. Tan, Z.Y. Chen, Q.J. Wang and R. Yang: *J. Mater. Sci. Technol.* **30–7** (2014) 706–709.
- 70) Y. Niu and M.Q. Li: *Mater. Sci. Eng. A.* **513–514** (2009) 228–232.
- 71) H.P. Ng, E. Douguet, C.J. Bettles and B.C. Muddle: *Mater. Sci. Eng. A.* **527** (2010) 7017–7026.
- 72) S. Kuppusami and R.H. Oskouei: *J. Biom. Eng.* **3-2** (2015) 9–14.
- 73) B. Sengupta, S. Shekhar and K.N. Kulkarni: *Mater. Sci. Eng. A.* **696** (2017) 478–481.
- 74) R.R. Boyer: *JOM.* (1994) 20–23.
- 75) R.R. Boyer and R.D. Briggs: *ASM. JMEPEG.* **14** (2005) 681–685.
- 76) P.J. Bania: *JOM.* (1994) 16–19.

- 77) F.J. Zanner: Metall. Trans. B. 10 (1979) 133–142.
- 78) T.B. Reed and E.R. Pollard: J. Cryst. Growth. **2** (1968) 243–247.
- 79) H. Usuki, N. Narutahi and Y. Yamane: J-STAGE. **61** (1995) 1001–1005.
- 80) R. Santhosh, M. Geetha, V.K. Saxena and M. Nageswararao: J. Alloy. Compd. **605** (2014) 222–229.
- 81) G. Srinivasu, Y. Natraj, A. Bhattacharjee, T.K. Nandy and G.V.S.N. Rao: Mater. Design. **47** (2013) 323–330.
- 82) G.S. Srinivasu and N.R. Raja: Int. J. Min. Met. Mater. **11** (2012) 953–960.
- 83) L. Meng, T. Kitashima, T. Tsuchiyama and M. Watanabe: Mater. Sci. Eng. A. (2019) Article in press.
- 84) E. Czarnowska, T. Wierzchon and A. Maranda-Niedbala: J. Mater. Sci. Technol. **92–93** (1999) 190–194.
- 85) F.H. Froes: ASM. Int. (2015)1–11.
- 86) H. Nasiri-Abarbekoh, A. Ekrami, A.A. Ziaei-Moayyed and M. Shohani: Mater. Design. **34** (2012) 268–274.
- 87) N. Niwa, T. Demura and K. Ito: ISIT. Int. **30** (1990) 773–779.
- 88) H.J. Beattie: J. Appl. Phys. **24** (1953) 1322–1324.
- 89) W. Hume-Rothery: J. Chem. Educ. London, (1954) 163–182.
- 90) H.J. Murphy, C.T. Sims and A.M. Beltran: J. Metal. (1968) 46–53.
- 91) D.K. Das, S.P. Rideout and P.A. Beck: Trans. TMS-AIME, **194** (1952) 1071–1075.
- 92) L. Pauling: Phys. Rev. **54** (1938) 899–904.
- 93) P. Greenfield and P. Beck: Trans. TMS-AIME. **200** (1953) 253–257.
- 94) P. Greenfield and P. Beck, Trans.TMS-AIME. **206** (1956) 265–276.
- 95) R.J. Barrows and J.B. Newkirk: Met. Trans. **3–11** (1972) 2889–2893.
- 96) M. Morinaga, N. Yukawa, H. Adachi and H. Ezaki: TMS. (1984) 523–532.
- 97) M. Morinaga, N. Yukawa, H. Adachi and H. Ezaki: J. Phys. Soc. Jpn. **53–2** (1984) 653–663.
- 98) Y. Xie and Z. Qiao: Phase. Equilibria. **17** (1996) 208–250.
- 99) K. Matsugi, Y. Murata, M. Morinaga and N. Yukawa: Sci. Eng. A. **172** (1993) 101–110.

- 100) K. Matsugi, T. Kashiwagi, Y.B. Choi and G. Sasaki: *Mater. Trans.* **52** (2011) 2189–2196.
- 101) Z.F. Xu, Y.B. Choi, T. Niimi, M. Yu, S. Motozuka, K. Matsugi and K. Suetsugu: *Mater. Trans.* **57** (2016) 553–557.
- 102) M. Morinaga, S. Nasu, H. A. Jsaio: *Phys. Condes. Matter.* **3** (1991) 6817–6828.
- 103) M. Morinaga: *Mater. Trans.* **57** (2016) 213–226.
- 104) X.L. Ma, K. Matsugi, Z.F. Xu, Y.B. Choi, R. Matsuzaki, J. Hu, X.G. Liu and H. Huang: *Mater. Trans.* **60** (2019) 2426–2434.
- 105) T. Koyama: *J. Japan. Inst. Metals.* **73** (2009) 891–905.
- 106) I. Ansara, B. Sundman and P. Willemin: *Acta Metall.* **36** (1988) 977–982.
- 107) K. Matsugi, T. Endo, Y.B. Choi and G. Sasaki: *Mater. Trans.* **51** (2010) 740–748.
- 108) M. Morinaga, N. Yukawa and H. Adachi: *J. Iron Steel Inst. Japan* **71** (1985) 1441–1451.

Chapter 2

Applicability of as-cast on β type titanium alloys proposed in the compositional region with different tensile deformation types

2.1 Introduction	32
2.2 Alloy design for the β alloys located on different regions in the Bo_T - Md_i diagram.	35
2.3 Experimental procedures	39
2.3.1 Materials and manufacturing process.....	39
2.3.2 Microstructural characterization and point analysis.....	43
2.3.3 Tensile test.....	43
2.4 Results and discussion	45
2.4.1 Microstructures and solute segregation in solidification.....	45
2.4.2 Tensile properties and fracture surface.....	50
2.4.3 Vickers hardness.....	54
2.4.4 As-cast application possibility of experimental alloys in the view of tension behaviors	55
2.5 Summary.....	57
References	58

2.1 Introduction

β type titanium (β -Ti) alloys have been widely investigated for their unique mechanical properties in ambient temperatures, excellent corrosion resistance, shape memory ability and high specific strength¹⁻⁴). Thus, β -Ti alloys are extensively used in aerospace, implant and industrial applications⁵⁻⁷). It is known that Ti ranks as the ninth most plentiful element and the fourth most abundant structural metal in the Earth's crust⁸). However, remaining drawbacks for Ti alloys is the higher cost than many other light metals because of the long design cycle time, poor refining efficiency, difficulty of melting and complexity of post treatment process etc⁹). Whereas the cost is the decisive factor for industrial manufacturers when they choose the materials¹⁰).

To reduce the cost of Ti alloys, some measurements are taken by researchers as follows. In the past, the alloy design and development of Ti alloys mainly relied on the repeated experiments and some empirical rules, which are high cost and inefficient, until the propose of d-electrons concept based on the theoretical calculation of electronic structures of alloys. The d-electrons concept was first published by Morinaga et al¹¹⁻¹³) and has been accepted by numerous Ti alloy researchers^{14, 15}). Two calculated parameters were mainly utilized in the d-electrons concept. The one is the d-orbital energy level (*Md*) of alloying transition elements, and the other is the bond order (*Bo*) that is a measure of the covalent bond strength between atoms. Moreover, Ti is very chemically reactive and easy to react with many elements like oxygen and hydrogen during the manufacturing process, which can greatly influence the properties of Ti alloys¹⁶⁻²⁰). The source of these elements usually derives from the gas environment of furnace and the contaminations of the crucible. Therefore, it is essential to control the vacuum level in furnaces and prevent impurities from contaminating. The cold crucible levitation melting (CCLM) method can suit these requests very well. The CCLM consists of a high frequency induction furnace and two electric coils. The upper electric coil is used for heating and the lower electric coil is utilized for levitation the molten metals^{21, 22}). The molten material can be levitated by the eddy current in the melting crucible so that the alloys can be melted without any contact between materials and the crucible. Moreover, a uniform composition of Ti alloys can be obtained by the diffusion

mixing effect and strong stirring from the electromagnetic force ²³⁾.

According to the previous reports and practical applications, many complex post-processing treatments were needed after casting for producing conventional β -Ti alloys with high strength and toughness ²⁴⁾, which further led to their high final costs. For example, one of the most widely applied β -Ti alloy Ti-15V-3Cr-3Sn-3Al with the ultimate tensile strength (σ_{UTS}) of 800~1400 MPa and fracture strain (ϵ_f) of 6~11% can be obtained after solution treated, aged, hot and cold working process ^{5,25)}. The complex post-processing treatments will lead to the high cost and high energy consumption, as shown in Fig. 2-1.

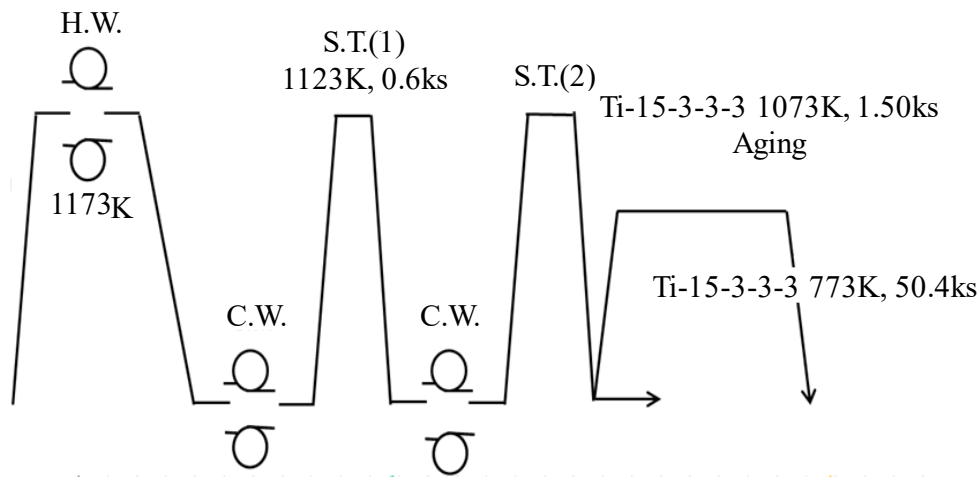


Fig. 2-1 Schematic drawing of thermomechanical process for Ti-15V-3Cr-3Sn-3Al alloy. H.W.: hot-working, C.W.: cold-working, and S.T.: solution-treatment.

Herein, when considering the final cost of the Ti alloy for aircraft applications, if the raw material cost is set as 1, the casting cost is about 0.5, the post-processing cost is about 1.5 and the secondary processing cost can be estimated to be 2 ²⁶⁾. The post-processing treatment cost is remarkably expensive compared with that of casting, because of the high energy consumption. The development of Ti alloys could be used in as-cast condition is urgent needed to reduce the post-processing and simplified manufacturing process. However, there are almost no precedent for Ti alloys with high alloy using in as-cast condition manufactured just by single casting process. Because the solidification segregation of alloying elements, emergence of non-equilibrium phase

and instability of the constituent phases usually appeared in the casting Ti alloys^{27, 28)}. In contrast, it is also reported that many light metals are developed to be applied in as-cast condition which may be an effective way to reduce energy consumption and production costs by omitting complex post-processing procedures, such as aluminum and magnesium alloys^{29, 30)}.

In view of the discussion above, the new composition of three β -Ti alloys were proposed to develop β -Ti alloys for as-cast application. In the present study, according to the d-electrons concept, the new three alloys were chosen by using mainly ubiquitous elements in the predicted regions showing the slip, twin and martensite dominant deformation behaviors in wide range β -Ti alloys area in the $B_{or}M_{di}$ diagram, respectively. The segregation of solute elements was major problem for as-cast application possibility of proposed alloys. The tensile and microstructural properties had to be also investigated in both as-cast and solution treated conditions. Moreover, the variant properties of three β -Ti alloys between as-cast and solution treated conditions as well as their as-cast application possibility were discussed in the present study.

2.2 Alloy design for the β alloys located on different regions in the Bo_t - Md_t diagram.

The Bo_t and Md_t values of three alloys were calculated by utilization of the discrete-variational $X\alpha$ (DV- $X\alpha$) cluster calculation method^{31,32}. The parameter values of each element were calculated on the MTi_{14} cluster model in the case of bcc Ti²³), as shown in Fig. 2-2. The models of (a) Bo and (b) Md level were shown in Fig. 2-3. The respective Bo and Md values of each for alloying elements in bcc Ti are listed in Table 2-1.

The mean values of Bo_t and Md_t were calculated from the following equations. (2-1) and (2-2).

$$Bo_t = \sum X_i (Bo)_i \quad (2-1)$$

$$Md_t = \sum X_i (Md)_i \quad (2-2)$$

Where X_i is the molar fraction of component i in the alloy, $(Md)_i$ and $(Bo)_i$ were the numerical values of Bo_t and Md_t for each component i , respectively³³). The compositions of three β -Ti alloys in both mol.% and mass% as well as their respective Bo_t and Md_t values are showed in Table 2-2 in detail.

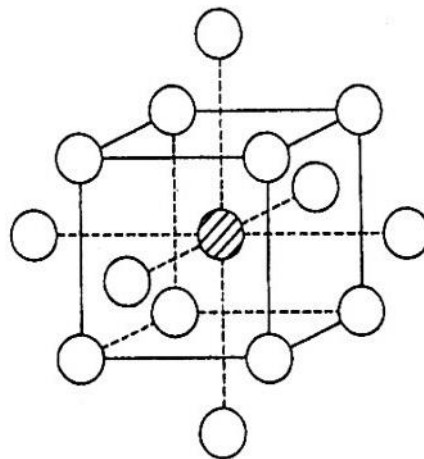


Fig. 2-2 MTi_{14} cluster model in the case of bcc Ti.

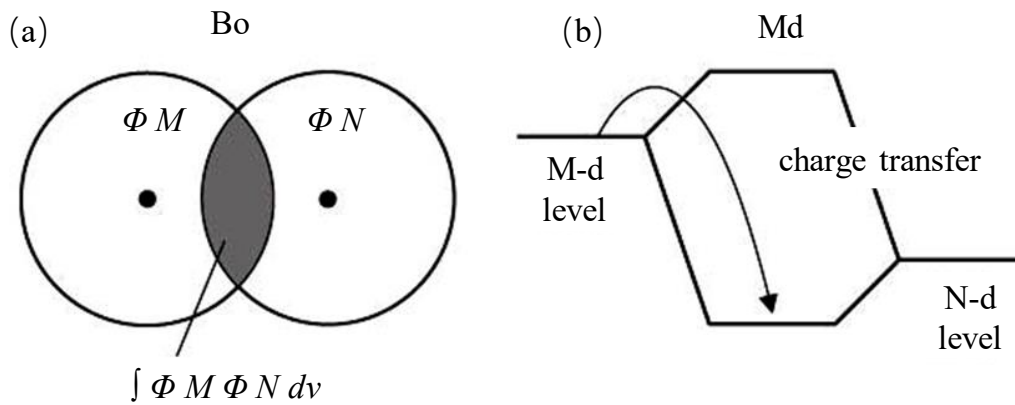


Fig. 2-3 Models of (a) Bo and (b) Md level.

Table 2-1 List of Bo and Md values for alloying elements in bcc Ti.

3d transition metals	Bo	Md	4d transition metals	Bo	Md	5d transition metals	Bo	Md
Ti	2.790	2.447	Zr	3.086	2.934	Hf	3.110	2.975
V	2.805	1.872	Nb	3.099	2.424	Ta	3.114	2.531
Cr	2.779	1.478	Mo	3.063	1.961	W	3.125	2.072
Mn	2.723	1.194	Non-transition metals	Bo	Md			
Fe	2.651	0.969						
Co	2.529	0.807	Al	2.426	2.200			
Ni	2.412	0.724	Si	2.561	2.200			
Cu	2.114	0.567	Sn	2.283	2.100			

Table 2-2 The compositions of proposed three β -Ti alloys in both mol.% and mass% and their Bo_t and Md_t values.

Predicted DT	Compositions		Bo_t	Md_t
	mol.%	mass%		
Slip	Ti-5.3Cr-4.9Mn-2.8Zr-2.5Fe	Ti-5.5Cr-5.4Mn-5.1Zr-2.8Fe	2.791	2.311
Twin	Ti-4.1Cr-2.2Mn-2.0Al	Ti-4.5Cr-2.5Mn-1.1Al	2.781	2.375
Martensite	Ti-5.7Mo-1.0Sn-1.9Al	Ti-10.8Mo-2.3Sn-1.0Al	2.794	2.411

The compositional locations of three β -Ti alloys were indicated in Fig. 2-4. The boundaries of α , $\alpha+\beta$ and β phases as well as different deformation types (DTs) were also showed in Fig. 2-4, they were identified by observing the phase types and deformation behaviors in the dozens of commercial and reported alloys^{11, 12, 34, 35}. The vectors pointing from pure Ti represent the location of Ti-2mass%M (M is alloying element selected in this study). This different DT in β -Ti alloys were determined by examining deformation bands which appeared around their Vickers indentations¹¹.

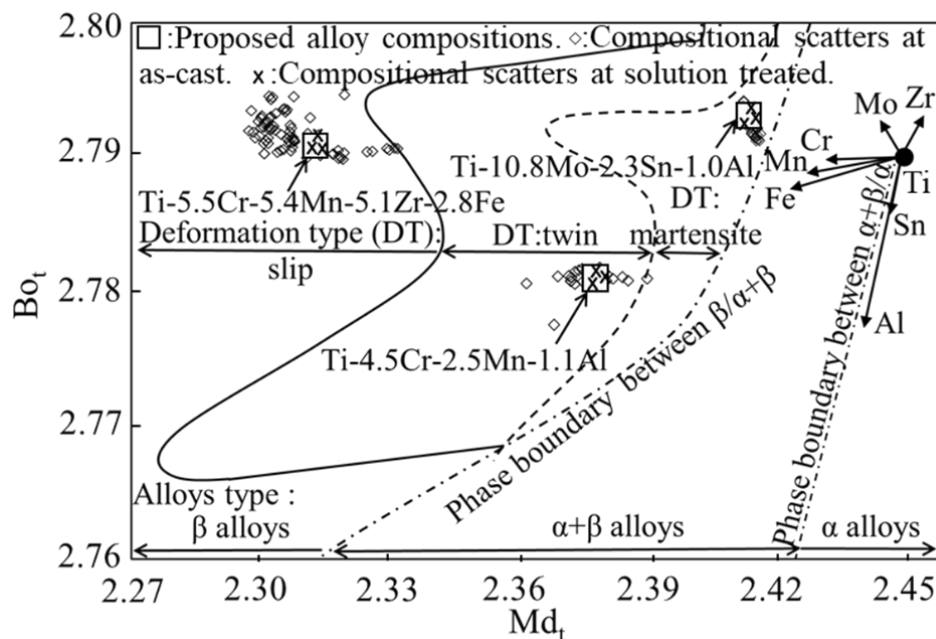


Fig. 2-4 The positions of three experimental alloys and their compositional scatters in as-cast and solution treated conditions in the Bo_t - Md_t diagram showing phase and deformation type boundaries. The vectors pointing from pure Ti represent the location of Ti-2mass%M. (M is an additional alloying element selected in this study)

The new Ti-5.5Cr-5.4Mn-5.1Zr-2.8Fe in mass% with the lowest Md_t or high alloy, Ti-4.5Cr-2.5Mn-1.1Al with the lowest Bo_t and Ti-10.8Mo-2.3Sn-1.0Al with the highest Md_t or low alloy, were chosen by using mainly ubiquitous elements in the predicted regions showing the slip, twin and martensite DTs in wide range β -Ti alloys area in the Bo_t - Md_t diagram, respectively. The Bo_t and Md_t values of Ti-5.5Cr-5.4Mn-5.1Zr-2.8Fe alloy were 2.791 and 2.311, which were approximately same as the Bo_t value of 2.790

of pure titanium and the Md_t value of 2.321 of Ti-15V-3Cr-3Sn-3Al commercial alloy³⁵), respectively. The Bo_t and Md_t values of Ti-4.5Cr-2.5Mn-1.1Al alloy were 2.781 and 2.375, respectively. They were determined approximately same as 2.784 and 2.375 of Ti-8Cr-6Sn-5Zr commercial alloy³⁶). The Bo_t value of 2.794 of Ti-10.8Mo-2.3Sn-1.0Al alloy was also approximately same with that of pure Ti. Moreover, the Md_t value of 2.411 of Ti-10.8Mo-2.3Sn-1.0Al alloy was the median value between Ti-4.5Cr-2.5Mn-1.1Al alloy of 2.375 and pure Ti of 2.447. The consideration of solute-segregation in solidification was essential which might cause a position shift for alloys in the Bo_t - Md_t diagram, especially for the multi-element alloys.

2.3 Experimental procedures

2.3.1 Materials and manufacturing process

For the present study, the purity of raw materials for preparing three β -Ti alloys were Ti, Cr, Mn, Fe, Al, Zr, Mo and Sn with 99.8, 99.9, 99.9, 99.9, 99.9, 98.0, 99.0 and 98.5 mass%, respectively. The chemical compositions of alloys were given in mass% units. All ingots were prepared through CCLM (Fuji-CCLM_{Fe} 1Kg / 100 + 60 kW, Japan) with a water-cooled copper crucible. The schematic diagram of equipment, vacuum chamber and crucible aspect pictures of CCLM were showed in the Figs. 2-5, 2-6 and 2-7, respectively. The enough mixing of raw materials during the melting process was done by two approaches. The first one was the procedures of filling raw materials, the shapes of raw materials for preparing titanium alloys were small sheet, granular or sponge with the sizes of 0.5 to 3 cm. In this case, the raw materials were uniformly filled in the crucible layer by layer. For example, the bottom layer were titanium sheets and the second layer of Zr sheets were uniformly placed on the titanium sheets. Then, the third layer of titanium sheets were putted on Zr sheets. According to the composition of alloys, next layer could be the granular aluminum and covered the titanium sheets again. By this method and the considering of melting points and the densities of additional alloying elements, the enough mixing of raw materials could be easily done. The second approach is the using of cold crucible levitation melting equipment and determination of heat up and hold time to make alloys ingots. The heating and holding time of the alloy ingots were determined by the results of repeated experiments. The cold crucible levitation melting equipment consists of two electric coils, the upper electric coil is used for heating and the lower electric coil is utilized for levitation the molten metals. The molten material can be levitated by the eddy current in the melting crucible and the uniform composition of Ti alloys can be obtained by the diffusion mixing effect and strong stirring from the electromagnetic force. When high-frequency current is passed through the coil, eddy current is induced in the crucible and the molten metal. Due to the electromagnetic repulsion between these currents, the molten metal floats from the crucible and melts by induction heating. This levitation force can be

calculated as follows, assuming that the alternating magnetic field is along the metal surface. Firstly, the input power W is determined by the equation (2-3):⁹⁾

$$W = \frac{1}{2} \cdot H_m^2 \cdot \sqrt{\frac{\omega \mu \rho}{2}} \quad (2-3)$$

Where ω : angular frequency ($= 2\pi f$: f is frequency (Hz)), μ : magnetic reluctance (H / m), ρ : metal resistivity ($\Omega \cdot m$), H_m : metal surface. The magnetic field strength (A / m) along. Next, the levitation force F acting on the metal as shown in (2-4):

$$F = \frac{\mu}{2} \cdot H_m^2 \quad (2-4)$$

From the above two formulas, the following formula is derived for convenience by the equation (2-5):

$$F = \sqrt{\frac{\mu}{\pi f \rho}} \cdot W \quad (2-5)$$

The contents of gaseous impurities of oxygen and nitrogen were lower than those (oxygen and nitrogen: 0.069 and 0.006 %, respectively) in the raw materials, because of highly vacuum level of 3×10^{-3} Pa were obtained by using rotary pump (RP) and diffusion pump (DP) as shown in Table 2-3. In addition, the images of ingot produced by CCLM with bottom, side and top views were shown in Fig. 2-8 (a), (b) and (c), respectively. The maximum temperature and holding temperature of CCLM are depending on the melting point of alloying elements. To completely melt the raw materials and well mix of molten metals, the alloys were held for 300 s in maximum temperature of 2300 K in melting process^{4, 32)}. The detailed profiles of temperature in molten metal, electric power in upper and lower coils and pressure in atmosphere of levitation melting and cooling process were given in Fig. 2-9. The atmosphere of CCLM was argon gas with purity of 99.99% after the pressure less than 3×10^{-3} Pa. Molten metals were solidified in the copper melting crucible after switching off electric power after the melting process. The as-cast specimens were cut directly from the ingot. Whereas, the solution treated specimens were encapsulated in a quartz tube filled with an inert argon atmosphere and held in 1173 K for 3.6 ks. Thereafter, solution treated specimens were water-quenched by breaking the quartz tube and dropped the specimens into cold water.

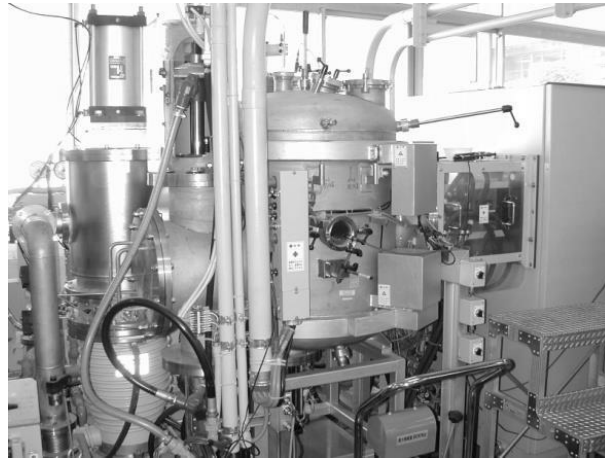


Fig. 2-5 Schematic diagram of vacuum chamber of CCLM.

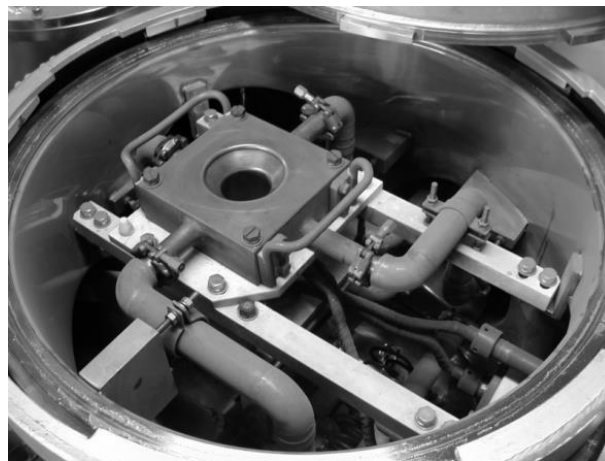


Fig. 2-6 Schematic diagram of crucible of CCLM.

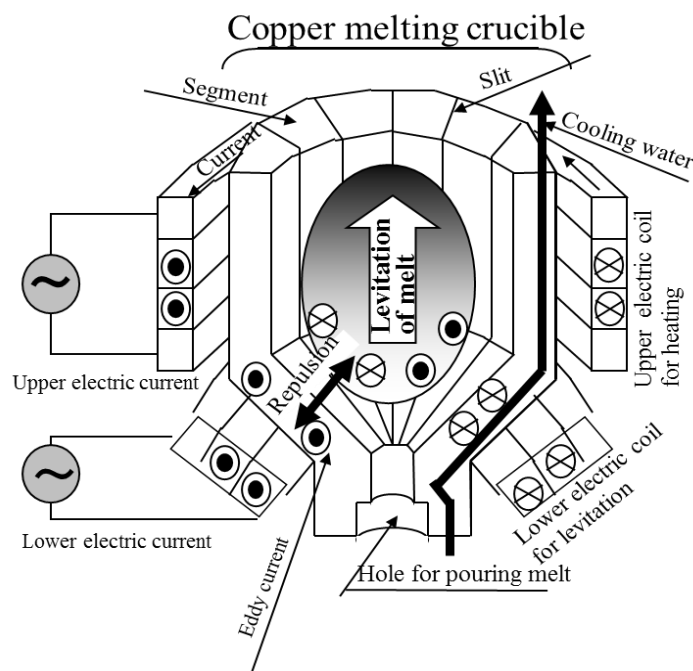


Fig. 2-7 Schematic illustrations of principle of CCLM.

Table 2-3 Chemical composition fractions of impurities in ingot produced by CCLM.

Impurities	O	N	C	H
Fractions in ingot, (mass%)	0.046	0.009	0.004	0.0007



Fig. 2-8 The images of ingot produced by CCLM, (a) bottom, (b) side and (c) top views.

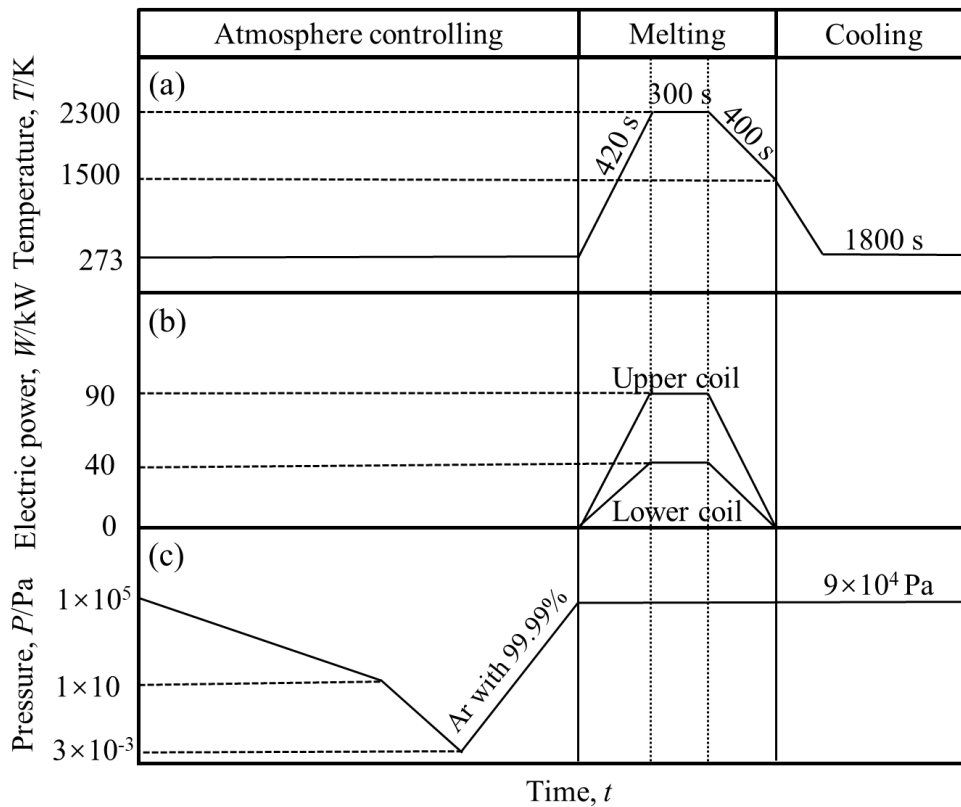


Fig. 2-9 Profiles of (a) temperature in molten metal, (b) electric power in upper and lower coils and (c) pressure in atmosphere of levitation melting and cooling process. Abscissa and ordinate are represented with arbitrary scales.

2.3.2 Microstructural characterization and point analysis

The specimens were mechanically polished by using different grades of polishing paper and etched by using a mixed solution of distilled water, nitric acid and hydrofluoric acid (95:3:2 in volume ratio) and microstructural observation of specimens in as-cast and solution treated conditions were carried out by using an optical microscope (OM). The constituent phases of alloys were determined by X-ray diffraction (XRD) with Cu K α radiation generated in 40 kV and 30 mA in the room temperature. The chemical compositions of three experimental alloys were measured by point analysis via the EPMA (JEOL JXA-8200, Japan). In order to determine segregation conditions, the compositional scatters through three alloy specimens in as-cast and solution treated conditions were detected with the electron beam of 5 μm in diameter by measuring of about 60 to 80 points. The points analysis thoroughly crossed two grains were measured with the interval of 15 μm between each two points. Moreover, the microstructures of plastic deformed Ti-4.5Cr-2.5Mn-1.1Al alloy in solution treated condition were observed by transmission electron microscopy (TEM). The specimens for TEM were prepared via electrolytic polishing in the solution containing 10% perchloric acid and 90% methanol in 18 V and 288 K (JEM-2000EX II, Japan).

2.3.3 Tensile test

The tensile specimens with a gauge size of 6 mm in diameter and 20 mm in length, and grips being 10 mm in diameter on both ends were applied in this study. The conditions for tensile test were with an initial strain rate of $1.9 \times 10^{-4} \text{ s}^{-1}$ in the room temperature. And an extensometer was used for all the tensile testing. The displacement and the constant strain rate were measured by Shimadzu SG 10-50 extensometer during the tensile process, and the stress-strain curve was got by using a mechanical testing machine (Autograph DCS-R-5000, Shimadzu Corporation, Japan). The Vickers hardness measurements were also tested with load of 300 N or 5 N for 10 s (FV-110, Japan). Cutting procedures of ingot prepared by CCLM were shown in Fig. 2-10 and the draft of tensile specimen were shown in Fig. 2-11, respectively.

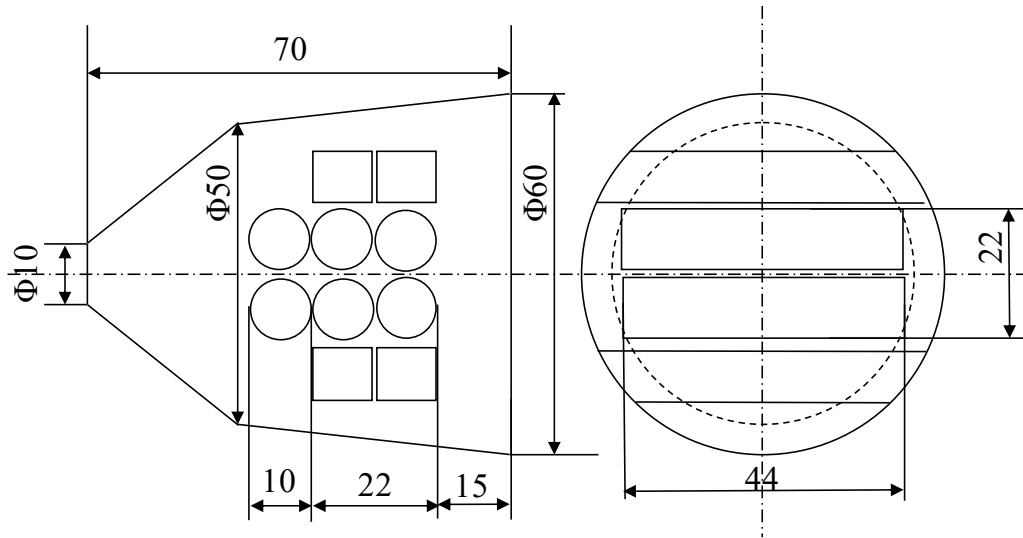


Fig. 2-10 Cutting procedures of melted ingot prepared by CCLM.

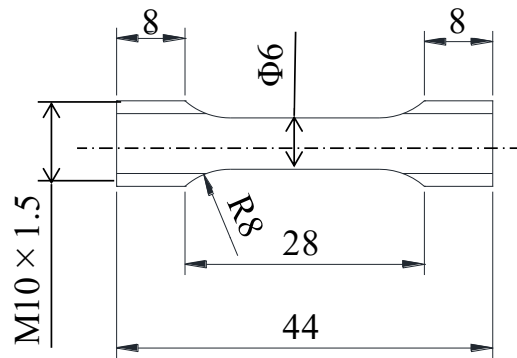


Fig. 2-11 Draft of specimen adopted for tensile test.

2.4 Results and discussion

2.4.1 Microstructures and solute segregation in solidification

OM images of three β -Ti alloys were presented in Fig. 2-12, and their constructed phases were identified using XRD profiles as shown in Fig. 2-13. For Ti-5.5Cr-5.4Mn-5.1Zr-2.8Fe alloy as shown in Fig. 2-12 (a) and (d), there was no significant difference in the microstructures, regardless of heat treatments. The average equiaxed mono β grain sizes of Ti-5.5Cr-5.4Mn-5.1Zr-2.8Fe alloy in as-cast and solution treated conditions were 350 and 390 μm , respectively. The mixed structure consisting of the β and orthorhombic α'' martensite phases precipitated in or near the grain boundaries were observed in the as-cast Ti-4.5Cr-2.5Mn-1.1Al alloy as shown in Fig. 2-12 (b). The content of α'' martensite phase was decreased by solution treatment, as seen in Fig. 2-12 (e). Their average grain sizes were 400 and 450 μm , in as cast and after solution treatment, respectively. In contrast, for Ti-10.8Mo-2.3Sn-1.0Al alloy, the α'' martensite phase observed in both as-cast and solution treated conditions were shown in Fig. 2-12 (c) and (f), which was consistent with its location showing martensite dominant deformation in the B_{0i} - Md_i diagram. Their average grain sizes were 420 and 460 μm , in as-cast and solution treated conditions, respectively. Ti-5.5Cr-5.4Mn-5.1Zr-2.8Fe and Ti-10.8Mo-2.3Sn-1.0Al had the Md_i values far and near that of pure Ti in the B_{0i} - Md_i diagram or showed the highest and lowest β phase stabilized alloys, respectively.

It was known that all three alloys showed slightly larger grain size in solution treated condition compared with their grain size in as-cast condition. The segment (1) and (2) or segment (2) and (3) in the images in both as-cast and solution treated conditions in Fig. 2-12, corresponded to the two adjacent grains, indicating the paths and directions of point analyses were from (1) to (3).

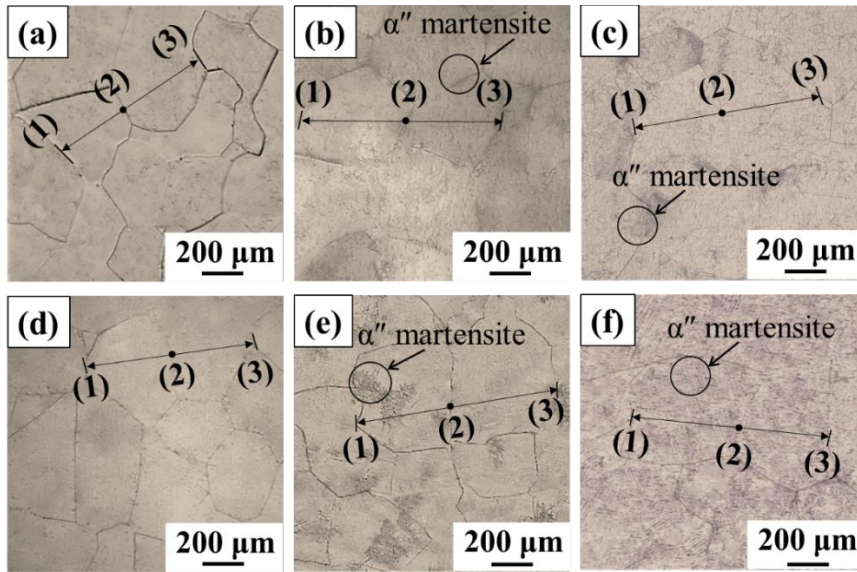


Fig. 2-12 OM images of (a) and (d) Ti-5.5Cr-5.4Mn-5.1Zr-2.8Fe, (b) and (e) Ti-4.5Cr-2.5Mn-1.1Al, (c) and (f) Ti-10.8Mo-2.3Sn-1.0Al alloys. (a), (b), (c) and (d), (e), (f) were obtained from as-cast and solution treated conditions, respectively. (1), (2) and (3) showing the paths and directions of point analysis measurement, corresponding to the ones in Fig. 2-14.

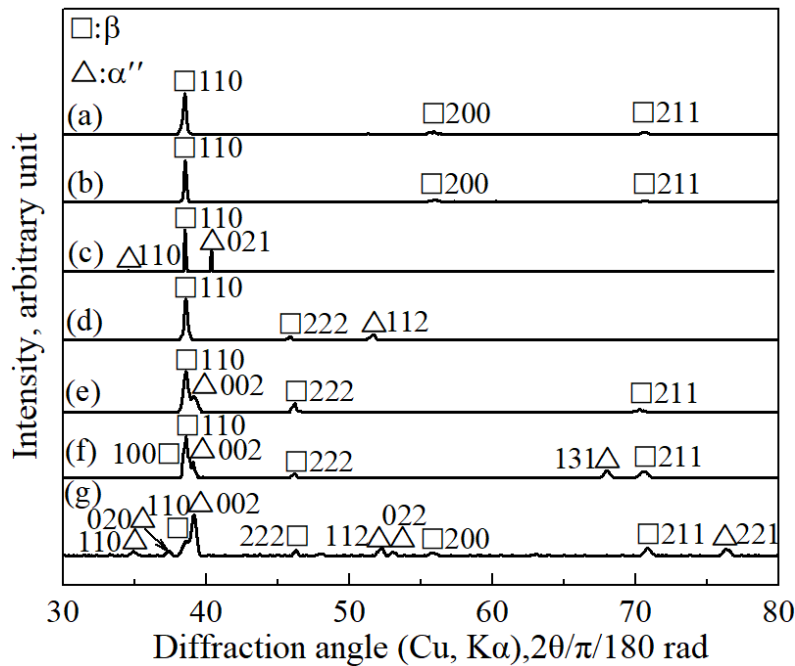


Fig. 2-13 X-ray diffraction profiles of (a) and (b) Ti-5.5Cr-5.4Mn-5.1Zr-2.8Fe, (c) and (d) Ti-4.5Cr-2.5Mn-1.1Al, (e) and (f) Ti-10.8Mo-2.3Sn-1.0Al alloys. (a), (c), (e) and (b), (d), (f) were obtained from as-cast and solution treated conditions, and (g) after tensile test for solution treated Ti-4.5Cr-2.5Mn-1.1Al alloy.

The elemental point analyses were performed on these segments for the determination of concentration heterogeneity or solidification path. The distribution profiles of alloying elements in Ti-5.5Cr-5.4Mn-5.1Zr-2.8Fe alloy in both as-cast and solution treated conditions were shown in Fig. 2-14 (a) and (b), respectively. The higher and lower contents of solute alloying elements and Ti were observed with the position closer to grain boundary. For Ti-4.5Cr-2.5Mn-1.1Al and Ti-10.8Mo-2.3Sn-1.0Al alloys in as-cast condition as shown in Fig. 2-14 (c) and (e), their solute-segregation conditions showed the same tendency with the as-cast Ti-5.5Cr-5.4Mn-5.1Zr-2.8Fe alloy, and their solution treated specimens showed the homogeneous concentrations.

The degree of segregation of solute elements in a grain caused by dendritic growth correlated to their kinds and amount. In contrast, serious segregation in three β -Ti alloys could to be caused by solidification conditions³⁷⁻³⁹). It is considered in this CCLM process, that the solutes enrichment strongly depending on their diffusion coefficient in liquid was caused keeping the local equilibrium in liquid ahead of solid and liquid interface under different concentrations between solid and infinity in liquid representing by the effective equilibrium coefficient and a certain thickness of boundary layer depending on the solidification rate and stir of liquid in this solidification process. The concentration profiles of Ti-5.5Cr-5.4Mn-5.1Zr-2.8Fe alloy as shown in Fig. 2-14 (a) corresponded to the initial, steady and final stages⁴⁰) in solidification according to the solute enrichment model mentioned above, which resulted in heavy micro-segregation. The solidification proceeded from Ti enriched dendritic arms to Mn, Zr and Fe enriched parts corresponding to center to grain boundaries in grains, respectively, as shown in Fig 2-14. In contrast, the micro Vickers hardness values were reflected the concentration profiles, as shown in Fig. 2-14 (a), which meant the heavy segregation even in a grain of as-cast Ti-5.5Cr-5.4Mn-5.1Zr-2.8Fe alloy.

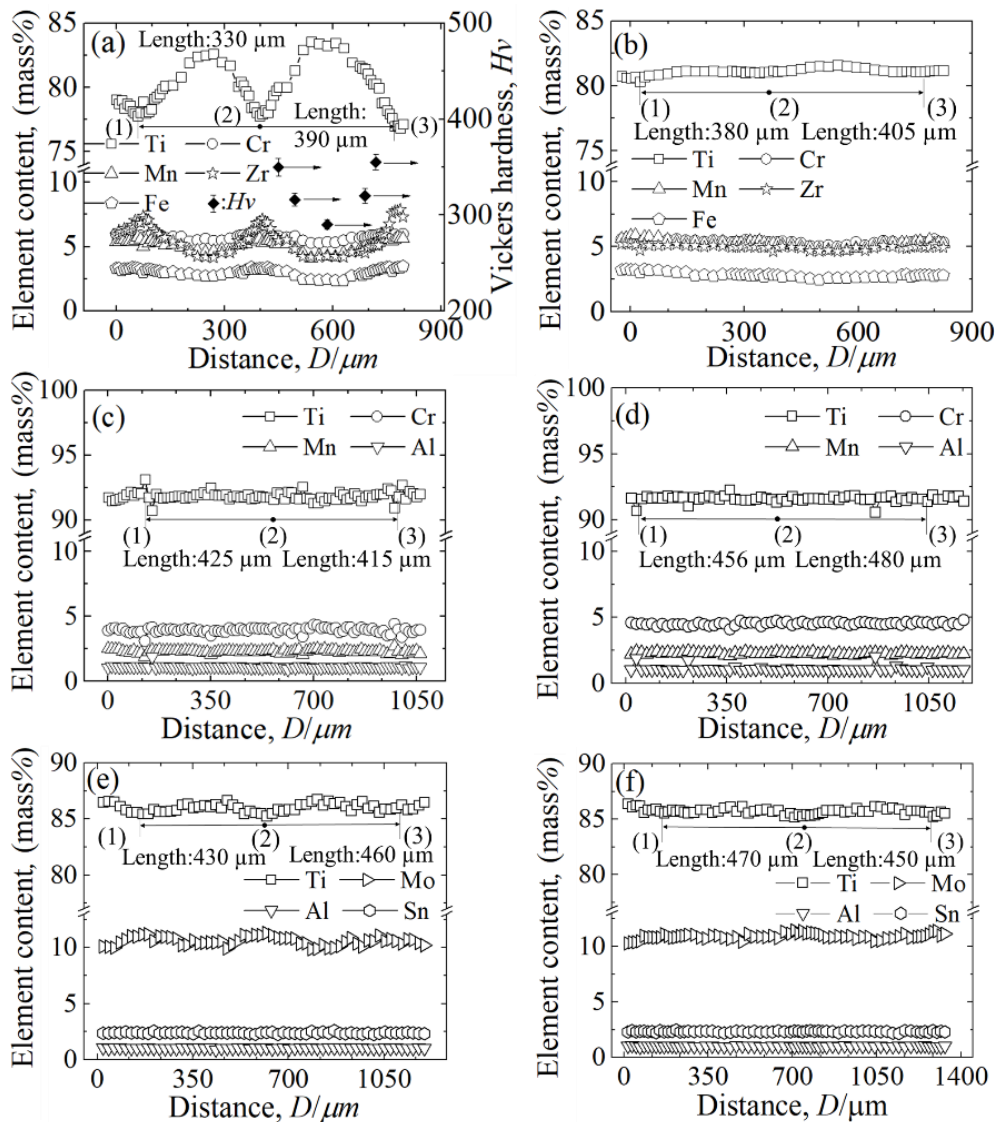


Fig. 2-14 The concentration profiles of alloying elements of (a) and (b) Ti-5.5Cr-5.4Mn-5.1Zr-2.8Fe, (c) and (d) Ti-4.5Cr-2.5Mn-1.1Al, (e) and (f) Ti-10.8Mo-2.3Sn-1.0Al alloys. (a), (c), (e) and (b), (d), (f) were obtained from as-cast and solution treated conditions, respectively. And the concentration profiles (a) corresponded to the Vickers hardness values in five positions. (1) to (3) corresponded to the ones in Fig. 2-12.

For all solution treated specimens, the diffusion of alloying elements occurred due to the presence of elemental concentration gradients. There were constant values in all concentrations by solution heat treatment, and they were close with their chemical compositions, as shown in Figs. 2-4 and 2-14. For convenience, the segregation degree in a grain, K was denoted using the Ti content. In addition, $BO_t max$, $BO_t min$, ΔBO_t and

$Md_{t\ max}$, $Md_{t\ min}$, ΔMd_t values of three β -Ti alloys in as-cast condition are also shown in Table 2-4. The segregation degree K was approximated by eq. (2-6) using $C_{Ti\ max}$, $C_{Ti\ min}$ and $C_{Ti\ total}$ showing concentrations of minimum, maximum and total Ti amounts, respectively.

$$K = (C_{Ti\ max} - C_{Ti\ min}) / C_{Ti\ total} \times 100 \% \quad (2-6)$$

The K values, $Bo_{t\ max}$, $Bo_{t\ min}$, ΔBo_t and $Md_{t\ max}$, $Md_{t\ min}$, ΔMd_t values of Ti-5.5Cr-5.4Mn-5.1Zr-2.8Fe alloy with the heaviest segregation in as-cast condition were 8.3%, 2.795, 2.790, 0.005 and 2.330, 2.298, 0.032, respectively. The higher ΔBo_t and ΔMd_t may correlated to segregation degree, which results in the heaviest segregation degree of 4.8 times, compared with Ti-10.8Mo-2.3Sn-1.0Al with the lowest segregation.

Table 2-4 The segregation coefficient, K , $Bo_{t\ max}$, $Bo_{t\ min}$, ΔBo_t and $Md_{t\ max}$, $Md_{t\ min}$, ΔMd_t values of three β -Ti alloys in as-cast condition.

Alloys	K	$Bo_{t\ max}$	$Bo_{t\ min}$	ΔBo_t	$Md_{t\ max}$	$Md_{t\ min}$	ΔMd_t
Ti-5.5Cr-5.4Mn-5.1Zr-2.8Fe	8.3	2.795	2.790	0.005	2.330	2.298	0.032
Ti-4.5Cr-2.5Mn-1.1Al	2.6	2.781	2.777	0.004	2.387	2.359	0.028
Ti-10.8Mo-2.3Sn-1.0Al	1.7	2.794	2.791	0.003	2.413	2.409	0.004

The relation between the segregation of alloying elements and positions of composition scatters in the Bo_t - Md_t diagram of as-cast Ti-5.5Cr-5.4Mn-5.1Zr-2.8Fe alloy with the heavy segregation was also discussed in Fig. 2-15. According to the vectors of Ti-2mass%M as shown in Fig. 2-4, it was known that the horizontal distribution of composition scatters in one grain was influenced by the changing in contents of Cr, Mn and Fe as shown in Fig. 2-15 (a) and (c), corresponding to the diversification of Md_t values. In contrast, the vertical distribution of composition scatters was mainly influenced by the changing in the content of Zr as shown in Fig. 2-15 (b), corresponding to the diversification of Bo_t values. Bo_t parameter describes the covalent bond strength between atoms and correlates with several physical parameters of alloys such as the activation energy of diffusion in β -Ti alloys and melting points

correlating to cohesion energy¹¹⁾. Therefore, the higher concentration deviation was shown by the addition of Zr with higher Bo_i , which meant the slowly diffusion of Zr in liquid and solid parts in solidification process. Moreover, it is found from the contents of impurities that the cleanly molten metals were created by utilization of CCLM without the reaction between the molten metal and water-cooled copper crucible, although the affinity of Ti with oxygen, carbon and nitrogen was strong.

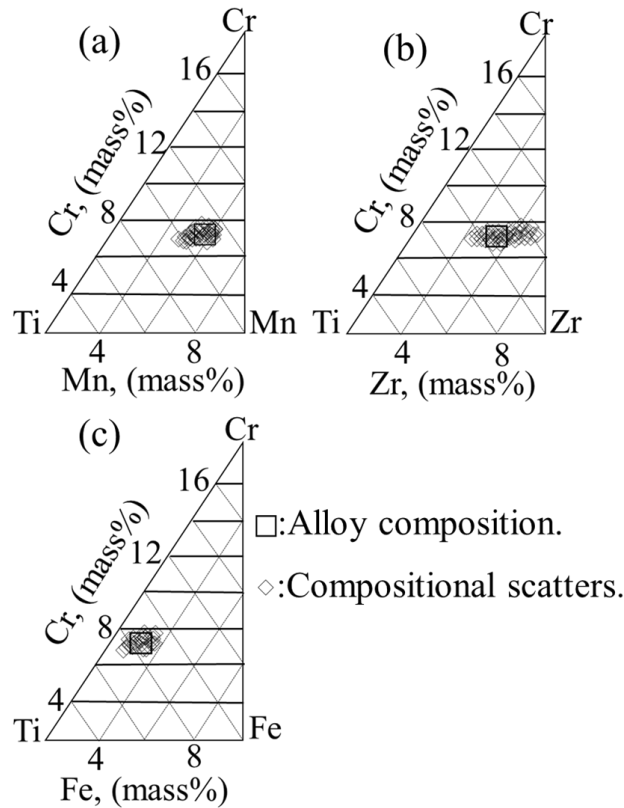


Fig. 2-15 Solidification paths of (a) Ti, Cr and Mn, (b) Ti, Cr and Zr and (c) Ti, Cr and Fe for Ti-5.5Cr-5.4Mn-5.1Zr-2.8Fe alloy in as-cast condition.

2.4.2 Tensile properties and fracture surface

The stress-strain curves of three β -Ti alloys in as-cast and solution treated conditions were shown in Fig. 2-16. Ti-5.5Cr-5.4Mn-5.1Zr-2.8Fe alloy showing highest β phase stability with the lowest Mdt among three β -Ti alloys, had the slip behavior in the stress-strain curves showing a classical elasto-plastic behavior, and led to the high yield strength and negligible elongation. It had been reported that the tensile properties of β -Ti alloys depend significantly on the DT, such as slip and twin. Moreover, the content

of the β phase stabilizing could greatly affect the formation of twin and slip⁴¹). There were high $\sigma_{0.2}$ more than 950 MPa, high σ_{UTS} more than 1000 MPa and ε_f more than 8 %, regardless with heat treatment conditions.

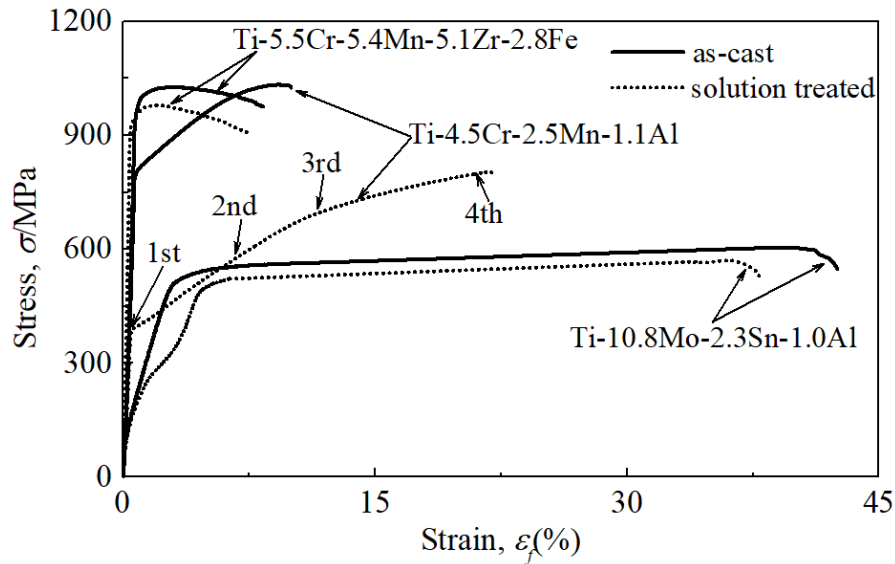


Fig. 2-16 Stress-strain curves of as-cast and solution treated three β -Ti alloys.

The fracture morphologies showing inter- and trans-granular or dimple fracture patterns, as shown in Fig. 2-17, that the same deformation behaviors were caused in both specimens, although there was their different segregation degree of solute elements, as seen in Fig. 2-14 (a) and (b). A TEM image of the solution treated Ti-5.5Cr-5.4Mn-5.1Zr-2.8Fe specimen after fracture was shown in Fig. 2-18 (a). Mono β phase was just observed even after tensile fracture. The dislocations corresponding to high flow stress levels, were already moved throughout β phase, which agreed with the predominant slip DT.

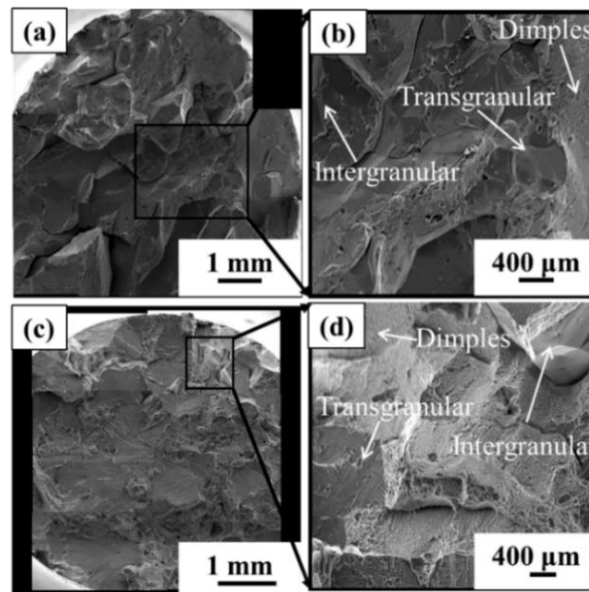


Fig. 2-17 Low and high magnified fractographies of tensile specimens for (a), (b) as-cast and (c), (d) solution treated Ti-5.5Cr-5.4Mn-5.1Zr-2.8Fe specimens, respectively.

The as-cast and solution treated Ti-4.5Cr-2.5Mn-1.1Al alloys showed the σ_{UTS} value of 1033 and 804 MPa and $\sigma_{0.2}$ value of 803 and 394 MPa with ϵ_f value of 9 and 22 %, respectively. There were large different flow stress levels between both specimens. The solution treated Ti-4.5Cr-2.5Mn-1.1Al showed typical four stages in the stress-strain curve. The first stage was the initial elastic region, the second stage was the transformation from a part of β phase to α'' phase caused by the stress-induced transformation. The third stage corresponded to the elastic deformation of both β and α'' phases. The last stage was the plastic deformation of β phase and α'' phase. This stress-strain curve classified into four stages has been observed in Zr and Nb addition alloys^{15,42}). The TEM images of the solution treated Ti-4.5Cr-2.5Mn-1.1Al specimen with two levels of 1 and 5% in plastic strain by cold rolling were shown in Fig. 2-18 (b) and (c). There was just β phase in the 1% strained specimen. In contrast, some twin bands were observed obviously in 5% strained specimen. A selected-area electron diffraction pattern was taken from $[\bar{1}11]$ β zone axis and the reflections indicated the new part corresponding to the formation of twin bands were still β phase, as seen in Fig. 2-18 (d), which agreed with previous literatures⁴³⁻⁴⁵). The tensile fractured samples showed some stress induced α'' martensite phase in the twin band, as shown in Fig. 2-

18 (e), which agreed with to the predominant twin DT. Moreover, this agreed with the result of XRD showing additional new peaks of α'' martensite phase, due to the formation of stress-induced α'' martensite phase, as seen in Fig. 2-13 (d) and (g). The as-cast Ti-10.8Mo-2.3Sn-1.0Al specimen indicated the σ_{UTS} value of 600 MPa and $\sigma_{0.2}$ value of 520 MPa but large uniform ϵ_f of approximately 40 %. In contrast, solution treated specimen indicated similar stress-strain behaviors to the as-cast one, showing the characteristic α'' martensite deformation^{46,47}. This agreed with to the predominant martensite DT, regardless of initial elastic parts. Experimental β -Ti alloys in as-cast and solution treated conditions showed the similar tensile behaviors. Ti-5.5Cr-5.4Mn-5.1Zr-2.8Fe alloy with the slip DT showed the close stress-strain behaviors, regardless of the different segregation degrees of solute elements. In contrast, alloys with the twin and martensite DTs showed different behaviors in initial elastic region, because of the different precipitated α'' martensite amount. Then, the predicted classification in β -Ti alloys by DT in the Bo_i - Md_i diagram, could be accuracy in three proposed β -Ti alloy systems.

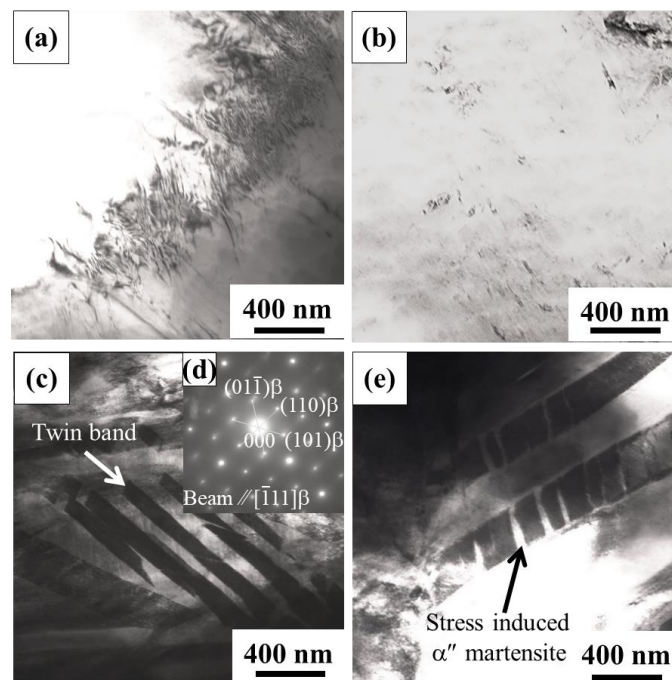


Fig. 2-18 TEM images of (a) solution treated Ti-5.5Cr-5.4Mn-5.1Zr-2.8Fe alloy in tensile fractured specimen, and solution treated Ti-4.5Cr-2.5Mn-1.1Al alloy in (b), (c) 1 and 5% plastic strained specimens, (d) SAED pattern along with $[111]$ of (c) and (e) tensile fractured specimen.

2.4.3 Vickers hardness

The Vickers hardness of three β -Ti alloys in as-cast and solution treated conditions were shown in Fig. 2-19. The Vickers hardness values were 320 and 240 in as-cast Ti-5.5Cr-5.4Mn-5.1Zr-2.8Fe and Ti-10.8Mo-2.3Sn-1.0Al samples, respectively. Their solution treated specimens showed 3 - 5 % lower H_v values, compared with as-cast ones. In contrast, solution treated Ti-4.5Cr-2.5Mn-1.1Al specimens showed 17% lower H_v value compared with as-cast one (330). They were similar to tensile behaviors, as shown in Fig. 2-16. All the three alloys showed higher hardness values in as-cast condition compared with their values in solution treated condition, which were attributed to the presence of segregation of solute elements. Moreover, it was clear that the linearity of four indentation edges was more accuracy of three solution treated specimens, compared with that of as-cast specimens, as shown in Fig. 2-20. The irregular indentation edges with expansion and poor symmetry of indentation might be caused by different forces from each direction due to different hardness. The difference in forces from each direction was attributed to the different solid solution strengthening due to the segregation behavior. This agreed with the correlation between segregation degree and corresponding hardness value for Ti-5.5Cr-5.4Mn-5.1Zr-2.8Fe with the highest segregation degree, as seen in Fig. 2-14 (a), although there was its highest hardness value as mean one, as shown in Fig. 2-19.

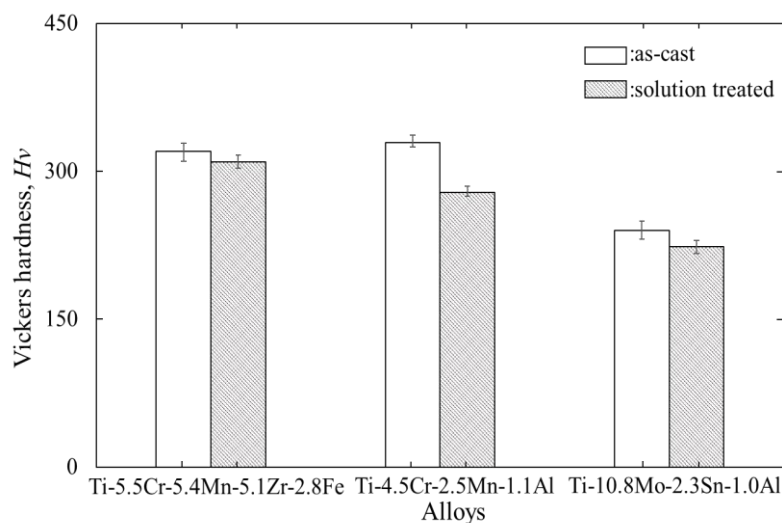


Fig. 2-19 Vickers hardness of Ti-5.5Cr-5.4Mn-5.1Zr-2.8Fe, Ti-4.5Cr-2.5Mn-1.1Al and Ti-10.8Mo-2.3Sn-1.0Al alloys for as-cast and solution treated specimens.

The β -Ti alloys were deformed by either slip or twin mechanism, depending on the stability of the β phase¹¹). The wavy slip bands appear when the slip mechanism was dominant, whereas straight twin bands appear when the twin mechanism was operating. The deformation bands around Vickers indentation of three β -Ti alloys were also shown in Fig. 2-20. In Fig. 2-20 (a) and (d), the observation results indicating the Vickers indentation of Ti-5.5Cr-5.4Mn-5.1Zr-2.8Fe alloy was wavy shape in both conditions, respectively. Moreover, the Vickers indentation around Ti-4.5Cr-2.5Mn-1.1Al alloy, as shown in Fig. 2-20 (b) and (e), in both conditions exhibited straight twin bands which meant the twin mechanism was dominant. The Ti-10.8Mo-2.3Sn- 1.0Al specimens with main twin bands were observed in Fig. 2-20 (c) and (f). The Vickers indentation scale of Ti-10.8Mo-2.3Sn-1.0Al alloy was largest among three β -Ti alloys, which also could be seen as a feature for the martensite alloy. These Vickers indentation results of three β -Ti alloys were highly consistent with their DT in tensile tests.

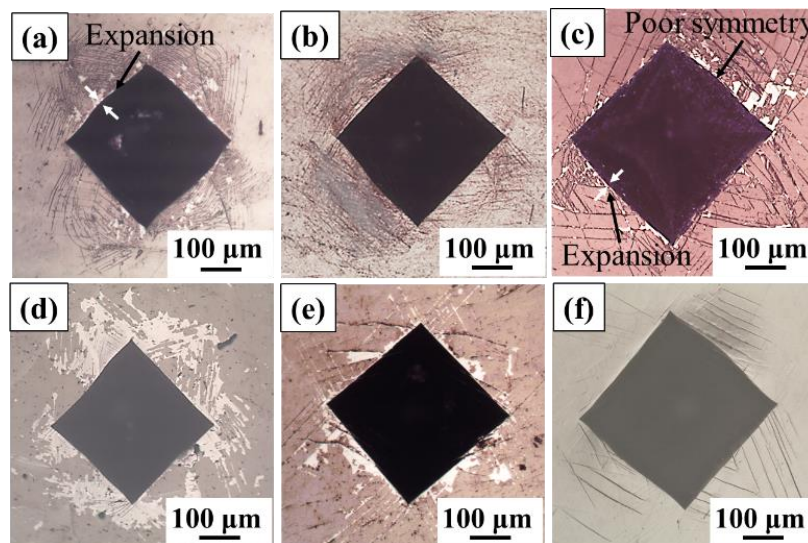


Fig. 2-20 Deformation bands around the Vickers indentations of (a) and (d) Ti-5.5Cr-5.4Mn-5.1Zr-2.8Fe, (b) and (e) Ti-4.5Cr-2.5Mn-1.1Al and (c) and (f) Ti-10.8Mo-2.3Sn-1.0Al alloys. (a), (b), (c) and (d), (e), (f) were obtained from as-cast and solution treated specimens, respectively.

2.4.4 As-cast application possibility of experimental alloys in the view of tension behaviors

The unit of fracture in tension as macro characterization was predominantly one grain even in the as-cast Ti-5.5Cr-5.4Mn-5.1Zr-2.8Fe having the highest segregation degree of solute elements as micro one. There was subsequent agreement in the stress-strain curves between its as-cast and solution treated samples. Other specimens showed a little difference in initial elastic regions of the curves, because of the different in the α'' martensite amount. For instance, the mean hardness values were obtained in three alloys by the mixture rule which consisted of the corresponding hardness in some area showing different concentration profiles. The tensile and hardness properties as macro properties were defined by mean strength, elongation and hardness values of experimental alloys, although there was the lower linearity of indentation edges and poor symmetry of indentation. It was found that as-cast application possibility of Ti-5.5Cr-5.4Mn-5.1Zr-2.8Fe alloy could not be refused in the view of tension behaviors. Promising alloys could be proposed accurately in short periods using the Bo_i-Md_i diagram which showed high level in the prediction of classification in β -Ti alloys by DTs.

2.5 Summary

(1) Ti-5.5Cr-5.4Mn-5.1Zr-2.8Fe alloy located in the slip DT showed mono β phase and the highest segregation degree of solute elements in experimental alloys. In contrast, Ti-4.5Cr-2.5Mn-1.1Al and Ti-10.8Mo-2.3Sn-1.0Al alloys located in the twin and martensite DTs showed the β phase and precipitated α'' martensite, respectively, regardless of heat treatment conditions.

(2) Ti-5.5Cr-5.4Mn-5.1Zr-2.8Fe alloy showing highest β phase stability with the lowest Md_t among three β -Ti alloys, had the slip behavior in the stress-strain curves showing a classical elasto plastic behavior, and led to the high $\sigma_{0.2}$ more than 950 MPa, high σ_{UTS} more than 1000 MPa and ε_f more than 8 %, regardless of the heat treatments.

(3) The Vickers hardness values were 320 and 240 in as-cast Ti-5.5Cr-5.4Mn-5.1Zr-2.8Fe and Ti-10.8Mo-2.3Sn-1.0Al specimens, respectively. Their solution treated specimens showed 3 - 5 % lower Hv values, compared with as-cast ones. Their hardness properties were similar to tensile behaviors.

(4) It was found that as-cast application possibility of Ti-5.5Cr-5.4Mn-5.1Zr-2.8Fe alloy could not be refused in the view of tension behaviors. Promising alloys for as-cast applications could be proposed accurately in short periods using the Bo_r - Md_t diagram which showed high level in the prediction of classification in alloys by DTs.

References

- 1) O.M. Ivasishin, P.E. Markovsky, Y.V. Matviychuk, S.L. Semiatin, C.H. Ward and S. Fox: *J. Alloy. Compd.* **457** (2008) 296–309.
- 2) J. Ryhanen, E. Niemi, W. Serlo, E. Niemela, P. Sandvik, H. Pernu and T. Salo: John Wiley & Sons, Inc. *J. Biomed. Mater. Res.* **35** (1997) 451–457.
- 3) J. Choi, D. Bogdanski, M. Koller, S.A. Esenwein, D. Muller, G. Muhr and M. Epple: *Biomaterials.* **24** (2003) 3689–3696.
- 4) K. Matsugi, H. Kishimoto, D. Yamakawa, Z.F. Xu and Y.B. Choi: *Mater. Trans.* **56** (2015) 1747–1755.
- 5) M.A.H. Gepreel and M. Niinomi: *J. Mech. Behav. Biomed. Mater.* **20** (2013) 407–415.
- 6) R.R. Boyer and R.D. Briggs: *J. Mater. Eng. Perform.* **14** (2005) 681–685.
- 7) I. Inagaki, T. Takechi, Y. Shirai and N. Ariyasu: Nippon Steel and Sumitomo Metal Technical Report. No. **106** (2014).
- 8) C. Leyens and M. Peters: Wiley-Vch Verlag GmbH and Co. KGaA, (2003) 1–36.
- 9) E.O. Ezugwu and Z.M. Wang: *J. Mater. Proc. Technol.* **68** (1997) 262–274.
- 10) F.H. Froes, H. Friedrich, J. Kiese and D. Bergoint: *JOM*, (2004) February.
- 11) M. Morinaga, N. Yukawa, T. Maya, K. Sone and H. Adachi: *Proc. 6th World Conf. on Ti, TMS*, (1988) 1601–1606.
- 12) M. Morinaga, N. Yukawa and H. Adachi: *Tetsu-to-Hagane*, **72** (1986) 555–562.
- 13) M. Morinaga, J. Saito and M. Morishita: *JJILM*, **42** (1992) 614–621.
- 14) P. Laheurte, F. Prima, A. Eberhardt, T. Gloriant, M. Wary and E. Patoor: *JMBBM.* **3** (2010) 565–573.
- 15) X.J. Jiang, Y.K. Zhou, Z.H. Feng, C.Q. Xia, C.L. Tan, S.X. Liang, X.Y. Zhang, M.Z. Ma and R.P. Liu: *Mater. Sci. Eng. A.* **639** (2015) 407–411.

- 16) C.P. Liang and H.R. Gong: *Int. Hydrogen. Energ.* **35** (2010) 3812–3816.
- 17) Y.Y. Zong, S.H. Huang, Y.J. Feng and D.B. Shan: *J. Alloy. Compd.* **541** (2012) 60–64.
- 18) W.J. Joost, S. Ankem and M.M. Kuklja: *Acta. Mater.* **105** (2016) 44–51.
- 19) J.R.S. Martins, J.R.O. Araújo, T.A.G. Donato, V.E. Arana-Chavez, M.A.R. Buzalaf and C.R. Grandini: *J. Mater. Sci.* **7** (2014) 232–243.
- 20) R. Sarkar, P. Ghosal, T.K. Nandy and K.K. Ray: *Mater. Sci. Eng. A.* **656** (2016) 223–233.
- 21) A. Gagnoud, J. Etay and M. Garnier: *Trans. ISIJ.* **28** (1988) 36–40.
- 22) A. Morita, H. Fukui, H. Tadano, S. Hayashi, J. Hasegawa and M. Niinomi: *Mater. Sci. Eng. A.* **280** (2000) 208–213.
- 23) K. Matsugi, H. Mamiya, Y.B. Choi, G. Sasaki, O. Yanagisawa and H. Kuramoto: *Inter. J. of Cast Metals Research.* **21** (2008), 156–61.
- 24) C. Brozek, F. Sun, P. Vermaut, Y. Millet, A. Lenain, D. Embury, P. J. Jacques and F. Prima: *Scr. Mater.* **114** (2016) 60–64.
- 25) M. Morinaga, M. Kato, T. Kamimura, M. Fukumoto, I. Harada and K. Kubo: *Proc. 7th World Conf. on Ti, TMS,* (1992) 217–224.
- 26) K. Ikeda: *JJILM,* **55** (2005) 97–102.
- 27) I.V. Okulov, H. Wendrock, A.S. Volegov, H. Attar, U. Kühn, W. Skrotzki and J. Eckert: *Mater. Sci. Eng. A.* **628** (2015) 297–302.
- 28) B. Cantor, I.T. H. Chang, P. Knight and A.J.B. Vincent: *Mater. Sci. Eng. A.* **375–377** (2004) 213–218.
- 29) V.B. Deev, V.A. Degtyar, A.I. Kutsenko, I.F. Selyanin, and A.P. Voitkov: *Steel. Transl.* **12** (2007) 33–36.
- 30) A.K. Dahle, Y.C. Lee, M.D. Nave, P.L. Schaffer and D.H. StJohn: *JLM.* **1** (2001) 61–72.
- 31) M. Morinaga: *Mater. Trans.* **57** (2016) 213–226.
- 32) R.J. Deeth: *J. Chem. Soc. Dalton Trans.* **0** (1990) 355–363.

- 33) K. Matsugi, T. Endo, Y.B. Choi and G. Sasaki: *Mater. Trans.* **51** (2010) 740–748.
- 34) M. Abdel-Hady, H. Fuwa, K. Hinoshita, H. Kimura, Y. Shinzato and M. Morinaga: *Scr. Mater.* **57** (2007) 1000–1003.
- 35) D. Kuroda, M. Niinomi, M. Morinaga, Y. Kato and T. Yashiro: *Mater. Sci. Eng. A.* **243** (1998) 244–249.
- 36) T. Chandra, N. Wanderka, W. Reimers and M. Ionescu: *Mater. Sci. Forum.* **638-642** (2010) 635–640.
- 37) A.K. Sample and A. Hellawell: *Metall. Trans. A.* **15A** (1984) 2163–2173.
- 38) D. Ruvalcaba, R.H. Mathiesen, D.G. Eskin, L. Arnberg and L. Katgerman: *Acta. Mater.* **55** (2007) 4287–4292.
- 39) H. Kato and J.R. Cahoon: *Metall. Trans. A.* **16A** (1985) 579–587.
- 40) W. Kurz and D.J. Fisher: *Fundamentals of Solidification.* Trans Tech Publications. (1998) 117–132.
- 41) X.H. Min, K. Tsuzaki, S. Emura, T. Nishimura and K. Tsuchiya: *Mater. Trans.* **52** (2011) 1611–1616.
- 42) A. Paradkar, S.V. Kamat, A.K. Gogia and B. P. Kashyap: *Mater. Sci. Eng. A.* **487** (2008) 14–19.
- 43) J.H. Gao, Y.H. Huang, D.K. Guan, A.J. Knowles, L. Ma, D. Dye and W.M. Rainforth: *Acta. Mater.* **152** (2018) 301–314.
- 44) L. Ren, W.L. Xiao, C.L. Ma, R.X. Zheng and L. Zhou: *Scr. Mater.* **156** (2018) 47–50.
- 45) F. Sun, J.Y. Zhang, M. Marteleur, T. Gloriant, P. Vermaut, D. Laille, P. Castany, C. Curfs, P.J. Jacques and F. Prima: *Acta. Mater.* **61** (2013) 6406–6417.
- 46) L.L. Chang, Y.D. Wang and Y. Ren: *Mater. Sci. Eng. A.* **651** (2016) 442–448.
- 47) H.Y. Kim, Y. Ikehara, J.I. Kim, H. Hosoda, S. Miyazaki: *Acta. Mater.* **54** (2006) 2419–2429.

Chapter 3

Possibility of as-cast applications on β type titanium alloys proposed in the newly expanded area of Bo_t-Md_t diagram

3.1 Introduction.....	62
3.2 Alloy design for the new β -Ti alloys located in the newly expanded area of Bo_t-Md_t diagram.....	62
3.3 Experimental procedures.....	69
3.3.1 Materials and manufacturing process	69
3.3.2 Microstructural characterization.....	71
3.3.3 Tensile tests.....	72
3.4 Results and discussion.....	73
3.4.1 Microstructures.....	73
3.4.2 Tensile properties and fracture surface.....	81
3.4.3 Vickers hardness	84
3.4.4 As-cast application possibility of proposed alloys in the newly expanded area in the Bo_t-Md_t diagram	85
3.5 Summary.....	87
References	88

3.1 Introduction

Titanium based alloys have been extensively investigated for a variety of applications due to their excellent material properties, such as its biocompatibility, excellent combination of high-temperature strength, and lightweight.¹⁻⁵⁾ In particular, β -type titanium (β -Ti) alloys with high strength, excellent corrosion resistance, shape memory ability, and high specific strength are widely used in aerospace, bio-implant, and industrial applications.⁶⁻⁹⁾ However, the higher cost of β -Ti alloys compared to other common structural alloys have limited their usage fields due to the high cost of raw materials, the term length of the development process and its complex post-treatment.^{10,11)} In addition, the relative complex deformation types of β -Ti alloys, including slip, twin, and martensite, make their mechanical control more difficult.¹²⁾ Generally, the β -Ti alloys with single or combined deformation types show divergence in mechanical properties and deformation behaviors.¹³⁾ Hence, the development of β -Ti alloys with low cost and controllable deformation types is important and meaningful.

In the past, repetitive experiments and empirical rules on the purpose of developing β -Ti alloys of reduced cost and controllable deformation types were implemented by researchers; these have been characterized by their high energy consumption and long development cycle.^{14,15)} The proposal of the d-electrons concept can design β -Ti alloys and shorten the development cycle without trial and error experiments.^{16,17)} The d-electrons concept based on the theoretical calculation of electronic structure theory has been applied to the design of high-performance materials such as Al, Bi, Ni, Zn, and Ti-based alloys.^{9,18-22)} Two calculated parameters are utilized in the d-electrons concept, the bond order (Bo), which is a measure of the covalent bond strength between Ti and an alloying element, and the d-orbital energy level (Md), which correlates the electronegativity and metallic radius of elements.^{23,24)} The d-electrons concept is easy and convenient to use in practical applications, compared with other alloy design methods such as the phase-field method and the thermodynamic modeling of ordered phases.^{19,25,26)} The compositional average values of Bo and Md of Ti alloys are represented by Bo_t and Md_t , respectively.¹⁷⁾ Ti alloys are classified into the α , $\alpha + \beta$, and β types according to the phases existing in alloys. Compositions of forty commercial

alloys were plotted on the Bo_i and Md_i coordinates; three types of titanium alloys were separated in the Bo_i - Md_i diagram.^{17,23)} β -Ti alloys with slip dominant deformation universally possess high strength and a controllable deformation process compared with Ti alloys with twin and martensite deformation types.²⁷⁾ However, β -Ti alloys located in the new region of the Bo_i - Md_i diagram with a higher amount of β stabilized elements and lower Md_i values than conventional β -Ti alloys are rarely discussed in previous literature, because of the emergence possibility of intermetallic compounds. Although this new region is a candidate area to develop β -Ti alloys with improved mechanical properties in as-cast condition, the superior solid solution hardening is foreseen for the β -Ti alloys located in the new region with the addition of sufficiently β stabilized elements.

Titanium has a high affinity toward oxygen and hydrogen at elevated temperatures, which can greatly influence the properties of Ti alloys.²⁸⁻³⁰⁾ These elements and other impurities are usually derived from the gas environment of the furnace and the contaminations of the crucible in the process of melting.^{9,17,31)} The choice of appropriate melting equipment is essential for the preparation of Ti alloys. Cold crucible levitation melting (CCLM) consists of a high-frequency induction furnace and two electric coils. Two electric coils are used for the heating and levitation of the metals in the crucible, respectively.³²⁾ The materials will be melted and suspended by the induction current without contact between the materials and copper crucible during the melting process. Furthermore, uniform composition and the high purity of Ti alloys can be obtained by the effect of the electromagnetic stirring force and higher vacuum performance of the furnace.^{17,31,33)}

The reported β -Ti alloys, TUT 1A (Ti-13V-3Al-3Cr-2Nb) and 15-3-3-3 (Ti-15V-3Cr-3Sn-3Al), have never been used in as-cast condition without post-treatments as structural materials, because of the resulting undesirable mechanical properties, according to previous reports.³⁴⁻³⁶⁾ In contrast, the 15-3-3-3 alloy, which was treated by solution treatment and aging was commonly used as sheet, plate, and airframe materials, and showed the ultimate tensile strength (σ_{UTS}) of approximately 1000 MPa and a fracture strain (ϵ_f) of 10%.^{6,35,36)} However, when calculating the cost of the Ti alloy for aircraft applications, if the raw material cost is set as unit 1, the cost of the casting

process is approximately 0.5, the post-treatment cost is approximately 1.5, and the cost of secondary processing is approximately 2.³⁷⁾ The post-treatment cost is remarkably expensive compared with that of casting, because of its high energy consumption. The cost reduction trend of Ti alloys is focused on the following methods;³⁷⁾ The first approach is the choice of cheaper raw materials. The second method is the development of new Ti alloys with improved mechanical properties, which can simplify or omit the post-treatment processes. The third way is to improve the efficiency of manufacturing and post-treatment equipment. Finally, the fourth method is the expansion of the production scale to reduce fringe costs. The high performance of titanium alloys with the σ_{UTS} of 1000 MPa and ϵ_f of 10% just as in as-cast condition is a landmark alloy-development for energy-saving measures, compared with conventional alloys such as 15-3-3-3 with high performance manufactured by complex post-processing. The development of light alloys applied in as-cast condition, such as aluminum and magnesium alloys, has proven to be an effective way to reduce their cost and energy consumption.^{22,38,39)}

In the present study, ten types of β -Ti alloys for as-cast applications were proposed, on the basis of the d-electrons concept, by using the Bo_r-Md_t diagram. To develop β -Ti alloys with an σ_{UTS} value of 1000 MPa and ϵ_f value of 10% in as-cast condition, the new compositions of ten types of β -Ti alloys were chosen using mainly ubiquitous elements in the newly expanded area, greatly differing from conventional alloys. This implies the choice of cheaper raw materials and the design of new β -Ti alloys with improved mechanical properties as cost reduction measures occur at the same time. Ingots of experimental alloys were produced by the CCLM technique as a single manufacturing process for saving energy; their microstructures were controlled by adjusting its cooling process parameters. The microstructure and mechanical properties of the ten types of β -Ti alloys were discussed in as-cast and solution treated conditions.

3.2 Alloy design for the new β -Ti alloys located in the newly expanded area of Bo_t - Md_t diagram.

The nominal compositions of ten types of β -Ti alloys were designed on the basis of d-electrons concept⁴⁰⁾ by using mainly ubiquitous elements. The Bo_t and Md_t values of ten types of β -Ti alloys were calculated by utilization of the discrete-variational $X\alpha$ (DV- $X\alpha$) cluster calculation method⁴¹⁾, on the MTi_{14} cluster model in the case of bcc Ti⁴²⁾. The mean Bo_t and Md_t values of each alloy were calculated by the following equations. (3-1) and (3-2).

$$Bo_t = \sum X_i (Bo)_i \quad (3-1)$$

$$Md_t = \sum X_i (Md)_i \quad (3-2)$$

Where X_i is the molar fraction of component i in Ti alloy, $(Bo)_i$ and $(Md)_i$ were the numerical values of Bo_t and Md_t for each component i , respectively.^{9,40-42)} By using equations (1) and (2), the Bo_t and Md_t values of 15-3-3-3 alloy were calculated conveniently. Firstly, the chemical composition unit of Ti-15V-3Cr-3Sn-3Al in mass% will be converted to Ti-14.18V-2.78Cr-1.22Sn-5.35Al in mol.%. In this case, the X_i values of Ti, V, Cr, Sn and Al were 0.7647, 0.1418, 0.0278, 0.0122 and 0.0535, respectively. The $(Bo)_i$ and $(Md)_i$ values of Ti, V, Cr, Sn and Al were 2.79 and 2.45, 2.81 and 1.87, 2.78 and 1.48, 2.28 and 2.10, and 2.43 and 2.20, respectively.²³⁾ The molar fraction of each element in alloy multiplied its respective Bo or Md value, then these values of all elements were summated to obtain the Bo_t and Md_t values of this alloy, as shown in follow:

$$Bo_t = X_{Ti}(0.7647) \times Bo_{Ti}(2.79) + X_V(0.1418) \times Bo_V(2.81) + X_{Cr}(0.0278) \times Bo_{Cr}(2.78) + X_{Sn}(0.0122) \times Bo_{Sn}(2.28) + X_{Al}(0.0535) \times Bo_{Al}(2.43) = 2.77$$

$$Md_t = X_{Ti}(0.7647) \times Md_{Ti}(2.45) + X_V(0.1418) \times Md_V(1.87) + X_{Cr}(0.0278) \times Md_{Cr}(1.48) + X_{Sn}(0.0122) \times Md_{Sn}(2.10) + X_{Al}(0.0535) \times Md_{Al}(2.20) = 2.32$$

The 2.77 and 2.32 were the Bo_t and Md_t values of 15-3-3-3 alloy calculated by taking its average chemical composition. Figure 3-1 shows the compositional locations of ninety-three commercial and reported β -Ti alloys. There are the indications of deformation modes consisting of slip, twin and martensite types, and the excellent mechanical properties have been produced by combinations of both compositional and

post manufacturing process approaches, such as TUT 1A (σ_{UTS} : 1400 MPa, ϵ_f : 6%).^{35,36} The positions of TUT 1A and 15-3-3-3 alloys in the Bo_t - Md_t diagram are also shown in Fig. 3-1. The β stabilized area in lower Md_t values is a candidate, or the “target area” indicated by solid black arrows in newly expanded area for as-cast applications of β -Ti alloys without post-treatments compared with conventional alloys. The promising mono β phase alloys with high strength and elongation can be proposed in this target area showing the expanded compositional area where is greatly different from ninety-three commercial and reported alloys.

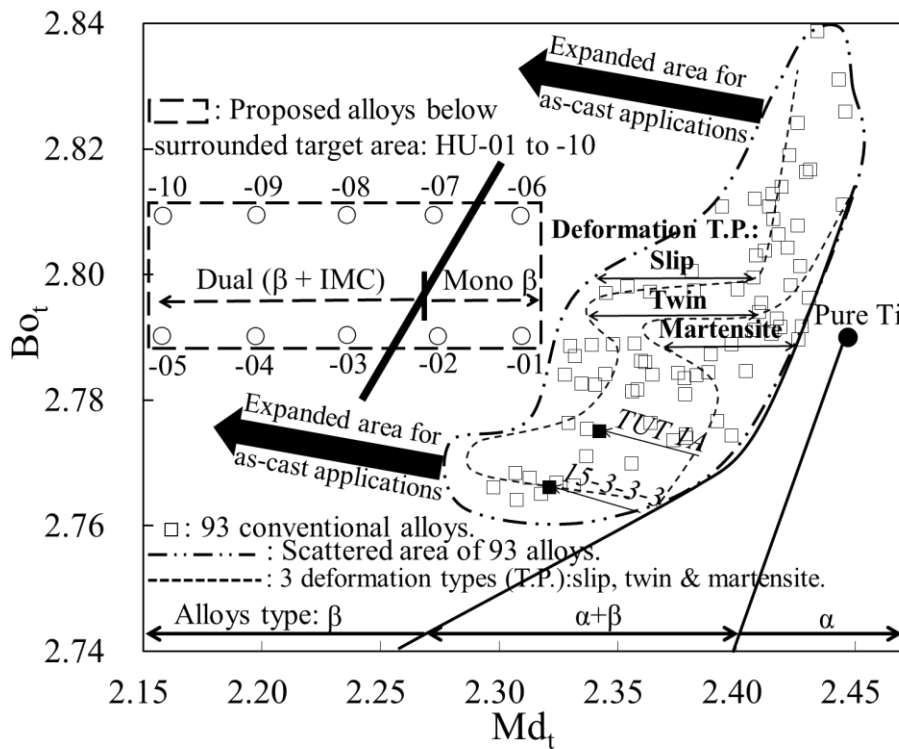


Fig. 3-1 The compositional positions of ten proposed alloys (HU-01 to -10) and 93 conventional β -Ti alloys in the Bo_t - Md_t diagram, which represented phase boundaries between β , $\beta+\alpha$ and α alloys, and deformation mode consisting of slip, twin and martensite types. The compositional range of 93 β -Ti alloys were Ti-(0-55)Ta-(0-41)Nb-(0-30)Zr-(0-8)Fe-(0-13)Cr-(0-22)V-(0-20)Mo-(0-6)Sn-(0-8)Al-(0-8)Mn in mass%. The line among the HU-02, HU-03, HU-06 and HU-07 alloys indicated the phase boundary between the mono β phase and dual β plus intermetallic compound phases, which was derived from this study.

The Bo_t value of 2.79 which is equal to that of pure Ti and five Md_t values of 2.16, 2.20, 2.24, 2.28 and 2.32 were selected to investigate the mono phase region. Another Bo_t value of 2.81 was chosen as the high Bo_t alloys for improvement of strength properties. According to the principle of the Bo_t values from 2.79 to 2.81 and the Md_t values from 2.32 to 2.16, the newly proposed β -Ti alloys were named from HU-01 to HU-10, as shown in Fig. 3-1. The compositions of ten newly proposed β -Ti alloys in mol% or mass%, and their respective Bo_t and Md_t values are listed in Table 3-1. The chemical compositions of the ten alloys in Table 3-1 are determined by considering the mean Bo_t and Md_t values to propose alloy in target area where is greatly different from ninety-three commercial and reported alloys in the Bo_t - Md_t diagram, the usage of ubiquitous elements to reduce the cost of alloy, and easy disposal of abandoned alloy.

Table 3-1 The compositions of ten proposed β -Ti alloys in both mol.% and mass%, and their Bo_t and Md_t values.

Alloys	Compositions		Bo_t	Md_t
	mol.%	mass%		
HU-01	Ti-5Cr-5Mn-2.5Zr-2Fe	Ti-5.1Cr-5.4Mn-4.6Zr-2.2Fe	2.79	2.32
HU-02	Ti-10.5Cr-5.4Mn-2.4Zr-0.9Al	Ti-11.0Cr-6.0Mn-4.4Zr-0.5Al	2.79	2.28
HU-03	Ti-12.5Cr-7.3Mn-2.2Zr	Ti-13.0Cr-8.0Mn-4.0Zr	2.79	2.24
HU-04	Ti-13.6Cr-10.1Mn-2.9Zr	Ti-14.0Cr-11.0Mn-5.3Zr	2.79	2.20
HU-05	Ti-15.6Cr-12Mn-3.3Zr	Ti-16.0Cr-13.0Mn-6.0Zr	2.79	2.16
HU-06	Ti-7.4Zr-6.0Cr-5.7Mn-5.1V	Ti-13.0Zr-6.0Cr-6.0Mn-5.0V	2.81	2.32
HU-07	Ti-6.5Zr-8.3Cr-4.9Mn-1.9Fe-3.6V-1.8Ta	Ti-11Zr-8.0Cr-5.0Mn-2.0Fe-3.4V-6.0Ta	2.81	2.28
HU-08	Ti-6.6Zr-10.5Cr-6.0Mn-2.3Fe-3.6V-2.0Ta	Ti-11.0Zr-10.0Cr-6.0Mn-2.4Fe-3.4V-6.6Ta	2.81	2.24
HU-09	Ti-17.2Cr-5.5Mo-4.8Mn-2.5Zr	Ti-17.0Cr-10.0Mo-5.0Mn-4.3Zr	2.81	2.20
HU-10	Ti-18.4Cr-6.4Mo-6.5Mn-2.0Zr-0.5V	Ti-18.0Cr-11.6Mo-6.7Mn-3.4Zr-0.5V	2.81	2.16

In addition, the vectors pointing from pure Ti represented the location of Ti-10mass%M (M is additional alloying element) are shown in Fig. 3-2 (a). The elements circled by square correspond to the alloying elements selected in the present study from the viewpoints of the Bo_t and Md_t values of alloy, low cost and easy disposal of abandoned alloy. The ubiquitous Cr and Mn elements were chosen as the major additional elements which had the high ability to shift the positions of β -Ti alloys to the target area with low Md_t values in the Bo_t - Md_t diagram. The Fe and V elements were auxiliary to move the β -Ti alloys to lower Md_t area in the Bo_t - Md_t diagram. The Zr, Mo, Al and Ta elements were chosen to adjust the Bo_t values of β -Ti alloys. The MTi_{14} cluster model in the case of bcc Ti is shown in Fig. 3-2 (b).

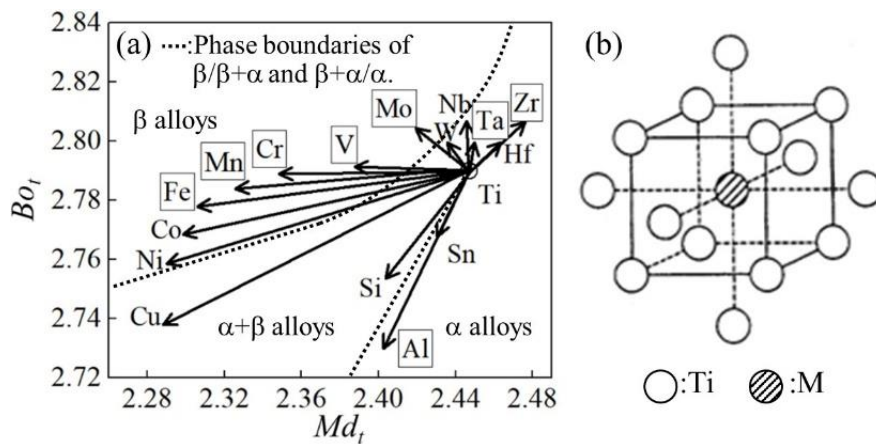


Fig. 3-2 The vectors pointing from pure Ti represented the location of Ti-10mass%M. (M were alloying elements). The elements circled by squares showing the positions of alloying elements selected in the present study corresponded to the Cr, Mn, Fe, V, Zr, Mo, Al, Sn and Ta, respectively.

3.3. Experimental procedures

3.3.1 Materials and manufacturing process

The purity of raw materials for preparing ten newly proposed β -Ti alloys were Ti, Cr, Mn, Fe, V, Zr, Mo, Al and Ta with 99.8, 99.9, 99.9, 99.9, 99.9, 98.0, 99.0, 99.9 and 99.8 mass%, respectively. Hereafter, the compositions of ten newly proposed β -Ti alloys were given in mass% in this paper. All ingots of ten proposed β -Ti alloys were prepared by CCLM (capacity of 1 kg in Fe melt / 100 + 60 kW, Fuji Corporation, Japan) and their microstructures were controlled by adjusting its process parameters. The 100 and 60 kW are the rated power of upper and lower electric coils of CCLM, respectively. The maximum temperature and holding temperature of CCLM were depending on the melting point of alloying elements¹⁷⁾. HU-01 alloy, for example, in order to completely melt the raw materials and fully stirring the molten metals, the molten metal with 150 cubic centimeters was heated to 2350 K in the heating process. Then, for its completely stirring, the molten metal was held for 300 s at the constant temperature of 2300 K which was above its melting point of approximately 2180 K. Subsequently, the molten metal was heated to 2350 K, as the pretreatment of solidification. Finally, the molten metal was cooling and solidified in the copper crucible after switching off electric power in upper and lower coils after the melting process. The detailed parameters of CCLM equipment during the melting process are shown in Fig. 3-3. The profiles of temperature in molten metal, electric power in upper and lower coils and pressure in atmosphere of levitation melting and cooling process are shown in Fig. 3-3 (a), (b) and (c), respectively. The upper and lower electric coils were utilized for heating by the high-frequency induction and levitation by the eddy current for molten metals. These functions were successfully acted, which led to the achievement of homogeneous mono β phase (mentioned in 4.1 section) and the low contents of gaseous impurities. The different grain sizes of alloys were obtained by the both cooling methods of molten metals, which meant the solidification in the melting copper (Cu) crucible and split-cold mold placed below the hole of melting Cu crucible in the bottom part of melting furnace.^{9,31)} In contrast, the different grain sizes could also be influenced by the

different Ar gas purity.³¹⁾ These Ti ingots were prepared in the solidification of the melting Cu crucible under the purity of 99.99 % Ar atmosphere in the present study. The contents of gaseous impurities of oxygen and nitrogen were lower than those (oxygen and nitrogen: 0.069 and 0.006 %, respectively) in the raw materials, because of highly vacuum level of 3×10^{-3} Pa were obtained by using rotary pump (RP) and diffusion pump (DP).

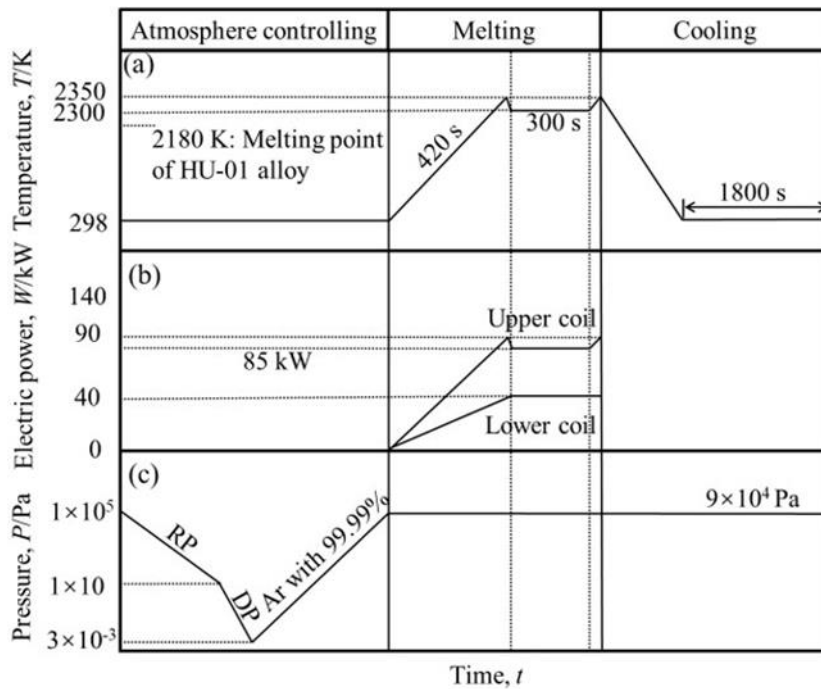


Fig. 3-3 Profiles of (a) temperature in molten metal, (b) electric power in upper and lower coils and (c) pressure in Ar atmosphere of levitation melting and cooling process. Abscissa and ordinate are represented with arbitrary scales.

The schematic illustrations of ingot produced by CCLM and tensile specimen showing both the equiaxed and columnar grains distribution and cutting position for a tensile specimen in an ingot are shown in Fig. 3-4. Dimensions of ingot and tensile specimen are given in millimeters (mm). The rectangle blocks were firstly cut by a wire cutting from the ingot. Then, the tensile specimens were also prepared in this rectangle blocks. The edge lengths of rectangle blocks were \overline{ab} , \overline{cd} , \overline{ef} and \overline{gh} of 30 mm, \overline{ad} , \overline{bc} , \overline{eh} and \overline{gf} of 10 mm and \overline{ae} , \overline{bf} , \overline{cg} and \overline{dh} of 35 mm, respectively. The equiaxed and columnar grains in ingot were further observed by the optical microscope

(OM) images obviously. The columnar grains with larger and various sizes were observed at the bottom and close to the lower part (tip part) of the ingot compared with those of equiaxed grains part with the uniform sizes in the upper part of ingot. Therefore, the positions with equiaxed grains were chosen for cutting the tensile specimens. The sizes of equiaxed grains were approximately $200\ \mu\text{m}$ in diameter as shown in the OM images in Fig. 3-4, and detailly discussed in Figs. 3-5 and 3-6, respectively. For the as-cast specimens, they were cut directly from the ingot. Whereas, the solution treatment was carried out at $1173\ \text{K}$ for $3.6\ \text{ks}$, the specimens cut from the ingot were sealed in a quartz tube under argon atmosphere following by quenching in the cold water.

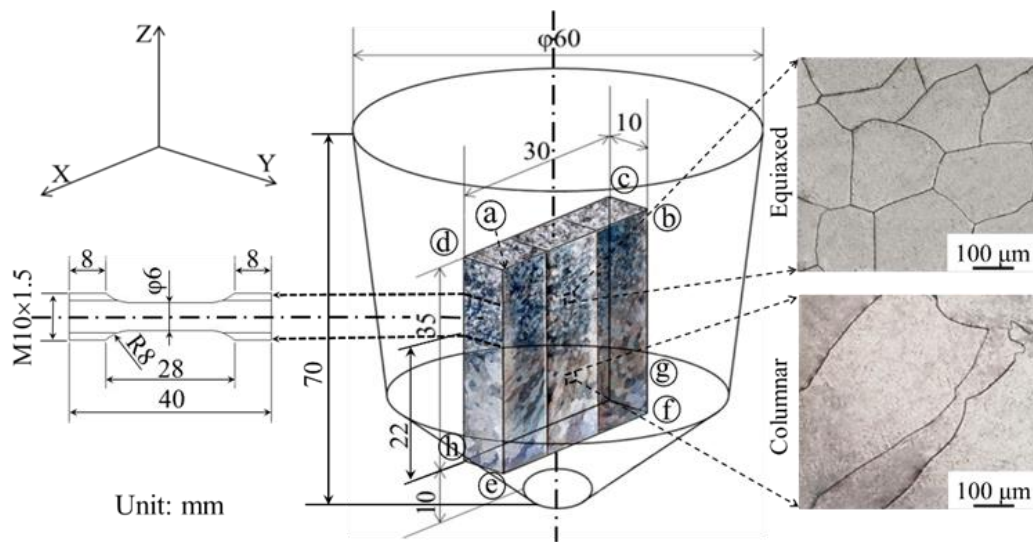


Fig. 3-4 Schematic illustrations of ingots produced by CCLM and tensile specimens showed the distribution of both equiaxed and columnar grains and cut positions for a tensile specimen with equiaxed grains of approximately $200\ \mu\text{m}$ in ingot. Dimensions of ingot and tensile specimen were given in millimeters (mm). The edge lengths of rectangle blocks were \overline{ab} , \overline{cd} , \overline{ef} and \overline{gh} of $30\ \text{mm}$, \overline{ad} , \overline{bc} , \overline{eh} and \overline{gf} of $10\ \text{mm}$ and \overline{ae} , \overline{bf} , \overline{cg} and \overline{dh} of $35\ \text{mm}$, respectively. OM images of equiaxed and columnar grains further showed the different grain size distributions in the ingot.

3.3.2 Microstructural characterization

The specimens were grinded, polished and etched by using sandpapers from 80 to

2500 mesh, different grades of polishing paper and a mixed solution of distilled water, nitric acid and hydrofluoric acid (95:3:2 in volume ratio), respectively. The microstructural observation of as-cast and solution treated specimens was carried out by using the OM imaging analysis. The constituent phases and lattice constants of ten experimental alloys were identified by X-ray diffraction (XRD) with Cu-K α radiation generated at 40 kV and 30 mA at ambient temperature. The chemical compositions of HU-01 and -05 alloys were measured by point analysis via the EPMA (JXA-8200, JEOL Corporation, Japan). For preparation of solidification paths, the points analysis thoroughly crossed two grains of each specimen were measured with the interval of 25 μm between each two points.

3.3.3 Tensile tests

The gauge sizes of tensile specimens were 6 mm in diameter and 20 mm in length with grips of 10 mm in diameter as shown in Fig. 3-4. The tensile tests were carried out at an initial strain rate of $1.9 \times 10^{-4} \text{ s}^{-1}$ under room temperature, the fracture strain values of tensile specimens were measured by extensometer (SG 10-50, Shimadzu Corporation, Japan) and the stress-strain curves were obtained by mechanical testing machine (Autograph DCS-R-5000, Shimadzu Corporation, Japan) during the tensile process. The Vickers hardness measurements were tested with load of 10 N for 10 s (FV-110, Future-tech Corporation, Japan).

3.4 Results and discussion

3.4.1 Microstructures

The OM images of ten types of β -Ti alloys in as-cast and solution treated conditions are presented in Figs. 3-5 and 3-6, and the area fraction of constructed phases of ten types of β -Ti alloys are presented in Fig. 3-7. For the HU-01 to HU-05 alloys with the constant Bo_t value of 2.79 in both as-cast and solution treated conditions, the mono β phase were observed in HU-01 and 02 alloys in both as-cast and solution treated conditions as shown in Fig. 3-5 (a) and (b), (c) and (d), respectively. In contrast, the presence of dual β plus intermetallic compound phases were observed in Fig. 3-5 (e) and (f), (g) and (h), (i) and (j), corresponding to the HU-03 to HU-05 alloys in both as-cast and solution treated conditions, respectively. The average grain sizes of HU-01 to HU-05 alloys in both as-cast and solution treated conditions were measured to be, on the basis of microstructure results, 290 and 305, 235 and 242, 210 and 215, 186 and 198, 175 and 185 μm , respectively. The decreasing of Md_t value, or higher alloying led to the decrease of grain sizes, regardless of post-treatments. The heterogeneous-nucleation was thought as the major factor response to the trend of smaller in grain size, regardless of Bo_t values^{43, 44}). The heterogeneous-nucleation means the additional alloying elements will provide more nucleation opportunities for the titanium alloys. The increased amount of nucleation will lead to the refinement of grain size.

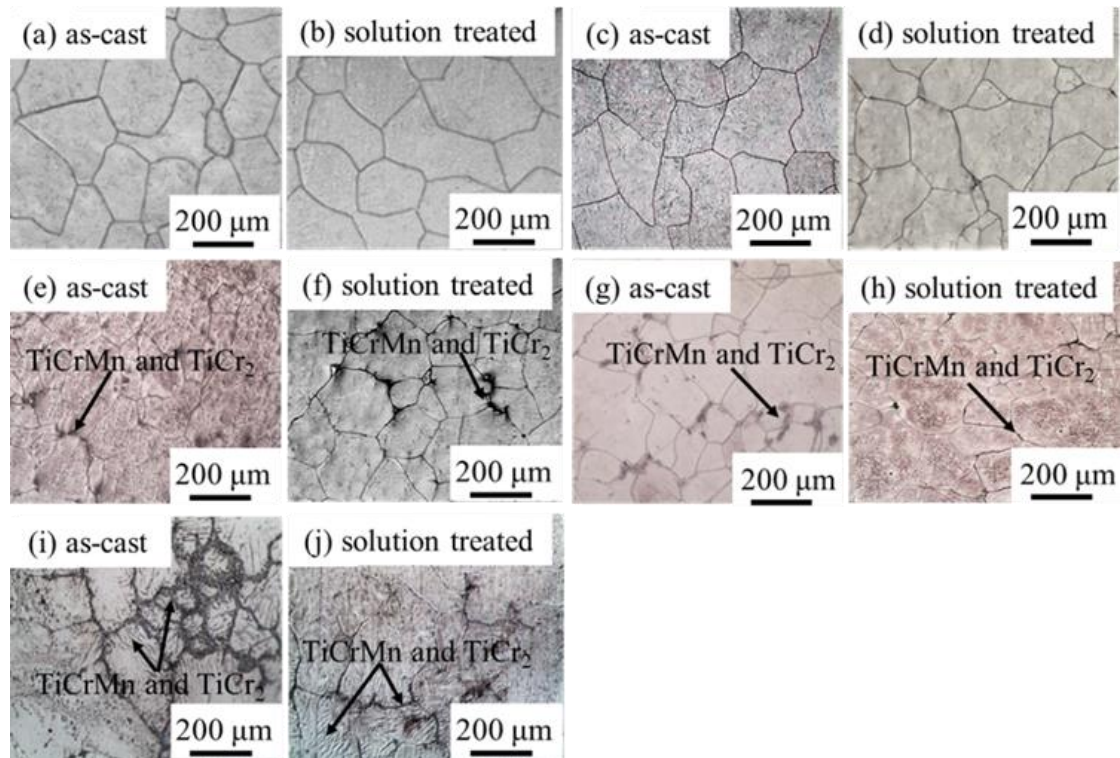


Fig. 3-5 OM images of (a) and (b) HU-01, (c) and (d) HU-02, (e) and (f) HU-03, (g) and (h) HU-04, (i) and (j) HU-05 alloys. (a), (c), (e), (g), (i) and (b), (d), (f), (h), (j) were obtained from as-cast and solution treated conditions, respectively.

For the HU-06 to HU-10 alloys with the constant Bo_i value of 2.81, the mono β phase were observed in HU-06 alloy in both as-cast and solution treated conditions as shown in Fig. 3-6 (a) and (b). In contrast, the presence of dual β plus intermetallic compound phases were observed in Fig. 3-6 (c) and (d), (e) and (f), (g) and (h), (i) and (j), corresponding to the HU-07 to HU-10 alloys in both as-cast and solution treated conditions, respectively. The average gran sizes of HU-06 to HU-10 alloys in both as-cast and solution treated conditions were 280 and 295, 230 and 245, 193 and 205, 191 and 205, 180 and 195 μm , respectively. There was the same relation between the Md_i values and grain sizes, regardless of the Bo_i values. The 3 to 8% increment in the grain sizes was measured by the solution treatment, regardless of the Bo_i values.

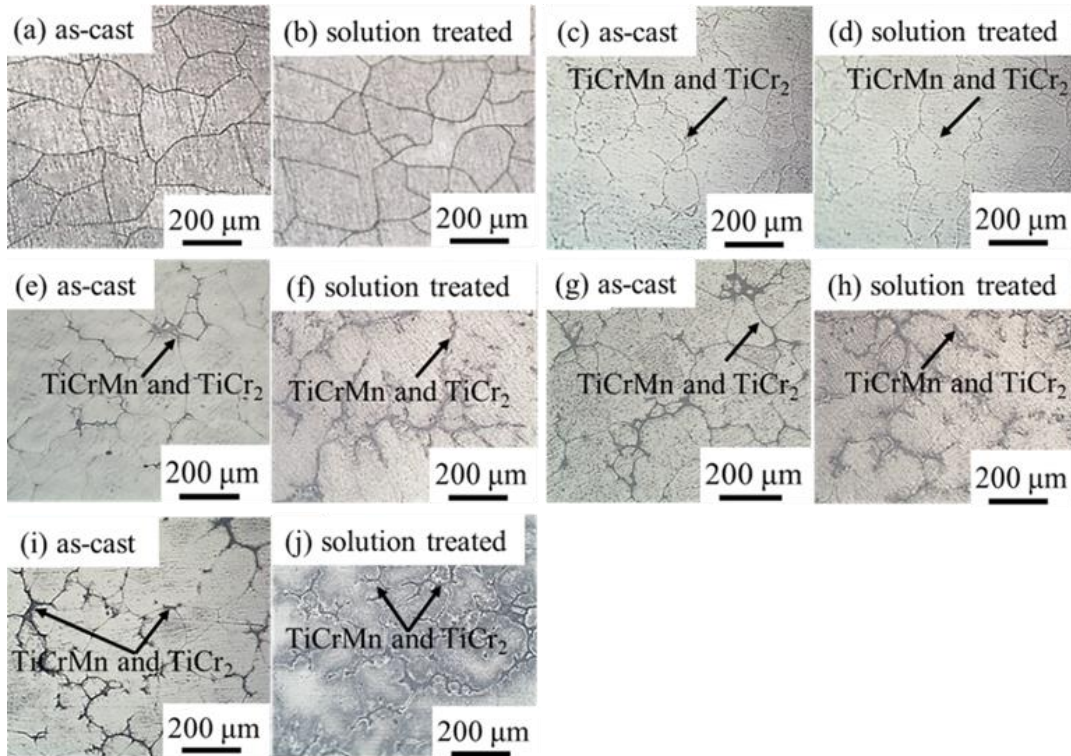


Fig. 3-6 OM images of (a) and (b) HU-06, (c) and (d) HU-07, (e) and (f) HU-08, (g) and (h) HU-09, (i) and (j) HU-10 alloys. (a), (c), (e), (g), (i) and (b), (d), (f), (h), (j) were obtained from as-cast and solution treated conditions, respectively.

Moreover, the occurrence positions of intermetallic compounds expanding from the grain boundaries toward to the inner of grains were observed obviously with increasing contents of additional elements in alloys. The contents of intermetallic compounds were evaluated by measuring their area fractions in ten types of β -Ti alloys in both as-cast and solution treated conditions, according to their OM results, respectively. The increment contents of intermetallic compounds were observed and measured from HU-03 to HU-05 β -Ti alloys, as shown in Fig. 3-7 (a). Simultaneously, the increased tendency in contents of intermetallic compounds were occurred from HU-07 to HU-10 alloys, as shown in Fig. 3-7 (b).

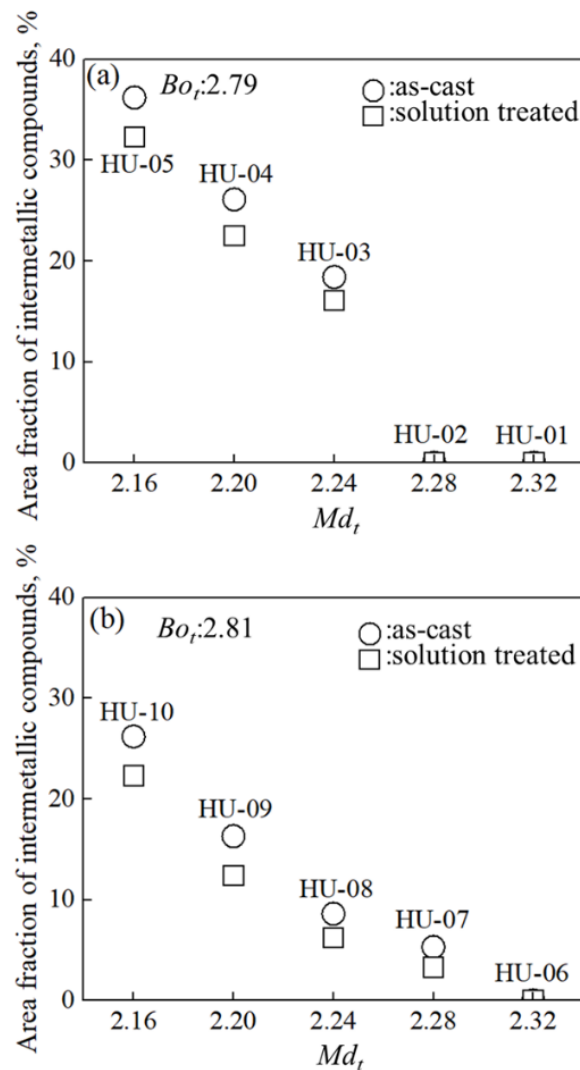


Fig. 3-7 Area fraction of intermetallic compounds of (a) in HU-01 to HU-05 alloys, (b) in HU-06 to HU-10 alloys, according to the results of OM images as shown in Figs. 3-5 and 3-6, respectively.

The area fractions of intermetallic compounds in HU-03 to HU-05 alloys in as-cast and solution treated conditions were 18.4% and 16.1, 26.1 and 22.5, 36.2 and 32.3 %, respectively. Meanwhile, the area fractions of intermetallic compounds in HU-07 to HU-10 alloys in as-cast and solution treated conditions were 5.3 and 3.3, 8.6 and 6.2, 16.3 and 12.4, 26.2 and 22.3%, respectively. In contrast, the absences of intermetallic compounds were observed in HU-01, HU-02 and HU-06 alloys. The $TiCr_2$ and $TiCrMn$ phases were detected by XRD as shown in Figs. 3-8 and 3-9, and these intermetallic compounds were known as brittle phases^{45, 46}). The ternary intermetallic $TiCrMn$ is

partially manganese substituted derivative of the TiCr_2 , and the substitution of the Cr by Mn in the lattice of TiCr_2 made the atomic stacking closer⁴⁷.

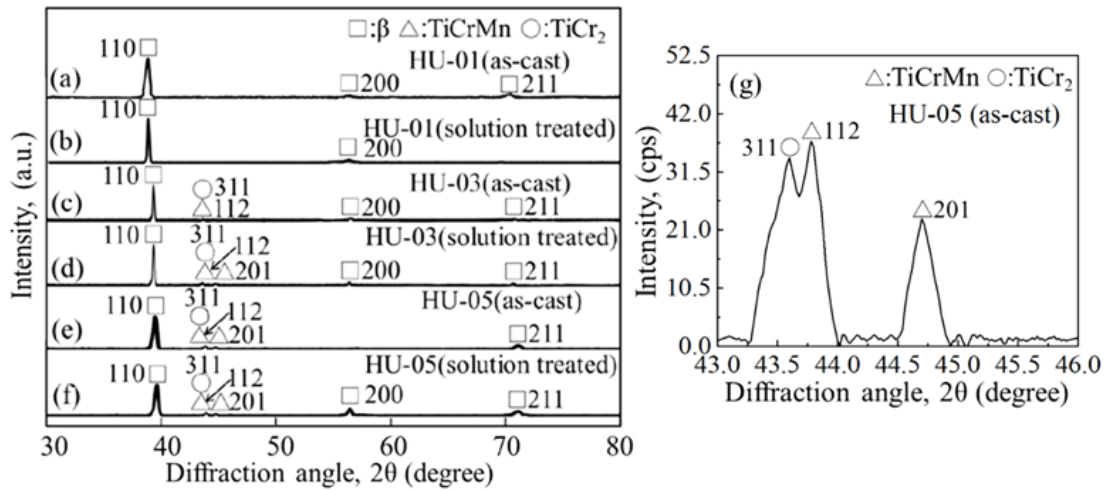


Fig. 3-8 X-ray diffraction profiles with Cu-K α radiation of (a) and (b) HU-01, (c) and (d) HU-03, (e) and (f) HU-05 alloys, and (g) the higher sensitive condition for identification of TiCrMn and TiCr_2 in the 2θ value of 43 to 46° for (e).

(a), (c), (e) and (b), (d), (f) were obtained from as-cast and solution treated conditions, respectively.

According to the microstructures of ten types of β -Ti alloys, the phase boundary between the mono β phase and the dual β plus intermetallic compound phases were roughly identified in the newly expanded area of $B_{0r}-M_{d_t}$ diagram for the first time. The lattice constants of ten types of β -Ti alloys were calculated from interatomic layer distances of the primary (110) reflections, using the results of Figs. 3-8 and 3-9. The higher sensitive condition for identification of TiCrMn and TiCr_2 in the 2θ value of 43 to 46° is also shown in Figs. 3-8 and 3-9 (g), respectively.

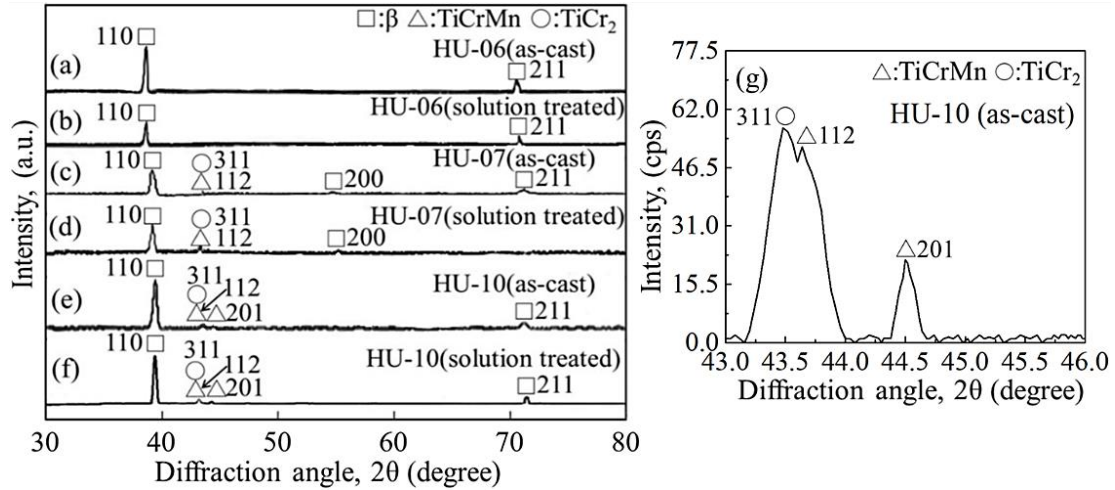


Fig. 3-9 X-ray diffraction profiles with Cu-K α radiation of (a) and (b) HU-06, (c) and (d) HU-07, (e) and (f) HU-10 alloys, and (g) the higher sensitive condition for identification of TiCrMn and TiCr₂ in the 2 θ value of 43 to 46° for (e).

(a), (c), (e) and (b), (d), (f) were obtained from as-cast and solution treated conditions, respectively.

The XRD experiments of each alloy were repeated and the data for the same alloy obtained from repeated experiments were compared with each other. The results showed the approximately same value and tendency as shown in Fig. 3-10. The detailed values of lattice constants of ten types of β -Ti alloys corresponded to the diffraction angle of (110) are shown in Fig. 3-10. The error bar from repeated experiments for the same alloy showed even smaller than the symbol used in Fig. 3-10, which mean the invisible error bar was inside the symbol range. For the HU-01 to HU-05 β -Ti alloys with B_{O_i} value of 2.79 in both as-cast and solution treated condition, the values of lattice constants of HU-01 to HU-05 alloys were 0.328, 0.325, 0.323, 0.321 and 0.321 nm, as shown in Fig. 3-10 (a), respectively. For the HU-06 to HU-10 β -Ti alloys with B_{O_i} value of 2.81 in both as-cast and solution treated conditions, as shown in Fig. 3-10 (b), the values of lattice constants of HU-06 to HU-10 β -Ti alloys were 0.327, 0.323, 0.323, 0.321 and 0.321 nm, respectively. In addition, the lattice constant of β -Ti metal with the value of 0.332 nm was also listed in Fig. 3-10 (a) and (b) as a comparison. The decreased lattice constants with decreasing of Md_i values were measured in each five β -Ti alloys with constant B_{O_i} value, due to the increasing of alloying elements with

smaller atomic radius which substituted the Ti in the crystal. The solid solution limits of ten types of β -Ti alloys were investigated by their respective values of lattice constants. For the two series of five β -Ti alloys with same Bo_t value, the fitting lines of two adjacent values of lattice constants were obtained as shown in Fig. 3-10 (a) and (b), respectively. The slope of fitting lines changed dramatically between HU-02 and HU-03, and HU-06 and HU-07, respectively. In view of the above results, the solid solution limit appeared in the interval between HU-02 and HU-03 for the β -Ti alloys with the Bo_t value of 2.79. In addition, the solid solution limit appeared in the interval between HU-06 and HU-07 for the β -Ti alloys with the Bo_t value of 2.81. The results of OM, XRD patterns indicating the $TiCr_2$ and $TiCrMn$ peaks and the values of lattice constant were highly in agreement with each other and by the combination of them, the phase boundary in the newly expanded area of Bo_t - Md_t diagram was identified in the present paper. The line among the HU-02, HU-03, HU-06 and HU-07 alloys as shown in Fig. 3-1, indicated the phase boundary between the mono β phase and the dual β plus intermetallic compound phases.

On the basis of the vectors which represent the location of Ti-10mass%M as shown in Fig. 3-2, the changing in Md_t values was mainly influenced by the increasing in contents of Fe, Cr and Mn. In addition, the intermetallic compounds, locating in the grain boundary, were consisting of $TiCr_2$ and $TiCrMn$. Therefore, the elements distribution of Cr and Mn in one grain of HU-01 and HU-05 alloys were investigated by the solidification paths. For preparation of solidification paths, the points analysis thoroughly crossed two grains of each specimen were measured with the interval of 25 μm between each two points by EPMA.²⁴⁾ The segregation degree and composition scatters of Cr and Mn elements in HU-01 and -05 alloys in as-cast and after solution treated conditions are shown in Fig. 3-11. The heavier segregation in HU-05 alloy was observed, compared with HU-01 alloy, regardless of the post-treatments. There was a little difference in compositional scatters between the as-cast and solution treated conditions in HU-01 alloy. The segregation degree and composition scatters of Cr and Mn elements were decreased by the solution treatment. The serious segregation and the formation of intermetallic compounds in HU-05 alloy were indicated by the widely distributed chemical composition scatters.

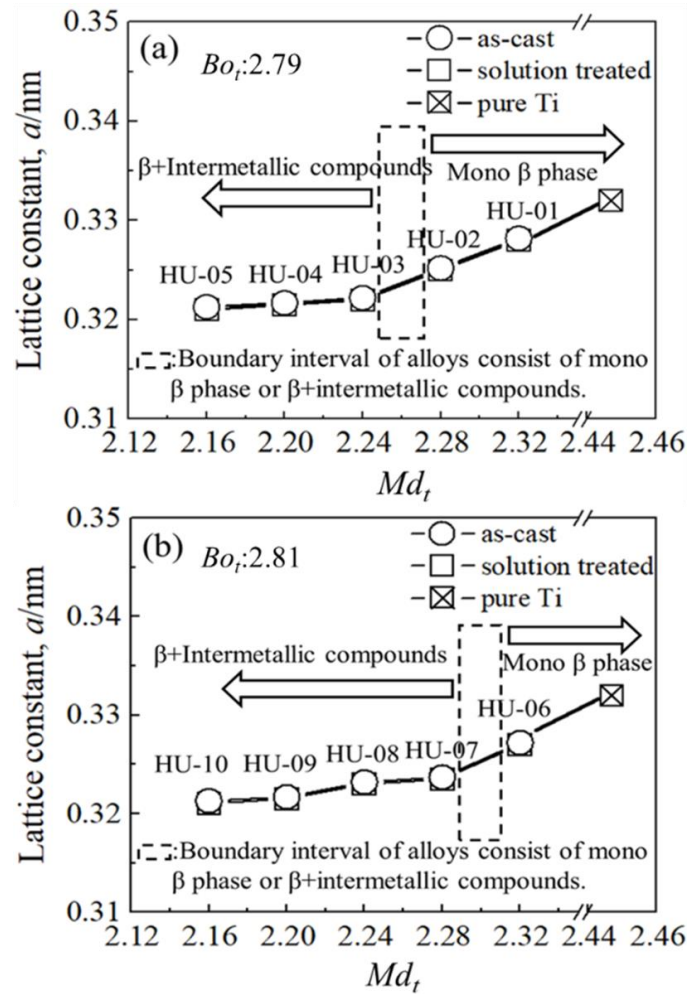


Fig. 3-10 Relation between the lattice constant calculated by the 2θ value of (110) plane and Md_t values of (a) HU-01 to HU-05 and (b) HU-06 to HU-10 alloys in as-cast and solution treated conditions.

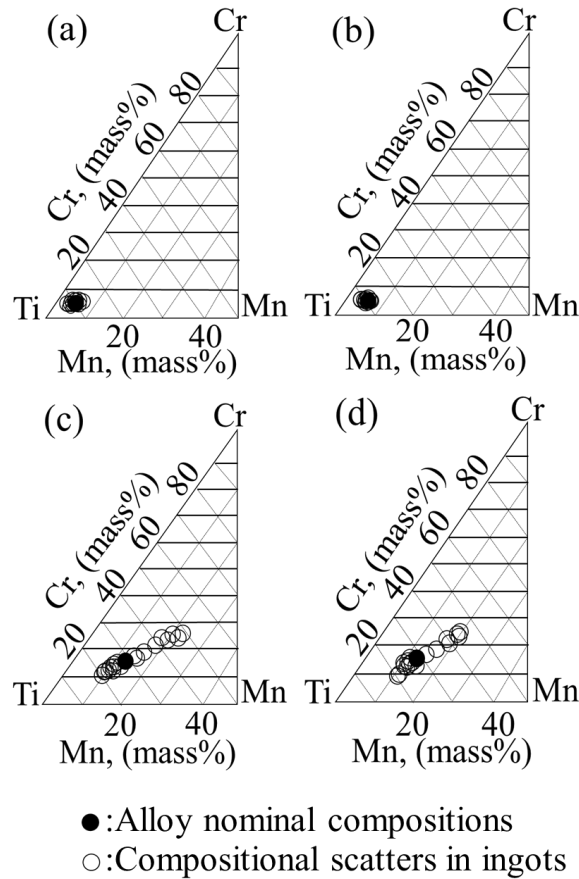


Fig. 3-11 Solidification paths of HU-01 (a) and (b), and HU-05 (c) and (d) β -Ti alloys, (a), (c) and (b), (d) were obtained from as-cast and solution treated conditions, respectively.

3.4.2 Tensile properties and fracture surface

The tensile curves of HU-02 and -03, and HU-06 and -07 alloys in both as-cast and solution treated conditions were chosen as typical specimens as shown in Fig. 3-12, respectively. The HU-02 and -06 alloys with the mono β phase showed the slip behavior consisting of a classical elastic-plastic tensile behavior, as mentioned in Fig. 3-1. They also showed high tensile strength and elongation values compared with those of HU-03 and -07 alloys with dual β plus intermetallic compound phases. The fracture morphologies of HU-02 and -06, and HU-03 and -07 alloys in as-cast condition were chosen as typical specimens, representing the alloys without or with the presence of

intermetallic compounds, respectively. The precipitation of brittle intermetallic compounds $TiCrMn$ and/or $TiCr_2$ located at the grain boundary, resulting in the fracture of specimens occurred during the elastic deformation stage in the tensile test process. The dimple fracture patterns appeared in HU-02 and 06 alloys in as-cast condition corresponded to the relative satisfaction ε_f values, as shown in Fig. 3-13 (a) or (b), and (e) or (f), respectively. In contrast, the inter- and trans-granular were observed obviously in Fig. 3-13 (c) or (d), and (g) or (h) corresponded to the HU-03 and -07 alloy in as-cast condition.

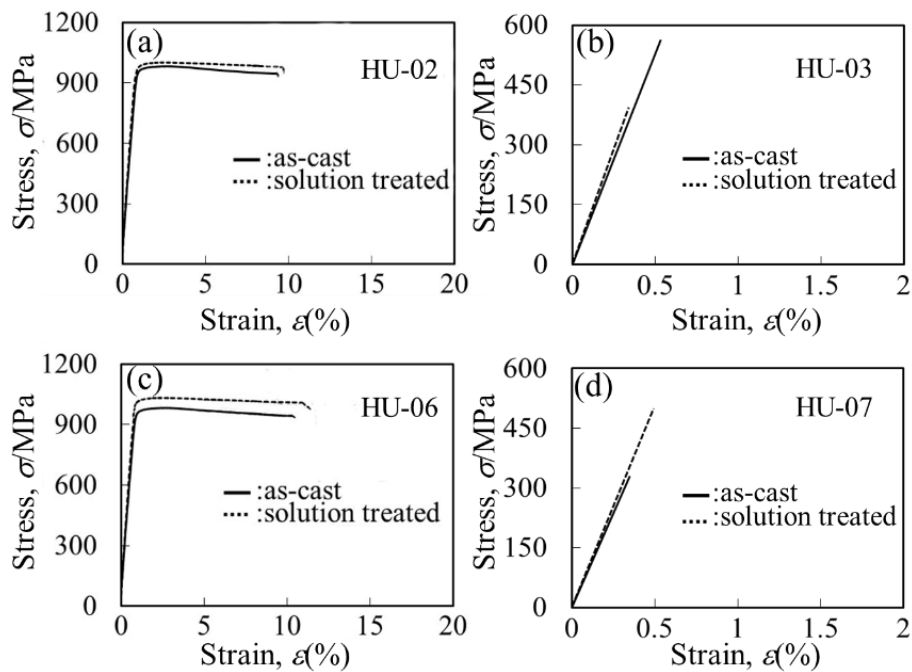


Fig. 3-12 Stress-strain curves of (a) HU-02, (b) HU-03, (c) HU-06 and (d) HU-07 alloys at as-cast and solution treated conditions.

The tensile properties of ten newly proposed β -Ti alloys with their respective σ_{UTS} and ε_f values in as-cast and solution treated conditions were shown in the Fig. 3-14 (a) and (b), corresponding to the β -Ti alloys with Bo_t values of 2.79 and 2.81, respectively. The as-cast and solution treated alloys showed their respective σ_{UTS} with ε_f values, they were 1027 and 979 MPa with 10.12 and 10.21 % for HU-01, 982 and 1002 MPa with 9.82 and 9.63 % for HU-02, 531 and 406 MPa with 0.55 and 0.44 % for HU-03, 279 and 155 MPa with 0.29 and 0.11 % for HU-04, 329 and 232 MPa with 0.17 and 0.16 % for HU-05, 984 and 1090 MPa with 10.32 and 10.63 % for HU-06, 340 and 463 MPa

with 0.40 and 0.50 % for HU-07, 208 and 316 MPa with 0.30 and 0.26 % for HU-08, 235 and 310 MPa with 0.23 and 0.27 % for HU-09, 188 and 213 MPa with 0.20 and 0.21 % for HU-10. HU-01 and -02 alloys with Md_t values of 2.32 and 2.28, respectively, showed the highest σ_{UTS} values among the five alloys with Bo_t value of 2.79. In contrast, σ_{UTS} values decreased dramatically, which corresponded to the decrease of ϵ_f values. The alloys with Md_t less than 2.24 also showed occurrence of $TiCr_2$ and $TiCrMn$ intermetallic compounds. The results showed the presence of brittle intermetallic compounds in alloys caused their serious deterioration in tensile properties. In addition, the HU-06 alloy with the Md_t value of 2.32 showed the highest σ_{UTS} value of 984 MPa and ϵ_f value of 10.32 % in as-cast condition among five alloys with Bo_t value of 2.81. The alloys at the Bo_t value of 2.81 showed the poor tensile properties with Md_t values less than 2.28 which was caused by the occurrence of $TiCr_2$ and $TiCrMn$ intermetallic compounds. The HU-01, -02 and -06 alloys showed the satisfaction in objective values of mechanical properties in as-cast and solution treated conditions, which led to development of alternate materials to the conventional β -type Ti alloys, since they reduced energy consumption and production costs by omitting complex post processing procedures.

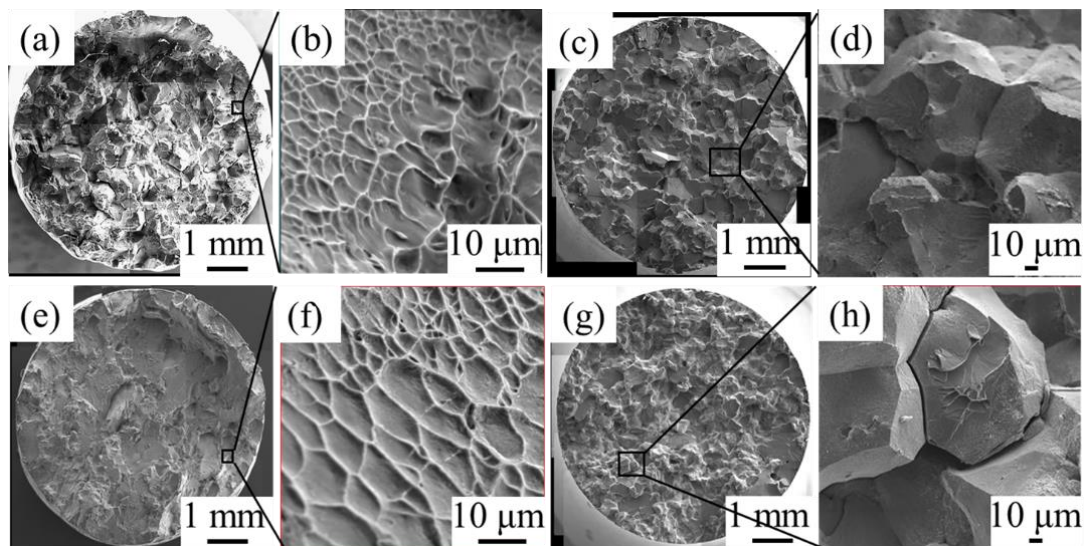


Fig. 3-13 Low and high magnified fractographies of tensile specimens of (a) and (b) for HU-02, (c) and (d) for HU-03, (e) and (f) for HU-06, and (g) and (h) for HU-07 alloys at as-cast condition, respectively.

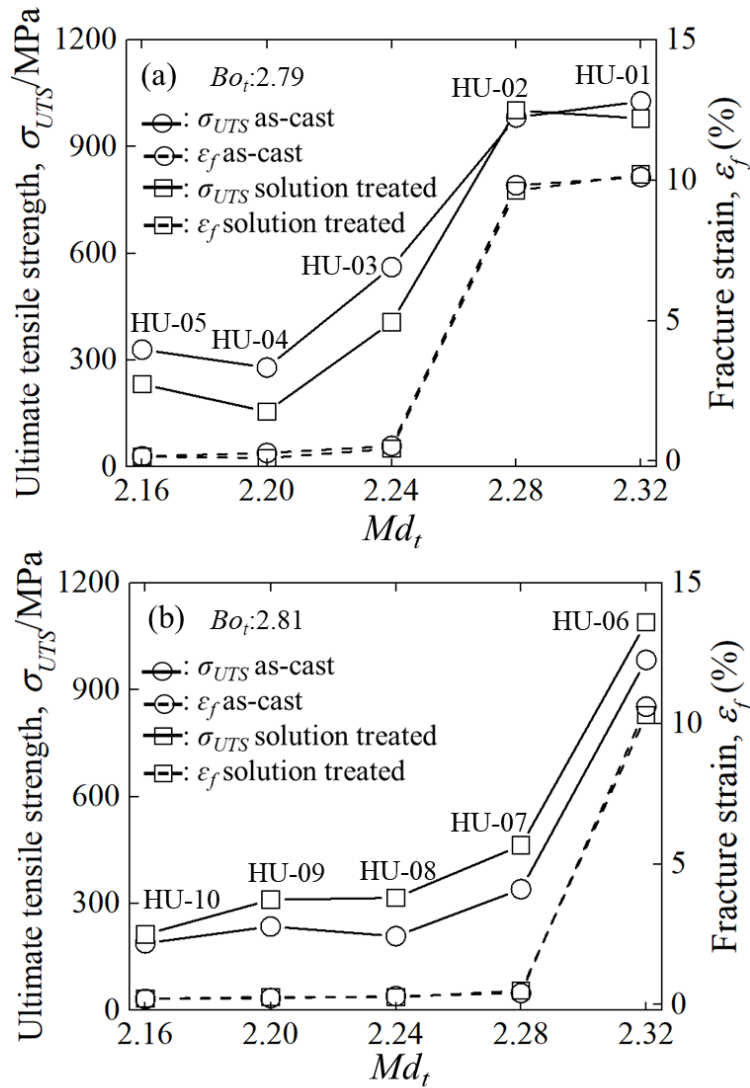


Fig. 3-14 Relation between the σ_{UTS} or ϵ_f and Md_t of (a) HU-01 to HU-05 and (b) HU-06 to HU-10 alloys in as-cast and solution treated conditions.

3.4.3 Vickers hardness

The Vickers hardness of ten types of β -Ti alloys in as-cast and solution treated conditions are shown in Fig. 3-15 (a) and (b). The Vickers hardness values of HU-01 to HU-10 alloys in as-cast and solution treated conditions were 325 and 332, 345 and 355, 366 and 372, 388 and 411, 422 and 466, 358 and 371, 410 and 433, 423 and 441, 436 and 446, 440 and 467, respectively. All the alloys excepted for HU-01, showed the lower Vickers hardness value in as-cast condition than that of solution treated condition. The Vickers hardness values increased with decreasing Md_t values by the solid solution

hardening for the alloys with same Bo_t value of either 2.79 or 2.81. Namely, the alloys with lower Md_t value meant the higher addition amount of β stabilized elements, possessing the superior solid solution hardening. The existence of $TiCr_2$ intermetallic compound led to the improvement in the hardness property of the reference 15-3-3-3 alloy which was attributed to the higher hardness of $TiCr_2$ intermetallic compound compared with that of its alloy matrix.⁴⁸⁾ The HU-05 alloy showed 29.8 and 40.7 % improvement in Vickers hardness values compared with those of HU-01 alloy in as-cast and solution treated conditions. While, the HU-10 alloy showed 22.9 and 25.6 % improvement in Vickers hardness values compared with those of HU-06 alloy in as-cast and solution treated conditions, respectively. Moreover, for the HU-06 alloy with Bo_t value of 2.81 showed higher Vickers hardness values than that of HU-01 alloy with Bo_t value of 2.79, which were attributed to effect of the Bo_t value correlating with the mechanical properties.¹⁵⁾ According to the chemical compositions of ten alloys and their respective Vickers hardness values, it was known that the Vickers hardness of five alloys with Md_t value of 2.79 were dominantly influenced by the changing in contents of intermetallic compounds, as shown in Figs. 3-7 (a) and 3-15 (a).

3.4.4 As-cast application possibility of proposed alloys in the newly expanded area in the Bo_t - Md_t diagram

There was agreement in the stress-strain curves and hardness values between its as-cast and solution treated samples for the mono β phase alloys of HU-01, -02 and -06. Their alloys even at the as-cast condition showed the excellent values in tensile properties, meaning the satisfaction in the initial objective values and the possibility of as-cast applications. The exact prediction of the phase boundary between the mono β phase and dual β plus intermetallic compound phases could be proposed in the newly expanded area large differing from compositional positions of conventional β alloys in the Bo_t - Md_t diagram.

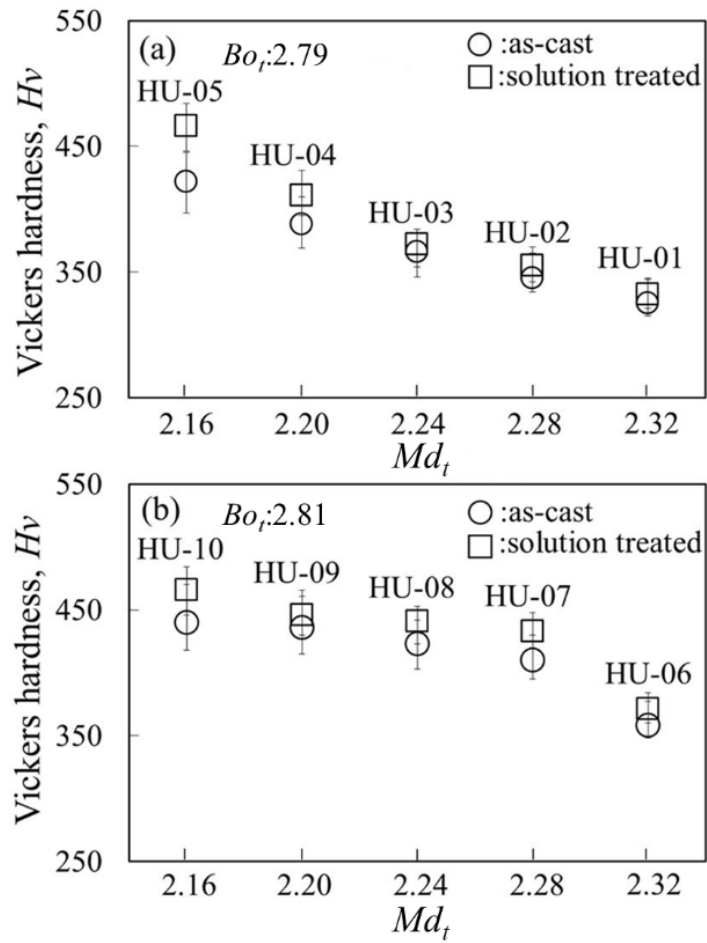


Fig. 3-15 Vickers hardness of (a) HU-01 to HU-05 and (b) HU-06 to HU-10 alloys in as-cast and solution treated conditions.

3.5 Summary

(1) The ten newly proposed alloys which were produced by the CCLM technique as the single manufacturing process, and their microstructures were approximately controlled to the same level at both as-cast and after solution treated conditions. The distribution of equiaxed and columnar grains in ingot were evaluated by the rectangle blocks and the cutting positions for tensile specimens were chosen in the upper part of ingot with equiaxed grains.

(2) The line among the HU-02, HU-03, HU-06 and HU-07 alloys indicating the phase boundary between the mono β phase and dual β plus intermetallic compound phases, were successful identified in the newly expanded area of Bo_t - Md_t diagram for the first time. The existence of brittle intermetallic compounds in proposed alloys caused their serious deterioration in tensile properties. The HU-01, HU-02 and HU-06 alloys, with mono β phase, showed the satisfaction in objective values of mechanical properties even at as-cast condition, which led to development of alternative materials to the conventional β -Ti alloys, since they reduced energy consumption and production costs by omitting complex post-treatments.

(3) For the alloys with same Bo_t value of either 2.79 or 2.81, the Vickers hardness values increased with decreasing Md_t values by the effect of solid solution hardening and the existence of hard intermetallic compounds. There were similar hardness values in both as-cast and solution treated specimens.

(4) The prediction of the phase boundary between the mono β phase and dual β plus intermetallic compound phases could be proposed in the newly expanded area large differing from compositional positions of conventional β alloys, indicating the possibility area in the Bo_t - Md_t diagram to develop β -Ti for as-cast applications.

References

- 1) A.H. Hussein, M.A.H. Gepreel, M.K. Gouda, A.M. Hefnawy and S.H. Kandil: *Mater. Sci. Eng. C.* **61** (2016) 574-578.
- 2) E. Eisenbarth, D. Velten, M. Muller, R. Thull and J. Breme: *Biomaterials.* **25** (2004) 5705-5713.
- 3) Z.Y. Yang, X.H. Zheng and W. Cai: *Scri. Mater.* **99** (2015) 97-100.
- 4) Y. Zhou, S.F. Wen, B. Song, X. Zhou, Q. Teng, Q.S. Wei and Y.S. Shi: *Materials and Design.* **89** (2016) 1199-1204.
- 5) M. Akita, Y. Uematsu, T. Kakiuchi, M. Nakajima, Y. Bai and K. Tamada: *Mater. Sci. Eng. A.* **627** (2015) 351-359.
- 6) R.R. Boyer and R.D. Briggs: *J. Mater. Eng. Perform.* **14** (2005) 681-685.
- 7) F. Sun, J.Y. Zhang, M. Marteleur, C. Brozek, E.F. Rauch, M. Veron, P. Vermaut, P.J. Jacques and F. Prima: *Scri. Mater.* **94** (2015) 17-20.
- 8) J.N. Laboulais, A.A. Mata, V.A. Borrás and A.I. Muñoz: *Electrochimic. Acta.* **227** (2017) 410-418.
- 9) K. Matsugi, H. Kishimoto, D. Yamakawa, Z.F. Xu and Y.B. Choi: *Mater. Trans.* **56** (2015) 1747-1755.
- 10) S.H. Hong, Y.J. Hwang, S.W. Park, C.H. Park, J.T. Yeom, J.M. Park and K.B. Kim: *J. Alloy. Compd.* **793** (2019) 271-276.
- 11) D. Banerjee and J.C. Williams: *Acta Mater.* **61** (2013) 844-879.
- 12) N. Sakaguchi, M. Niinomi, T. Akahori, J. Takeda and H. Toda: *Mater. Sci. Eng. C.* **25** (2005) 363-369.
- 13) S. Sadeghpour, S.M. Abbasi, M. Morakabati, A. Kisko, L.P. Karjalainen and D.A. Porter: *J. Alloy. Compd.* **746** (2018) 206-217.
- 14) Y. Mantani and M. Tajima: *Mater. Sci. Eng. A.* **438-440** (2006) 315-319.
- 15) M. Morinaga, N. Yukawa, T. Maya, K. Sone and H. Adachi: *Proc. 6th World Conf. on Ti, TMS, (1988)* 1601-1606.
- 16) M.A. Hady, K. Hinoshita and M. Morinaga: *Scri. Mater.* **55** (2006) 477-480.
- 17) K. Matsugi, T. Endo, Y.B. Choi and G. Sasaki: *Mater. Trans.* **51** (2010) 740-748.

- 18) K. Matsugi, Y. Murata, M. Morinaga and N. Yukawa: *Sci. Eng. A.* **172** (1993) 101-110.
- 19) K. Matsugi, T. Kashiwagi, Y.B. Choi and G. Sasaki: *Mater. Trans.* **52** (2011) 2189-2196.
- 20) Z.F. Xu, Y.B. Choi, T. Niimi, M. Yu, S. Motozuka, K. Matsugi and K. Suetsugu: *Mater. Trans.* **57** (2016) 553-557.
- 21) M.Q. Yu, K. Matsugi, Z.X. Xu, Y.B. Choi, J.K. Yu, S. Motozuka, Y. Nishimura and K. Suetsugu: *Mater. Trans.* **59** (2018) 303-310.
- 22) K. Matsugi, S. Yamamura, Z.F. Xu, Y.B. Choi, K. Sugio, G. Sasaki and N. Oda: *Mater. Trans.* **56** (2015) 1675-1682.
- 23) M. Morinaga: *Mater. Trans.* **57** (2016) 213-226.
- 24) X.L. Ma, K. Matsugi, Z.F. Xu, Y.B. Choi, R. Matsuzaki, J. Hu, X.G. Liu and H. Huang: *Mater. Trans.* **60** (2019) 2426-2434.
- 25) T. Koyama: *J. Japan. Inst. Metals.* **73** (2009) 891-905.
- 26) I. Ansara, B. Sundman and P. Willemin: *Acta Metall.* **36** (1988) 977-982.
- 27) H.S. Kim, S.H. Lim, I.D. Yeo and W.Y. Kim: *Mater. Sci. Eng. A.* **449-451** (2007) 322-325.
- 28) H. Dong and X.Y. Li: *Mater. Sci. Eng. A.* **280** (2000) 303-310.
- 29) W.J. Joost, S. Ankem and M.M. Kuklja: *Acta. Mater.* **105** (2016) 44-51.
- 30) E.T. Gutelmacher and D. Eliezer: *JOM.* September (2005) 46-49.
- 31) K. Matsugi, G. Sasaki and O. Yanagisawa: *Mater. Trans.* **48** (2007) 195-204.
- 32) A. Gagnoud, J. Etay and M. Garnier: *Trans. ISIJ.* **28** (1988) 36-40.
- 33) M.F. Ijaz, D. Laillé, L. Héraud, D.M. Gordin, P. Castany and T. Gloriant: *Mater. Lett.* **177** (2016) 39-41.
- 34) C. Brozek, F. Sun, P. Vermaut, Y. Millet, A. Lenain, D. Embury, P.J. Jacques and F. Prima: *Scr. Mater.* **114** (2016) 60-64.
- 35) M. Morinaga, M. Kato, T. Kamimura, M. Fukumoto, I. Harada and K. Kubo: *Proc. 7th World Conf. on Ti, TMS,* (1992) 217-224.
- 36) N. Niwa, T. Demura and K. Ito: *ISIT. Int.* **30** (1990) 773-779.
- 37) M. Ikeda: *JJILM,* **55** (2005) 97-102.
- 38) A.K. Dahle, Y.C. Lee, M.D. Nave, P.L. Schaffer and D.H. Stjohn: *JLM.* **1** (2001)

61-72.

- 39) V.B. Deev, V.A. Degtyar, A.I. Kutsenko, I.F. Selyanin, and A.P. Voitkov: *Metallurgist*, **58** (2015) 1123-1127.
- 40) P. Castany, T. Gloriant, F. Sun and F. Prima: *C.R. Physique* **19** (2018) 710-720.
- 41) M. Morinaga, J. Saito and M. Morishita: *JJILM*, **42** (1992) 614-621.
- 42) M. Morishita, M. Chikuda, Y. Ashida, M. Morinaga, N. Yukawa and H. Adachi: *Mater. Trans. JIM*, **32** (1991) 264-271.
- 43) B.S. Murty, S.A. Kori and M. Chakraborty: *Int. Mater. Rev.* **47** (2002) 3-29.
- 44) K. Matsugi, H. Mamiya, Y.B. Choi, G. Sasaki, O. Yanagisawa and H. Kuramoto: *Int. J. Cast. Metal. Res.* **21** (2008) 156-161.
- 45) X.M. Peng, C.Q. Xia, K. Ma and X.Y. Dai: *Mater. Chem. Phys.* **107** (2008) 158-163.
- 46) S. Zholdayakova, R. Gemma, H.H. Uchida, M. Sato and Y. Matsumura: *e-J. Surf. Sci. Nanotech.* **16** (2018) 298-301.
- 47) Z.S. Nong, J.C. Zhu, X.W. Yang, Y. Cao, Z.H. Lai, Y. Liu and W. Sun: *Solid State Sci.* **32** (2014) 1-7.
- 48) H.C. Lina and L.M. Wang: *Mater. Chem. Phys.* **126** (2011) 891-897.

Optimization of both composition and manufacturing process for α -type titanium alloys and their characterizations

<i>4.1 Introduction</i>	<i>92</i>
<i>4.2 Alloy design for the α alloys in the Bo_T-Md_t diagram</i>	<i>94</i>
<i>4.3 Experimental procedure</i>	<i>98</i>
<i>4.3.1 Materials and manufacturing processes</i>	<i>98</i>
<i>4.3.2 Evaluation of some properties</i>	<i>99</i>
<i>4.4 Results and discussion.....</i>	<i>103</i>
<i>4.4.1 Microstructures</i>	<i>103</i>
<i>4.4.2 Tensile properties</i>	<i>107</i>
<i>4.4.3 Hot salt corrosion resistance abilities</i>	<i>112</i>
<i>4.4.4 The mechanism of hot salt corrosion test of titanium alloys.....</i>	<i>118</i>
<i>4.5 Summary.....</i>	<i>121</i>
<i>References</i>	<i>123</i>

4.1 Introduction

α -type titanium (α -Ti) alloys which contain α stabilizing (aluminum) and neutral elements (zirconium and tin) are widely used for chemical, cryogenic applications and building materials of offshore drilling, due to their high specific resistance, low magnetic susceptibility, low specific heat, low thermal conductivity, high electrical resistivity ability ¹⁻⁵). When small amount of β stabilizing elements (molybdenum, vanadium, silicon, and copper etc.) were added in the α -Ti alloys, the β phase occurred in alloys with the fraction of less than 5 wt.%, which is named near- α titanium alloys ¹). The near- α titanium alloys were widely used for high-temperature applications in aircraft engines, because of their excellent combination of high-temperature strength and lightweight properties ⁵). However, it was found that the reactions between α and near- α titanium alloys and salts in the air above ocean at elevated temperatures limited the service life of α and near- α titanium alloys ⁶). To solve this problem and further expand the application fields of α titanium alloys, the development of new α and near- α titanium alloys with improved mechanical strength and corrosion resistance ability was important.

In the past, the design of Ti alloys mainly relying on the repeated experiments and some empirical rules which were high cost and inefficient, until the proposed of d-electrons concept which is based on the theoretical calculation of electronic structures of alloys ⁷). The application of Dv-X α method to design β -type titanium alloys were widely used and accepted ⁸). In contrast, the reliability of Dv-X α method to design α and near- α titanium alloy were still not well checked. In our group, the dependability of Dv-X α method on design α and near- α titanium alloy were estimated ⁹). Moreover, the mechanical properties of α and near- α titanium alloys are usually affected by the presence of impurities ^{10, 11}). The impurities in titanium alloys would lead to the variation properties ^{12, 13}). Therefore, it is also important to develop Ti alloys with extra low interstitial (ELI) level composition to control their performances. The source of these impurities usually derives from the gas environment of furnace and the contaminations of the crucible. The cold crucible levitation melting (CCLM) technique can prevent impurities from contaminating and control the vacuum level in furnace ¹⁴.

¹⁵⁾ The molten material can be levitated by the eddy current in the melting crucible and melted without any contact between materials and the crucible. The cooling solidification rate of molten alloys could appropriately control by CCLM. A uniform composition of Ti alloys is obtained by the diffusion mixing effect and strong stirring from the electromagnetic force.

In the present study, new designed alloy was proposed on the microstructural and mechanical properties prediction lines in the in the Bo_t - Md_t diagram with both electron parameters (Bo_t and Md_t). The mechanical properties and corrosion resistance of new designed alloy Ti-5Al-4Zr-3.6Sn (Bo_t : 2.422, Md_t : 3.430), modified alloy Ti-6Al-1.7Sn-1.3Zr (Bo_t : 2.422, Md_t : 3.485) and reference alloy Ti-5Al-2.5Sn (Bo_t : 2.422, Md_t : 3.485) were compared in both as-cast and solution treatment. The values of 790 MPa and 15% in the σ_{UTS} and fracture strain (ϵ_f) of practically reference alloy were set as objectives. The corrosion resistance ability of Ti-5Al-2.5Sn was chosen as target value. The relationship between corrosion resistance ability and Md_t values of three α alloys were discussed in this section. In addition, the design near- α titanium Ti-6Al-2Sn-5Zr-1Mo-0.3Si (Bo_t : 2.427, Md_t : 3.489), the modified near- α titanium alloy Ti-6Al-3Sn-9Zr-1Cu-0.2Si was proposed with same bond order (Bo) value of 2.424 and d-orbital energy level (Md) value of 3.485 eV to the reference alloy Ti-6Al-2.7Sn-4Zr-0.4Mo-0.45Si. One of the most recently developed commercial near- α titanium alloy TIMETAL 1100 with the chemical compositions of Ti-6Al-2.75Sn-4Zr-0.4Mo-0.45Si (mass%) was chosen as reference alloy. The reference alloy was developed by America with ultimate tensile strength (σ_{UTS}) value of 1000 MPa and fracture strain (ϵ_f) value of 10% after solution treatment (ST) and hot working processes. These values and the corrosion resistance ability of reference alloy were also chosen as objectives. All experimental alloys were produced by the CCLM technique as the single manufacturing process, and their microstructural were controlled by CCLM with same cooling solidification condition. The mechanical properties and hot salt corrosion resistance of experimental α and near- α titanium alloys in both as-cast and solution treated conditions were evaluated in this paper.

4.2 Alloy design for the α alloys in the Bo_t - Md_t diagram

New designed α -type titanium alloys were proposed with both electron parameters (Bo_t and Md_t). The chemical composition of two new α -Ti alloys were designed based on the cluster DV- $X\alpha$ method. And the parameter values of each element were calculated on the MTi_{18} cluster model in the case of hcp Ti ^{16, 17}), as shown in Fig. 4-1, their mean values of Bo_t and Md_t were calculated from the following equations (4-1) and (4-2).

$$Bo_t = \sum X_i (Bo)_i \quad (4-1)$$

$$Md_t = \sum X_i (Md)_i \quad (4-2)$$

Where X_i is the molar fraction of component i in the alloy, $(Md)_i$ and $(Bo)_i$ were the numerical values of Bo_t and Md_t for each component i , respectively. The respective Bo and Md values for each alloying element in hcp Ti are shown in Table 4-1. The alloying effect of each element in Ti and the boundaries of α , $\alpha+\beta$ and β phases was shown in Fig. 4-2. The vectors in the Bo_t - Md_t diagram represented the location of Ti-10 wt.% M binary alloys (M: alloying element in the binary alloy).

The locations of α type new designed alloy Ti-5Al-4Zr-3.6Sn (Md_t : 2.430, Bo_t : 3.487), modified alloy Ti-6Al-1.7Sn-1.3Zr (Md_t : 2.422, Bo_t : 3.487) and reference alloy Ti-5Al-2.5Sn (Md_t : 2.422, Bo_t : 3.487) in the Bo_t - Md_t diagram and the boundaries of α , $\alpha+\beta$ and β phases are shown in Fig. 4-3. The boundaries were identified by observing the phase types in the dozens of commercial and reported alloys ^{18, 19}). These results calculated on

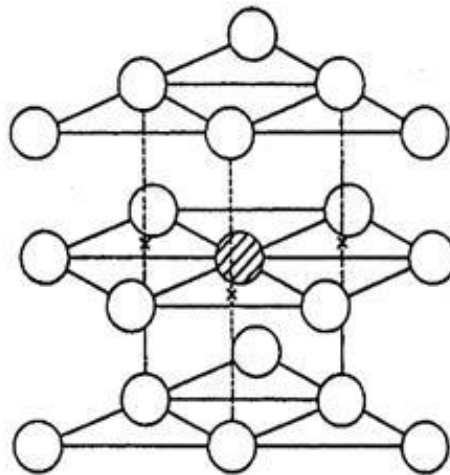


Fig. 4-1 MTi_{18} cluster model in the case of hcp Ti.

Table 4-1 List of Bo and Md values for alloying elements in hcp Ti.

3d transition metals	Bo	Md	4d transition metals	Bo	Md	5d transition metals	Bo	Md
Ti	3.513	2.447	Zr	3.696	2.934	Hf	3.664	2.975
V	3.480	1.872	Nb	3.767	2.424	Ta	3.720	2.531
Cr	3.485	1.478	Mo	3.759	1.961	W	3.677	2.072
Fe	3.428	0.969	Non-transition metals	Bo	Md			
Co	3.368	0.807	Al	3.297	2.200			
Ni	3.280	0.724	Si	3.254	2.200			
Cu	3.049	0.567	Sn	2.782	2.100			

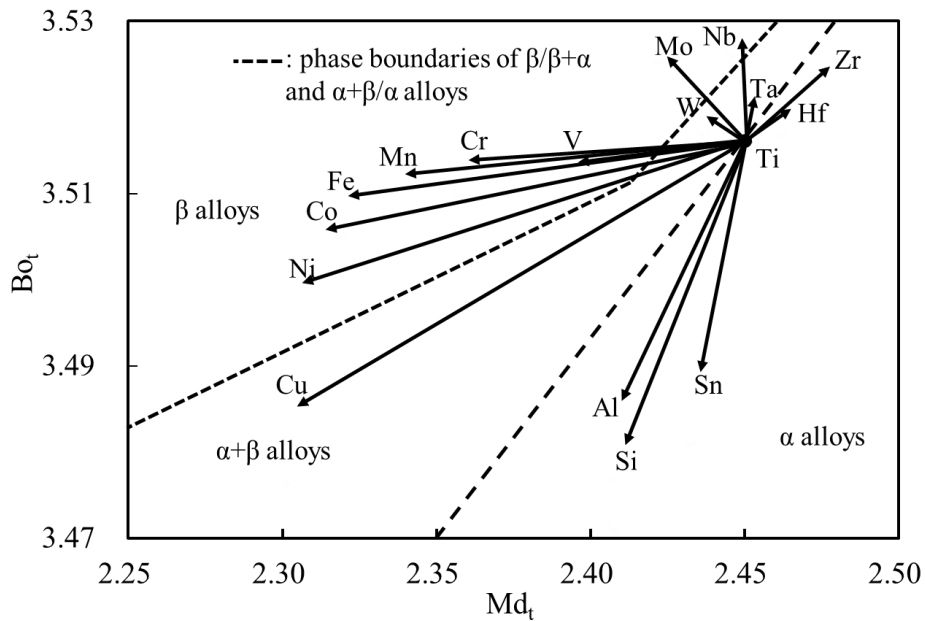


Fig. 4-2 The Bo_t - Md_t line of Ti-M binary alloys. The vectors represent the location of Ti-10mass%M. (M is alloying element in binary alloy)

the MTi₁₈ cluster model in the case of hcp Ti were agreement with calculation results of bcc Ti cluster model. The modified alloy was chosen the same Bo_t and Md_t values with those of reference alloy. The contour lines estimating the σ_{UTS} values could be indicated by connecting the reported α and near- α titanium alloys in the Bo_t - Md_t diagram. The reference α titanium alloy Ti-5Al-2.5Sn and modified α titanium alloy Ti-6Al-1.7Sn-1.3Zr were located in the contour line with the σ_{UTS} value of above 700 MPa. The designed alloy Ti-5Al-4Zr-3.6Sn was proposed inside the contour line with the σ_{UTS} value of above 800 MPa. The locations of near- α type new designed alloy Ti-6Al-4Zr-2Sn-2Mo-0.3Si (Md_t : 2.427, Bo_t : 3.489), modified alloy Ti-6Al-9Zr-3Sn-1Cu-0.2Si (Md_t : 2.424, Bo_t : 3.485) and reference alloy Ti-5Al-2.5Sn (Md_t : 2.424, Bo_t : 3.485) in the Bo_t - Md_t diagram, as shown in Fig. 4-4. The respect Bo_t and Md_t values of each α and near- α titanium alloys are shown in Table 4-2. The reference near- α alloy Ti-6Al-4Zr-2.75Sn-0.4Mo-0.45Si and modified near- α alloy Ti-6Al-9Zr-3Sn-1Cu-0.2Si were located in the contour line with the σ_{UTS} value of above 1000 MPa. The designed near- α alloy Ti-6Al-4Zr-2Sn-2Mo-0.3Si was proposed inside the contour line with the σ_{UTS} value of above 1100 MPa.

Table 4-2 The nominal composition, Bo_t and Md_t values of each α and near- α titanium alloys.

Alloys	Compositions (mass%)	Bo_t	Md_t
Designed α -Ti	Ti-5Al-4Zr-3.6Sn	3.487	2.430
Modified α -Ti	Ti-6Al-1.7Sn-1.3Zr	3.487	2.422
Reference α -Ti	Ti-5Al-2.5Sn	3.487	2.422
Designed near- α Ti	Ti-6Al-4Zr-2Sn-2Mo-0.3Si	3.489	2.427
Modified near- α Ti	Ti-6Al-9Zr-3Sn-1Cu-0.2Si	3.485	2.424
Reference near- α Ti	Ti-6Al-4Zr-2.75Sn-0.4Mo-0.45Si	3.485	2.424

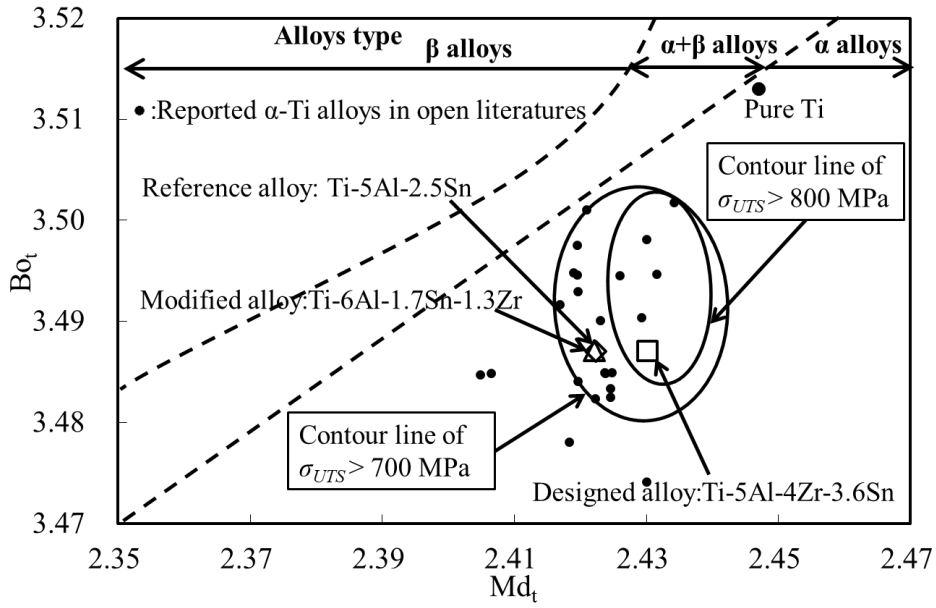


Fig. 4-3 Bo_t - Md_t diagram showing phase boundaries, and contour lines of σ_{UTS} obtained from reported alloys, and the positions of experimental α -Ti alloys.

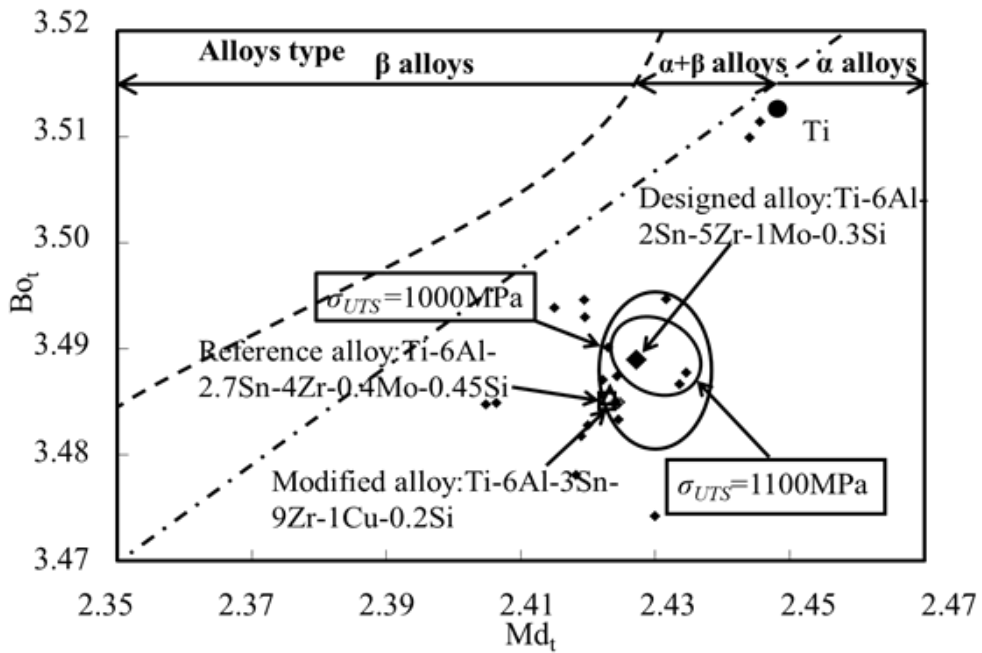


Fig. 4-4 Bo_t - Md_t diagram showing phase boundaries, and contour lines of σ_{UTS} obtained from reported alloys, and the positions of experimental near- α Ti alloys.

4.3 Experimental procedure

4.3.1 Materials and manufacturing processes

For the present study, the purity of raw materials for preparing two near- α titanium alloys were Ti, Al, Zr, Mo, Sn, Cu and Si alloy with 99.8, 99.9, 98.0, 99.0, 98.5, 99.0 and 99.0 mass%, respectively. All ingots were prepared through CCLM (capacity of 1Kg in Fe melt / 100 + 60 kW, Fuji Corporation, Japan) with a water cooled copper crucible, and the atmosphere of CCLM was argon gas with a purity of 99.99%²⁰). Their microstructures were controlled by adjusting its process parameters. The maximum temperature and holding temperature of CCLM are depending on the melting point of alloying elements. Furthermore, to complete melting the raw materials and enough mixing of molten metals, the alloys were holding for 300 s in maximum temperature (2300 K) in melting process, respectively²¹). Finally, the molten metals were cooling and solidified in the copper crucible after switching off electric power in upper and lower coils after the melting process.

The detailed parameters of CCLM equipment during the melting process were shown in Fig. 4-5. The profiles of temperature in molten metal, electric power in upper and lower coils and pressure in atmosphere of levitation melting and cooling process were shown in Fig. 4-5 (a), (b) and (c), respectively. The upper and lower electric coils were utilized for heating by the high-frequency induction and levitation by the eddy current for molten metals. These Ti ingots were prepared in the solidification of the melting Cu crucible under the purity of 99.99 % Ar atmosphere in the present study.

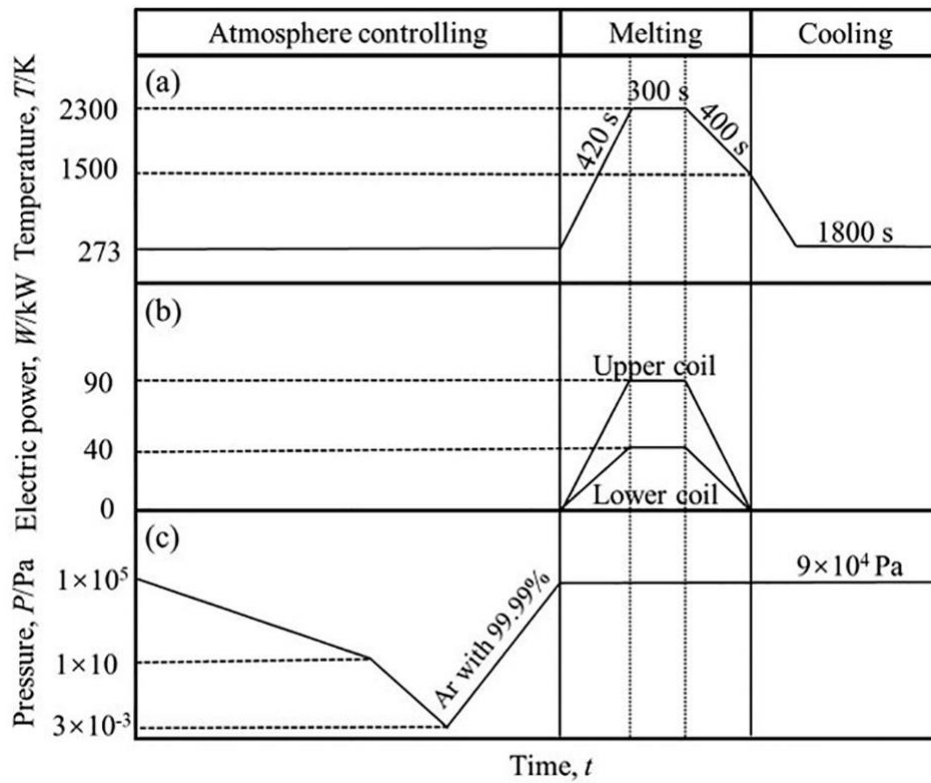


Fig. 4-5 Profiles of (a) temperature in molten metal, (b) electric power in upper and lower coils and (c) pressure in atmosphere of levitation melting and cooling process. Abscissa and ordinate are represented with arbitrary scales.

4.3.2 Evaluation of some properties

The β transus temperature of both α and near- α titanium alloys were measured by the thermal expansion equipment (NETZSCH, German). The solution treatment of α -Ti and near- α titanium alloys were carried out under inert argon atmosphere in 1375 and 12730 K for 7.2 ks, respectively. The solution treatment temperature was decided by the results of thermal expansion test, as shown in Figs. 4-6 and 4-7. The start, peak, and final points were discussed in Fig. 4-6 showing the phase transformation process.

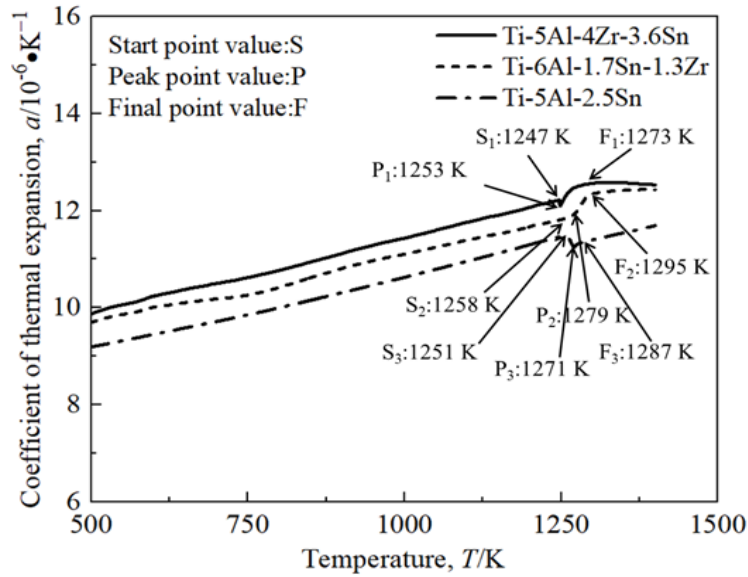


Fig. 4-6 Coefficient of thermal expansion for α titanium of designed alloy Ti-5Al-4Zr-3.6Sn, modified alloy Ti-6Al-1.7Sn-1.3Zr and reference alloy Ti-5Al-2.5Sn.

In order to completely transformed of α phase, usually the solution treatment temperature was set above the temperature of final point. In contrast, the analysis processes were omitted in Fig. 4-7 which just indicating the β transus temperature of near- α titanium alloys.

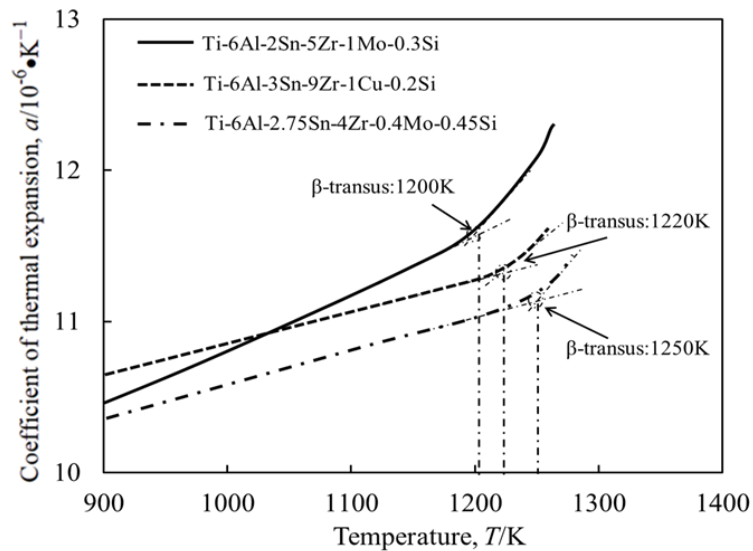


Fig. 4-7 Coefficient of thermal expansion for near- α titanium alloy of designed alloy Ti-6Al-4Zr-2Sn-2Mo-0.3Si, modified alloy Ti-6Al-9Zr-3Sn-1Cu-0.2Si and reference alloy Ti-6Al-4Zr-2.75Sn-0.4Mo-0.45Si.

All ingots were encapsulated in quartz tubes before solution treatment and then water-quenched through breaking the quartz tubes. In order to check the solution treatment time, the diffusion constant and activation energy of the element Zr with the largest activation energy in the composition were investigated, and the longest distance 971.43 μ m of the maximum distance in one grain was taken as the diffusion distance. The solution treatment time of the alloy is obtained using the following formula (4-3) and (4-4) ²²⁾:

$$D = D_0 \exp[-\Delta H / (RT)] \quad (4-3)$$

$$X \approx (Dt)^{1/2} \quad (4-4)$$

Where the D is Diffusion coefficient, D_0 is Diffusion constant, ΔH is the activation energy, R is gas constant and T is the heat treatment temperature. In addition, the X means diffusion distance and t corresponding to heat treatment time.

The microstructures of alloys were observed by optical microscope (OM) in as-cast condition and after ST. The specimens were grinded, polished and etched by using sandpapers from 80 to 2500 mesh, different grades of polishing paper and a mixed solution of distilled water, nitric acid and hydrofluoric acid (95:3:2 in volume ratio), respectively. The microstructural observation of specimens in as-cast and solution treated conditions were carried out by using the OM and image analysis. The constituent phases and lattice constants of ten experimental alloys were identified by X-ray diffraction (XRD) with Cu-K α radiation generated in 40 kV and 30 mA in ambient temperature. The tensile specimens with a gauge size of 6.0 mm in diameter and 20.0 mm in length and a grip of 10.0 mm in diameter were applied in the present study.

The specimens for hot salt corrosion were cut by wire cutting with the size of 10 \times 5 \times 1.5 mm and the six surfaces were grinded with abrasive paper grit 80-2000, respectively. The specimens were precisely weighed before the hot salt corrosion test. Then, the hot salt corrosion test was carried out in molten salts of Na₂SO₄-45mol% NaCl in 923 K for 43.2 ks and the data of weight loss was measured every two hours. The temperature of the hot salt corrosion test was decided by the practice application of titanium alloys as engine materials in aerospace industry. The crucible containing the molten salt is a high-purity alumina crucible with an outer diameter of 46 mm, a height of 36 mm and a capacity of 30 ml. The molten salt in crucible was directly exposed in

the air atmosphere condition, which is similar with the prarticle application conditions. The specimens hanging by a platinum wire to kept the six faces had sufficient contact with the fused salt (Na_2SO_4 -45mol% NaCl)²³). Then, the specimens were immersion in the 9.4 mol% NaOH -0.67 mol% KMnO_4 boiling solution held for 30 min to wash out the solidified salt which were attached on the surfaces of specimen. Subsequently, washing the specimens for 20 min in the 0.88mol% $(\text{NH}_4)_2\text{HC}_6\text{H}_5\text{O}_7$ boiling solution to washed out the residue salt and KMnO_4 . Finally, the specimen was rinsed, dried and weighing, respectively²⁴). The observation of the hot salt corrosion layer was performed via the electron probe micro-analyzer (EPMA). The chemical compositions of experimental alloys were also measured by point analysis via the EPMA (JXA-8200, JEOL Corporation, Japan). The procedure of the hot salt corrosion test was shown in Fig. 4-8.

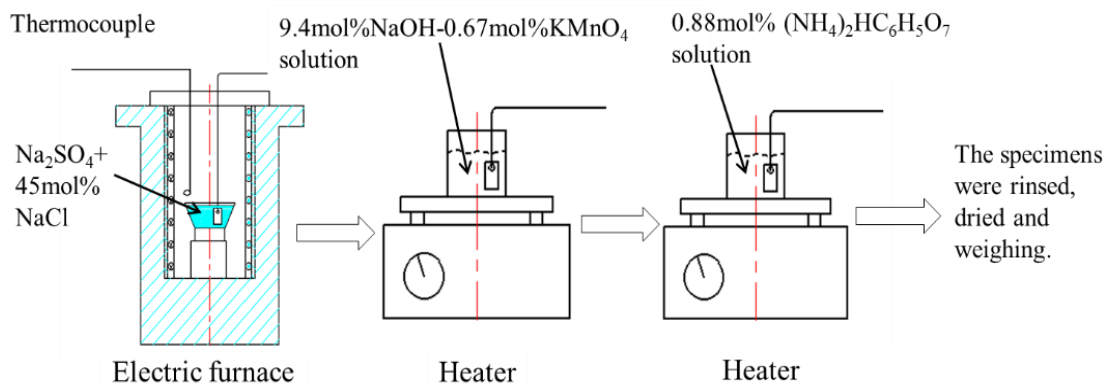


Fig. 4-8 Schematic diagrams of the hot salt corrosion test process.

4.4 Results and discussion

4.4.1 Microstructures

The OM image of designed, modified and reference α -Ti alloys in both as-cast and solution treated conditions were shown in Fig. 4-9 (a)-(f), respectively. The mono α phase with the grain size of about 600 μm were observed in three α -type alloys. In addition, the OM image of designed, modified and reference near- α titanium alloys in as-cast and solution treated conditions were shown in Fig. 4-10 (a)-(f), respectively. The same level of grain size and homogeneous microstructures in both α and near- α titanium alloys were attribute to the effect of CCLM. They were produced by the cold crucible levitation melting (CCLM) technique as the single manufacturing process, which cooling solidification rate were controlled by adjusting its magnitude of current. However, the relative coarse grain size of three α -type alloys compared with that of practically commercial reference alloy were obtained in the present research. The lower mechanical properties of reference alloy Ti-5Al-2.5Sn than those of the practically commercial alloy Ti-5Al-2.5Sn was foreseeable. The lamellae structure with complex orientation were observed in three α -Ti alloy in as-cast condition. Furthermore, for three α -Ti alloy after solution treatment, their layer's thickness become thinner compared with those in as-cast, were measured by the image method. When the alloy solidification from liquid, the β phase formed firstly, the beta phase will transform to the alpha phase with decreasing of temperature. The six slip planes and the two slip directions of the titanium unit cell give a maximum of 12 variants of orientation. This variety of orientations is also reflected in the metallographic microstructure. Within the prior β grains, which can be as large as several millimeters, individual lamellar packets nucleate and grow. There are 12 orientation relationships in the β phase, the individual lamellar packets having a common orientation within them. The large but limited to 12 number of possible orientations results in multiple repetitions of the orientation of the lamellar packets. It is known that the lamellae microstructure is a typical structure of α titanium alloys. The α phase strictly compliance the orientation of prior beta grains. Usually, the α phase grows start from the grain boundary to the inside of grain.

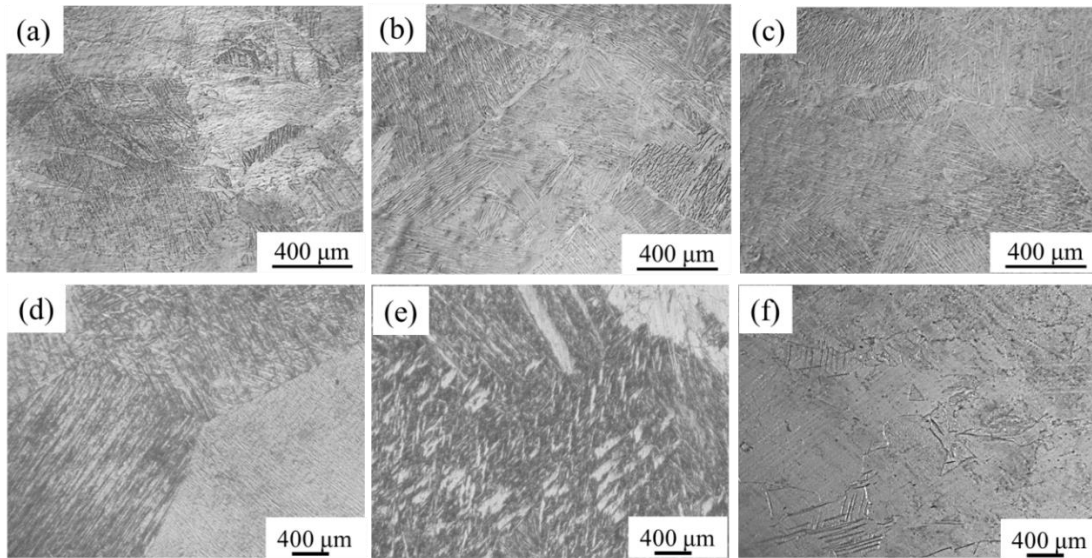


Fig. 4-9 OM images of (a) and (d) Ti-5Al-4Zr-3.6Sn, (b) and (e) Ti-6Al-1.7Sn-1.3Zr, and (c) and (f) Ti-5Al-2.5Sn α titanium alloys in as-cast and solution treated conditions, respectively.

The OM images of three near- α titanium alloys in as-cast and solution treated conditions were shown in Fig. 4-10 (a)-(f). The microstructures of three near- α titanium alloys in as-cast condition is shown in Fig. 4-10 (a), (b) and (c), respectively. The thin films of β phase between adjacent two layers of α interfaces and Widmanstätten microstructure as well as the prior β boundaries were observed in three near- α alloys in as-cast condition. The OM image of modified alloy in as-cast condition showed almost the same microstructure with reference alloy in corresponding condition. However, in solution treated condition, there were acicular α or α' phase occurrence, as shown in Fig. 4-10 (d), (e) and (f), respectively. The solution treatment with water-quenched process usually resulted in the insufficient diffusion of additional elements which caused local increases in the level of the α -stabilizing elements^{25, 26}. The reference alloy in solution treated condition as shown in Fig. 4-10 (f), also showed the coincident microstructures with modified alloy in corresponding condition. Moreover, all three alloys showed difference microstructures between in as-cast condition and after solution treated treatment. For example, the thin films of β phase and α phase of three near- α Ti alloys in as-cast condition were disappeared and the acicular α or α' phase occurred in solution treated condition. Simultaneously, the volume fraction of prior β grain boundaries also decreased in solution treated condition compared with that of as-cast condition, which

should be corresponding to the transformation from β phase to α or α' phase.

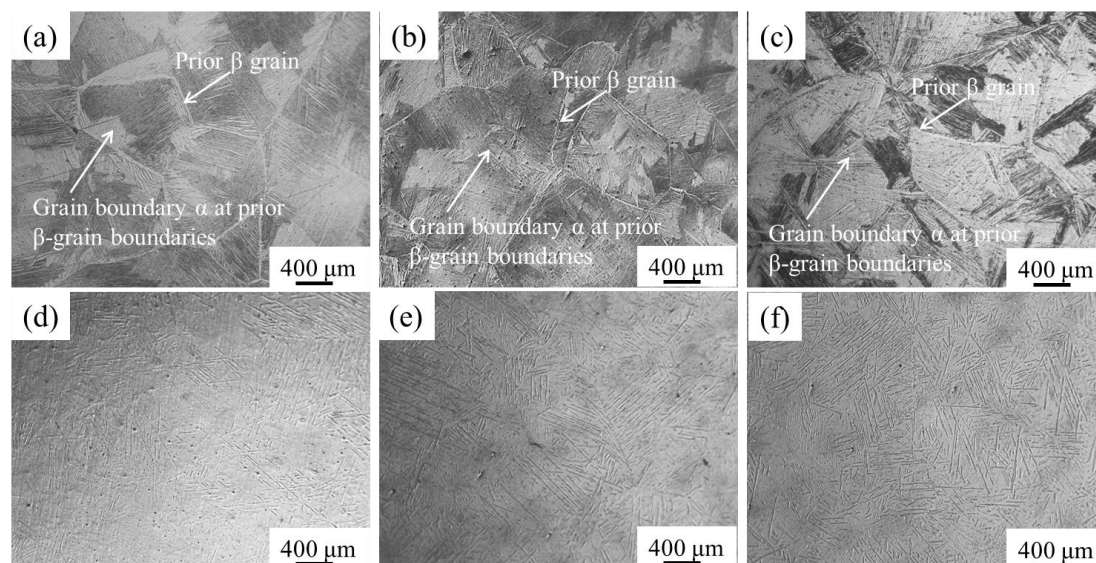


Fig. 4-10 OM images of (a) and (d) Ti-6Al-2Sn-4Zr-2Mo-0.3Si, (b) and (e) Ti-6Al-3Sn-9Zr-1Cu-0.2Si, and (c) and (f) Ti-6Al-2.75Sn-4Zr-0.4Mo-0.45Si near- α titanium alloys in as-cast and solution treated conditions, respectively.

The XRD patterns of experimental α -Ti alloys were shown in Fig. 4-11 (a)-(f), respectively. The XRD patterns showed mono α phase in three α -Ti alloys in both as-cast and solution treated conditions. The increasement in number of peaks appeared in designed α -Ti alloys compared with those of modified and reference α -Ti alloys in the XRD patterns with the occurrence of the colony structure were observed in designed α -Ti alloys. These results were consistent with their locations in the *Bo_r-Md_t* diagram and the microstructures observed by OM images. The XRD patterns of near- α titanium alloys were shown in Fig. 4-12 (a)-(f), respectively. The XRD patterns showed both α and β phases in three near- α titanium alloys in both as-cast and solution treated conditions. For three near- α titanium alloys in as-cast condition, as shown in Fig. 4-12 (a), (c) and (e) corresponding to the designed, modified and reference alloys. Their β phase amount were higher compared with those of designed, modified and reference near- α titanium alloys in solution treated condition, which should be corresponding to the transformation from β phase to α or α' phase. The decreased tendency in β phase amount in three near- α titanium alloys were observed in Fig. 4-12 (b), (e) and (f), with the decreased intensity of β phase in the XRD profiles. The XRD results also showed

highly agreement with the microstructure observations.

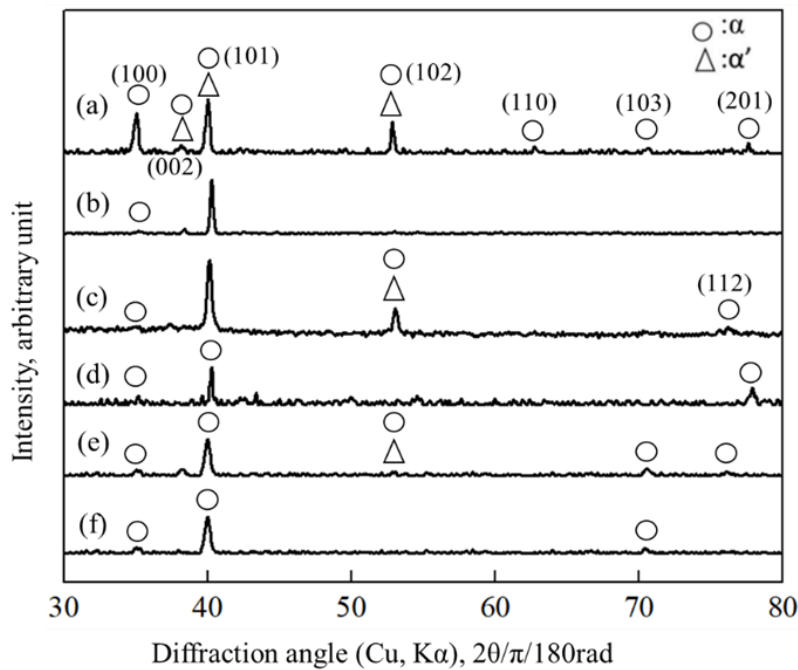


Fig. 4-11 XRD profiles of (a) and (b) Ti-5Al-4Zr-3.6Sn, (c) and (d) Ti-6Al-1.7Sn-1.3Zr and (e) and (f) Ti-5Al-2.5Sn alloys in as-cast and solution treated conditions.

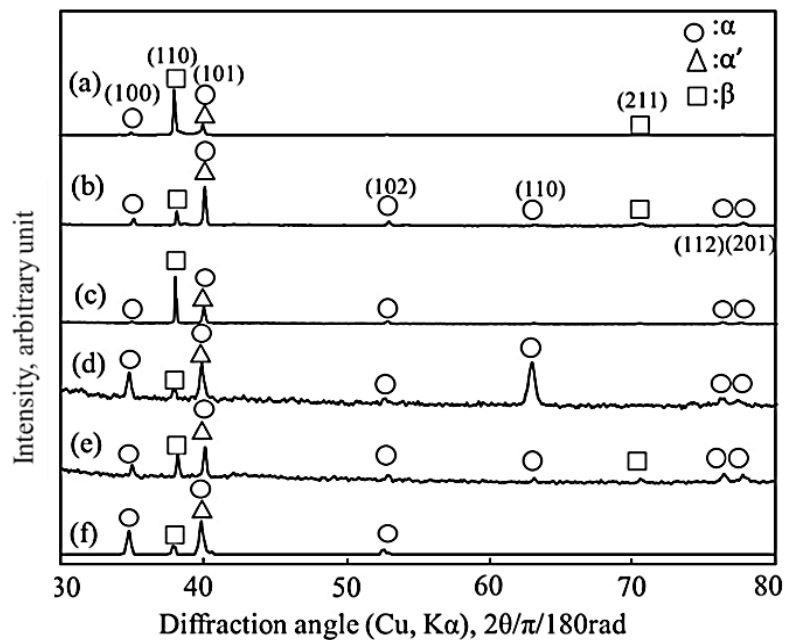


Fig. 4-12 XRD profiles of (a) and (b) Ti-6Al-2Sn-4Zr-2Mo-0.3Si, (b) and (e) Ti-6Al-3Sn-9Zr-1Cu-0.2Si and (c) and (f) Ti-6Al-2.75Sn-4Zr-0.4Mo-0.45Si alloys in as-cast and solution treated conditions.

4.4.2 Tensile properties

The tensile properties of experimental α -Ti alloys were shown in Fig. 4-13. The σ_{UTS} and ϵ_f values were shown on Ti-5Al-4Zr-3.6Sn alloy: 801 MPa, 16% and Ti-6Al-1.7Sn-1.3Zr alloy: 695 MPa, 15%, respectively. Their values were improved, compared with those of reference alloy: 598 MPa, 15%. The different values of experimental alloys in tension was attribute to their different levels of solid solution strengthening. The designed alloy Ti-5Al-4Zr-3.6Sn with optimized composition showed the highest σ_{UTS} value of 801 MPa among three α -Ti alloys. The lower σ_{UTS} value of reference alloy Ti-5Al-2.5Sn (598 MPa) produced by CCLM than that of the practically commercial alloy Ti-5Al-2.5Sn (790 MPa) should be caused by the coarse grain size. This should be the reason for the modified and reference alloys showed disagree in σ_{UTS} values with contour lines predicted results in the present research. The σ_{UTS} and ϵ_f of experimental alloys in solution treated condition were shown in Fig. 4-13. The σ_{UTS} , $\sigma_{0.2}$ and ϵ_f values were shown on designed alloy Ti-5Al-4Zr-3.6Sn alloy: 970, 840 MPa and 13%, modified alloy Ti-6Al-1.7Sn-1.3Zr alloy: 888, 837 MPa and 10% and reference alloy Ti-5Al-2.5Sn: 664, 645 MPa and 17% in solution treated condition, respectively. The α -Ti alloys were commonly free of solution treatment, because of the consideration of phase stability. However, according to the results of the present study, all experimental α -Ti alloys showed improvement in tensile strength in solution treated condition compared with those of three α -Ti alloys in as-cast condition. In addition, the tensile test results indicated that both designed and modified alloys with optimized composition showed better strengthening response to the solution treatment than that of reference alloy. For the α -Ti alloys to be applied in ambient temperature, the solution treatment might be a method to improve their tensile strength as cost save measures. The stress-strain curves of designed, modified and reference alloys were shown in Fig. 4-14. The values of σ_{UTS} and ϵ_f of designed alloy in as-cast condition were 989 MPa and 11.6%, respectively. For modified alloy, it showed the values of σ_{UTS} 993 MPa and ϵ_f of 13.5% in as-cast condition. The stress-strain curve of reference alloy in as-cast condition, the values of σ_{UTS} and ϵ_f were 991 MPa, and 12.7%, respectively. In addition, the values of σ_{UTS} and ϵ_f of designed alloy in solution treated condition were 1118 MPa

and 3.4%. While the values of σ_{UTS} and ϵ_f of modified alloy in solution treated condition were 1354 MPa and 2.3%. The values of σ_{UTS} and ϵ_f of reference alloy were 1238 MPa and 3.1% in solution treated condition. The results indicated the modified alloy possessed comparable mechanical properties with the reference alloy has been successfully designed on the basis of the d-electrons concept. The increasing of σ_{UTS} and drastic decreasing of ϵ_f of three alloys in solution treated condition compared to those in as-cast condition was attributed to the occurrence of acicular α or α' phase. Meanwhile, the precipitate of silicide in the grain boundary of near- α alloys after solution treatment were also widely reported in open literatures.

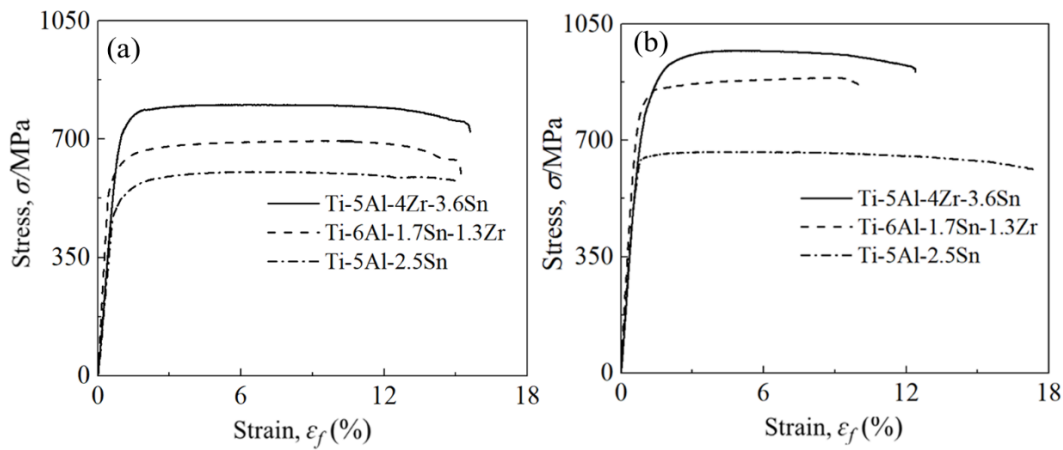


Fig. 4-13 Stress-strain curves of experimental α -Ti alloys in (a) as-cast and (b) solution treated conditions.

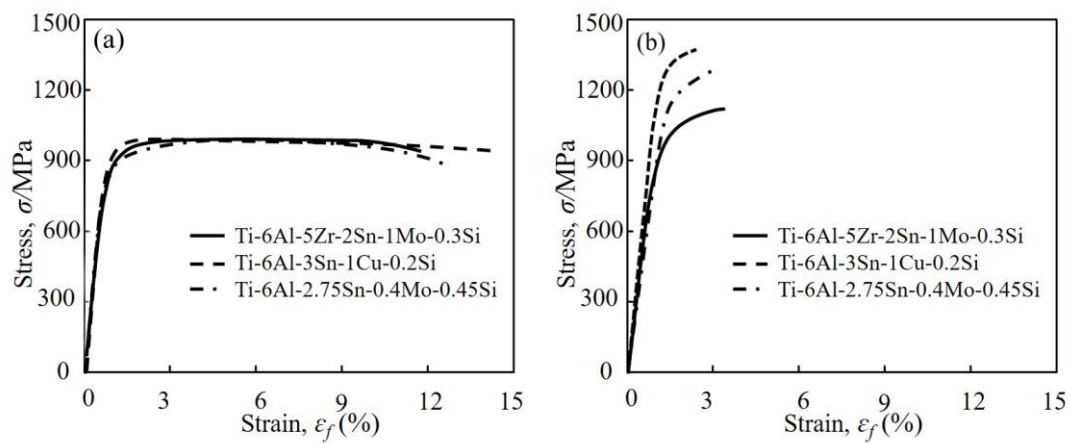


Fig. 4-14 Stress-strain curves of experimental near- α titanium alloys in (a) as-cast and (b) solution treated conditions.

The segregation degree of the Ti-5Al-2.5Sn and Ti-5Al-4Zr-3.6Sn α alloys were compared in the Fig. 4-15 by measuring their concentration profiles. The point analysis was applied to obtain the concentration profiles of both alloys in as-cast and solution treated conditions. The conditions of point analysis were similar with that of previously mentioned in chapter 2. The interval between each two points is 50~60 μm depending on their respective grain sizes. The as-cast and solution treated α -Ti alloys showed larger difference in mechanical properties compared to those of the β -Ti alloys located in the slip area of the *Bo_r-Md_t* diagram. Their segregation degree showed the distribution of alloying elements in α -Ti alloys became more homogeneous after the solution treatment than that of as-cast condition, which was thought as the major impact to the various in mechanical properties. The slightly segregation in β -Ti alloys showed almost no influence on their mechanical properties, as discussed in the chapter 2. However, for the α -Ti alloys, the difference in segregation degree is important and cannot be ignored when evaluating their mechanical properties. The heterogeneity of alloying elements will lead to the various in strength in the different local positions of specimens, because of the solid solution strengthening effect.

The fracture morphologies of three α titanium alloys in as-cast and solution treated conditions were shown in Fig. 4-16 (a)-(f), and their respective corresponded high magnified fractographies were shown in Fig. 4-16 (a')-(f'), respectively. The dimple fracture patterns appeared in three α titanium alloys in both as-cast and solution treated conditions, corresponded to the relative satisfaction ε_f values, as shown in Fig. 4-16 (a')-(f'), respectively. The dimples usually appeared in the ductile-fracture specimens, each dimple corresponding to a void. It is frequently possible to observe the inclusion responsible for nucleating the void within the depth of the dimple. When a material contains relatively hard inclusions which do not deform in the same rate as the matrix, voids are nucleated to accommodate the incompatibility. The nucleation event may involve, for example, the fracture of the inclusion, or decohesion in the inclusion-matrix interface. For the designed α titanium alloy Ti-5Al-4Zr-3.6Sn, which possessed highest amounts of additional elements among three alloys, showed the fine and deep dimples. In contrast, the other two α titanium alloys showed the fracture morphologies of dimples

linking. The voids are also a typical morphology of ductile fracture mode and have been observed in the fractographies of reference alloy Ti-5Al-2.5Sn. The fine and deep dimples were observed in three α titanium alloys in solution treated condition, corresponded to the relative satisfaction ε_f values. The reduction of area (RA) of designed, modified and reference α titanium alloys were 27.4, 18.6 and 22.6 % in as-cast condition, and 20.7, 15.6 and 28.2 % in solution treated condition, respectively.

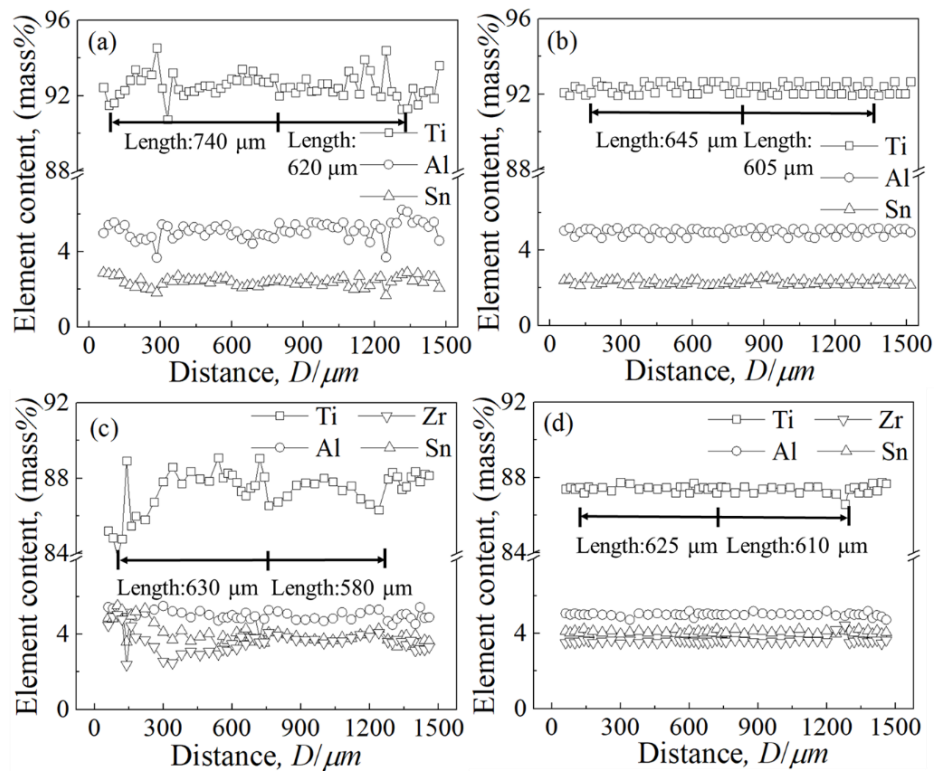


Fig. 4-15 The concentration profiles of alloying elements of (a) and (b) Ti-5Al-2.5Sn, and (c) and (d) Ti-5Al-4Zr-3.6Sn alloys. (a), (c) and (b), (d) were obtained from as-cast and solution treated conditions, respectively.

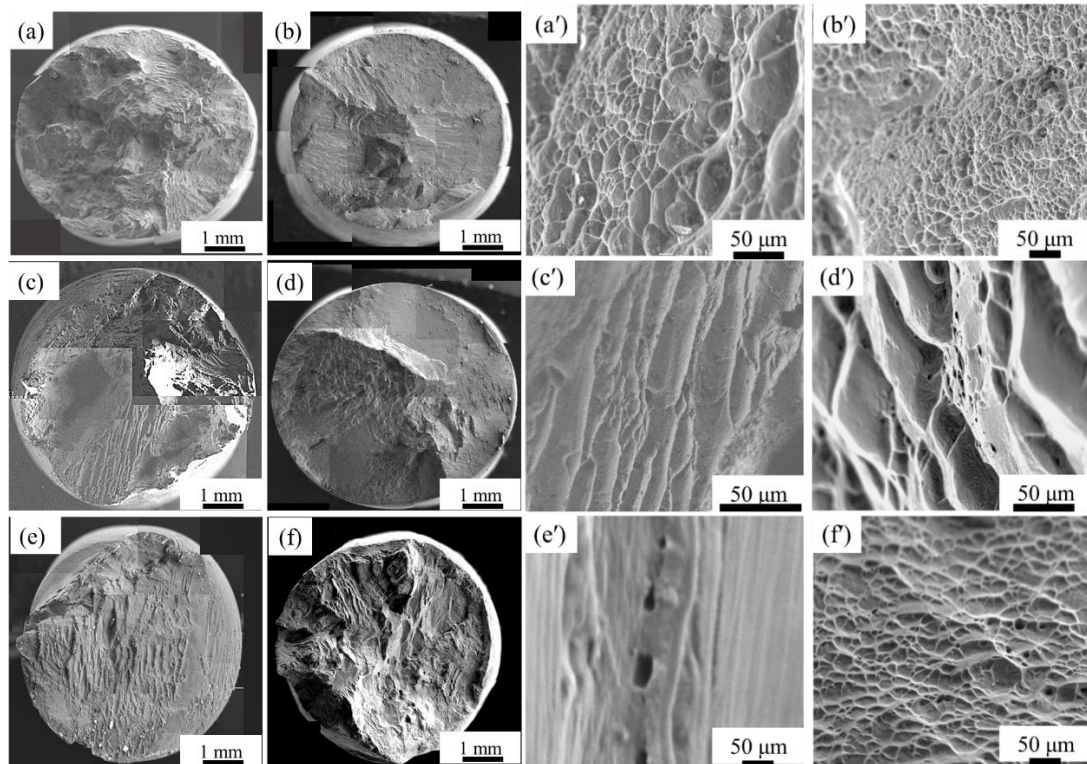


Fig. 4-16 Fractographies of tensile specimens of (a) and (b) Ti-5Al-4Zr-3.6Sn, (c) and (d) Ti-6Al-1.7Sn-1.3Zr and (e) and (f) Ti-5Al-2.5Sn alloys in as-cast and solution treated conditions, and their respective corresponded high magnified fractographies of (a') and (b') Ti-5Al-4Zr-3.6Sn, (c') and (d') Ti-6Al-1.7Sn-1.3Zr and (e') and (f') Ti-5Al-2.5Sn alloys in as-cast and solution treated conditions, respectively.

The fracture morphologies of three near- α titanium alloys in as-cast and solution treated conditions were shown in Fig. 4-17 (a)-(f), and their respective corresponded high magnified fractographies were shown in Fig. 4-17 (a')-(f'), respectively. The dimple fracture patterns appeared in three near- α titanium alloys in as-cast condition, corresponded to the relative satisfaction ϵ_f values, as shown in Fig. 4-17 (a'), (c') and (e'), respectively. In contrast, the brittle fracture patterns were observed in three near- α titanium alloys in solution treated condition, as shown in Fig. 4-17 (b'), (d') and (f'), respectively. The trans-granular were observed obviously in three near- α titanium alloys in solution treated condition. The reduction of area of designed, modified and reference near- α titanium alloys were 13.5, 16.7 and 18.3 % in as-cast condition. While almost no reduction of area of three near- α titanium alloys were measured in solution treated condition.

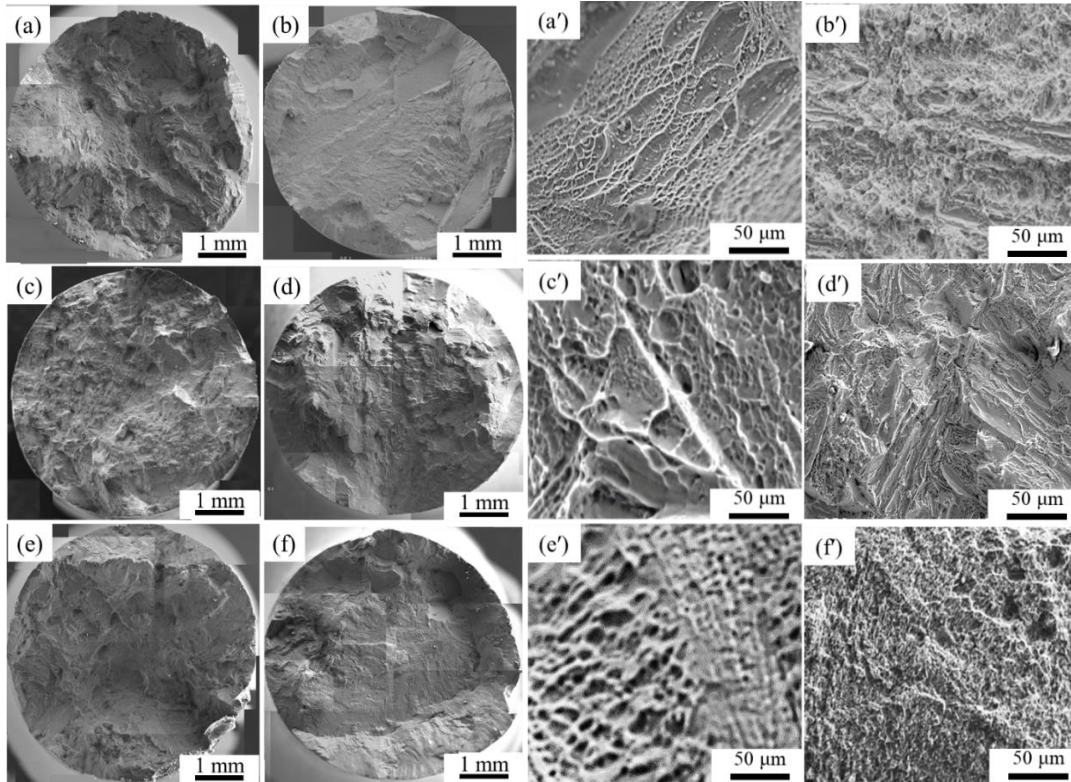


Fig. 4-17 Fractographies of tensile specimens of (a) and (b) Ti-6Al-2Sn-4Zr-2Mo-0.3Si, (b) and (e) Ti-6Al-3Sn-9Zr-1Cu-0.2Si and (c) and (f) Ti-6Al-2.75Sn-4Zr-0.4Mo-0.45Si alloys in as-cast and solution treated conditions, and their respective corresponded high magnified fractographies of tensile specimens of (a') and (b') Ti-6Al-2Sn-4Zr-2Mo-0.3Si, (c') and (d') Ti-6Al-3Sn-9Zr-1Cu-0.2Si and (e') and (f') Ti-6Al-2.75Sn-4Zr-0.4Mo-0.45Si alloys in as-cast and solution treated conditions, respectively.

4.4.3 Hot salt corrosion resistance abilities

The ratio of weight loss results of experimental α and near- α titanium alloys in as-cast and solution treated conditions were shown in Fig. 4-18. The linear regression was established by fitting the immersion time and the ratio of weight loss to initial weight. The ratio of weight loss was 3.81%, 4.16% and 4.87% after 43.2 ks hot salt corrosion test corresponded to the designed, modified and reference α -Ti alloys in as-cast condition, respectively. Both designed and modified alloys showed improvement in hot salt corrosion resistance ability compared with that of reference one, which showed connection to the increasement in content of solute elements. The designed alloy Ti-5Al-4Zr-3.6Sn with the highest content of solute elements showed the highest hot salt

corrosion resistance ability among three alloys. Meanwhile, the reference alloy Ti-5Al-2.5Sn with the lowest content of solute elements showed the lowest hot salt corrosion resistance ability among three α -Ti alloys. The ratio of weight loss was 1.98, 2.37% and 2.44 % after 43.2 ks hot salt corrosion test corresponded to the designed, modified and reference α -Ti alloys in solution treated condition, respectively. In addition, the ratio of weight loss was 2.22, 2.98 and 2.99% after 43.2 ks hot salt corrosion test corresponded to the designed, modified and reference near- α alloys in as-cast condition, respectively. The ratio of weight loss of designed near- α alloy Ti-6Al-4Zr-2Sn-2Mo-0.3Si was 1.99% in solution treated condition. While the ratio of weight loss of modified near- α alloy Ti-6Al-9Zr-3Sn-1Cu-0.2Si was 2.24 % compared with that of 2.51 % of reference alloy in solution treated condition. The ratio of weight loss of six Ti alloys in as-cast and solution treated conditions after 43.2 ks are summarized in Table 4-3.

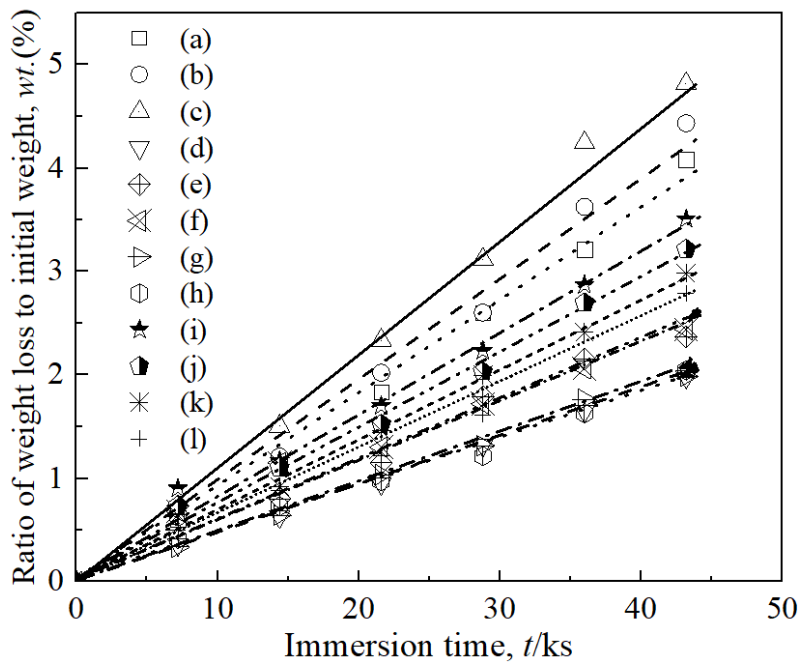


Fig. 4-18 Relation between immersion time and ratio of weight loss to initial weight obtained from immersion in Na_2SO_4 -45mol%NaCl molten salt in 923K for experimental α -Ti alloys (a) and (d) of Ti-5Al-4Zr-3.6Sn, (b) and (e) of Ti-6Al-1.7Sn-1.3Zr, and (c) and (f) of Ti-5Al-2.5Sn in as-cast and solution treated conditions, and for near- α titanium alloys (g) and (j) of Ti-6Al-2Sn-4Zr-2Mo-0.3Si, (h) and (k) of Ti-6Al-3Sn-9Zr-1Cu-0.2Si and (i) and (l) of Ti-6Al-2.75Sn-4Zr-0.4Mo-0.45Si in as-cast and solution treated conditions, respectively.

Table 4-3 The compositions of α and near- α Ti alloys in mass%, the ratio of weight loss of specimens after immersion in molten salts after 43.2 ks, and their Bo_t and Md_t values.

Alloys	Compositions (mass%)	Bo_t	Md_t	Ratio of weight loss (wt.%)	
				As-cast	Solution treated
Designed α -Ti	Ti-5Al-4Zr-3.6Sn	3.487	2.430	3.81	1.98
Modified α -Ti	Ti-6Al-1.7Sn-1.3Zr	3.487	2.422	4.16	2.37
Reference α -Ti	Ti-5Al-2.5Sn	3.487	2.422	4.87	2.44
Designed near- α Ti	Ti-6Al-4Zr-2Sn-2Mo-0.3Si	3.489	2.427	2.72	1.99
Modified near- α Ti	Ti-6Al-9Zr-3Sn-1Cu-0.2Si	3.485	2.424	3.48	2.24
Reference near- α Ti	Ti-6Al-4Zr-2.75Sn-0.4Mo-0.45Si	3.485	2.424	3.49	2.51

To investigate the mechanism of hot salt corrosion and the reliability of the ratio of weight loss results, the compositional images and EPMA mappings of experimental α -Ti alloys after immersion in hot salts for 28.8 ks were shown in Fig. 4-19 (a), (b) and (c), respectively. The cross section of experimental α -Ti alloys showed the thickness of corrosion layers and the elements distribution in alloys after hot salt corrosion test continuously for 28.8 ks. To reduce the measurement error of thickness of corrosion layers, the immersion time was confirmed before the occurrence of corrosion layer shedding from the surface of specimens. The thickness of corrosion layers of designed, modified and reference α -Ti alloys in as-cast condition were 4.98, 5.65 and 7.25 μm , respectively. The thickness of corrosion layers and the ratio of weight loss results showed the designed α -Ti alloy possessing the highest hot salt corrosion resistance ability with the thinnest corrosion layer and the least weight loss compared with those of modified and reference α -Ti alloys. In addition, both the diffusion behavior of solute elements close to or away from the interface between alloy and fused salts and the salt elements diffusion into specimens were not observed in three experimental α -Ti alloys by the EPMA mappings results. The reaction between α -Ti alloys and fused salts was happened on the contact surface of specimens. The surface of specimens showed dense outer oxide layer of oxidation products and porous inner oxide layer. The general

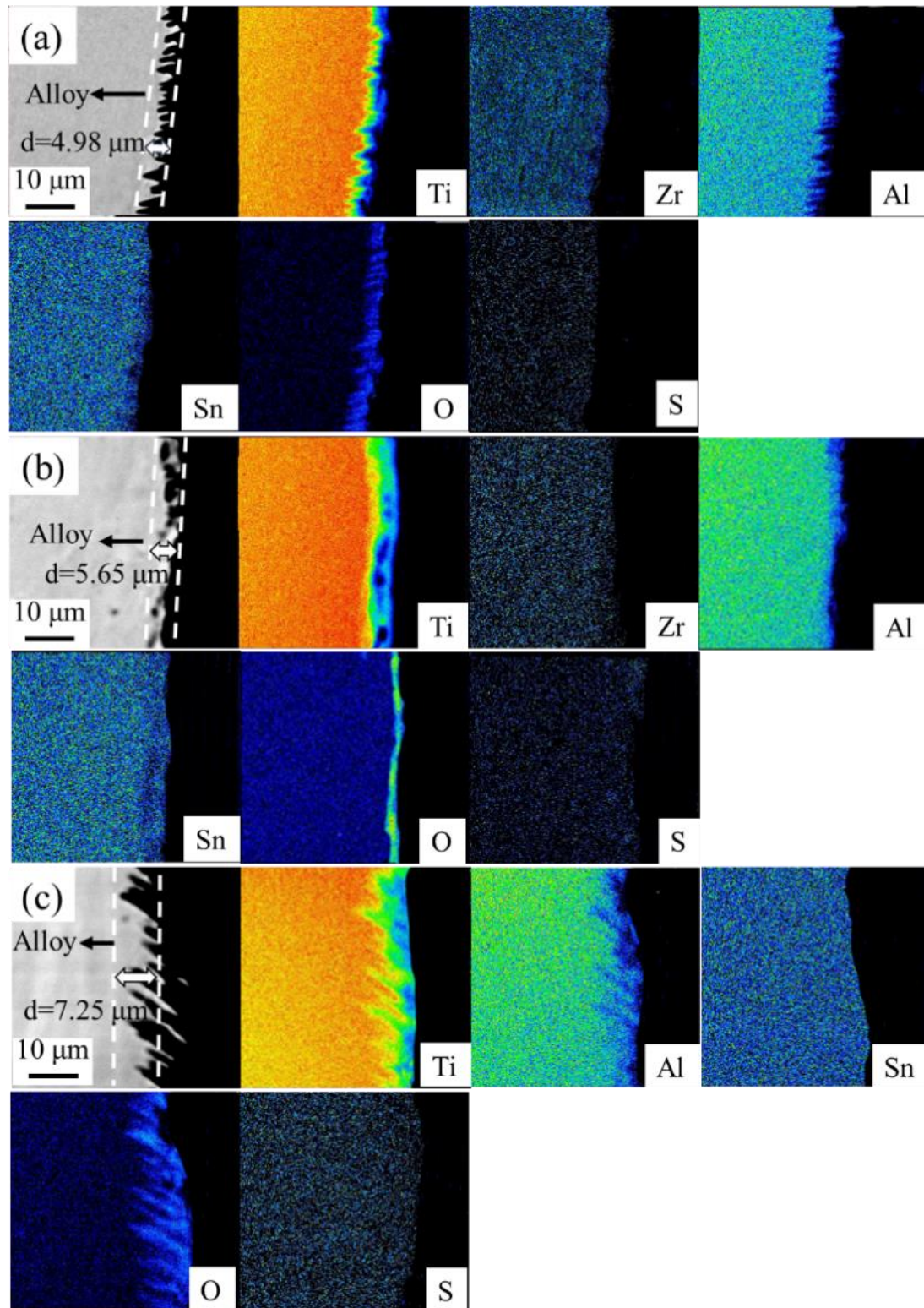
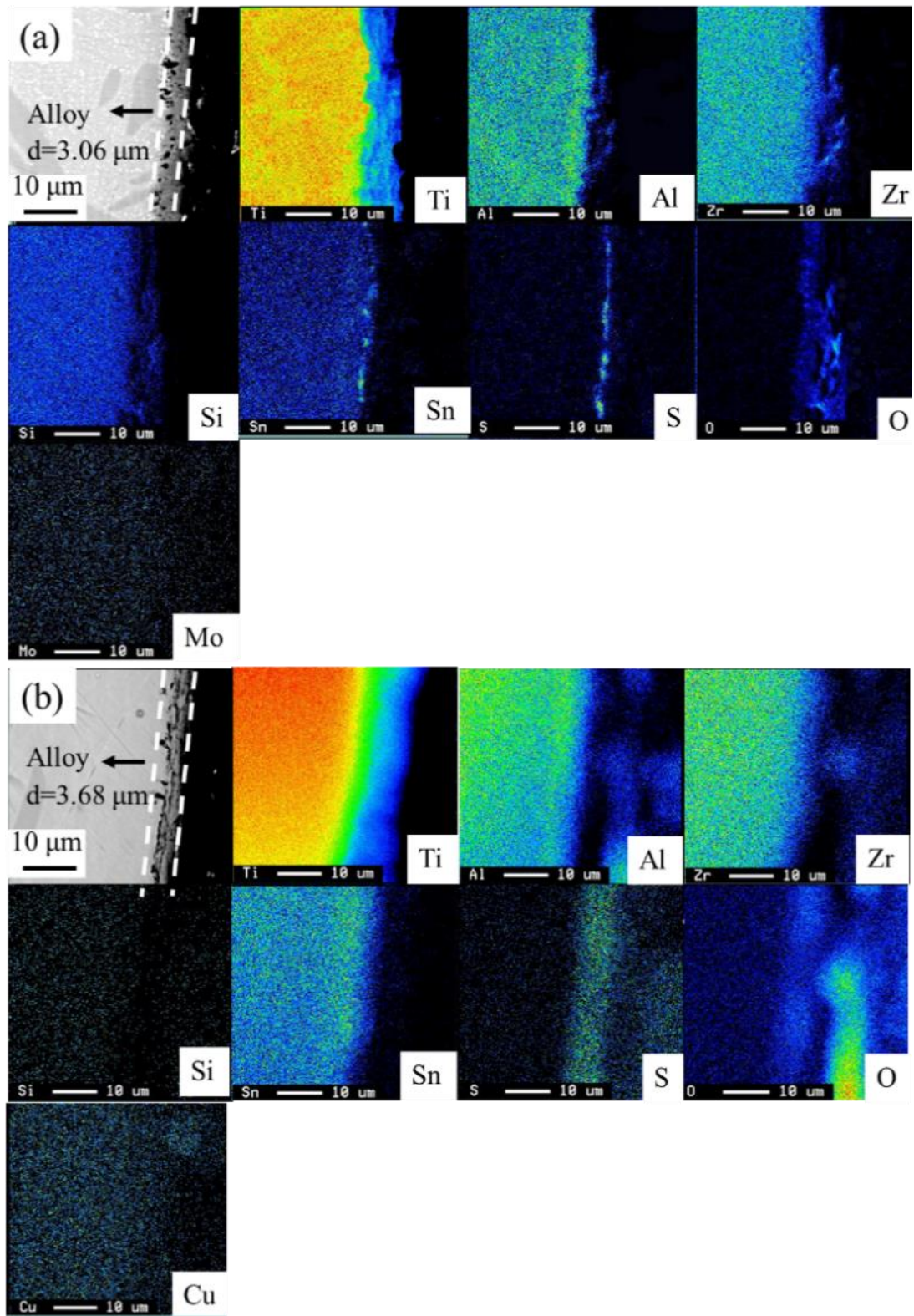


Fig. 4-19 Compositional images of (a) Ti-5Al-4Zr-3.6Sn, (b) Ti-6Al-1.7Sn-1.3Zr and (c) Ti-5Al-2.5Sn alloys in as-cast condition, and EPMA mappings showing the distribution of Ti, Zr, Al, Sn, O, and S, respectively.

corrosion was observed in the whole surface of three α -Ti specimens corresponded to the widespread metal loss across the surface. However, the electrochemical attacked behavior in local was also observed corresponded to the difference corrosion rate and the formation of jagged interface on the surface of specimens. The electrochemical attacked of metal or alloys was called concentration-cell corrosion and usually happened with the presence of small volumes of stagnant solution ²⁷).

The thickness of corrosion layers of designed, modified and reference near- α titanium alloys in solution treated condition were 3.06, 3.68 and 4.89 μm , respectively. the compositional images and EPMA mappings of experimental near- α Ti alloys after immersion in hot salts for 28.8 ks were shown in Fig. 4-20 (a), (b) and (c), respectively.



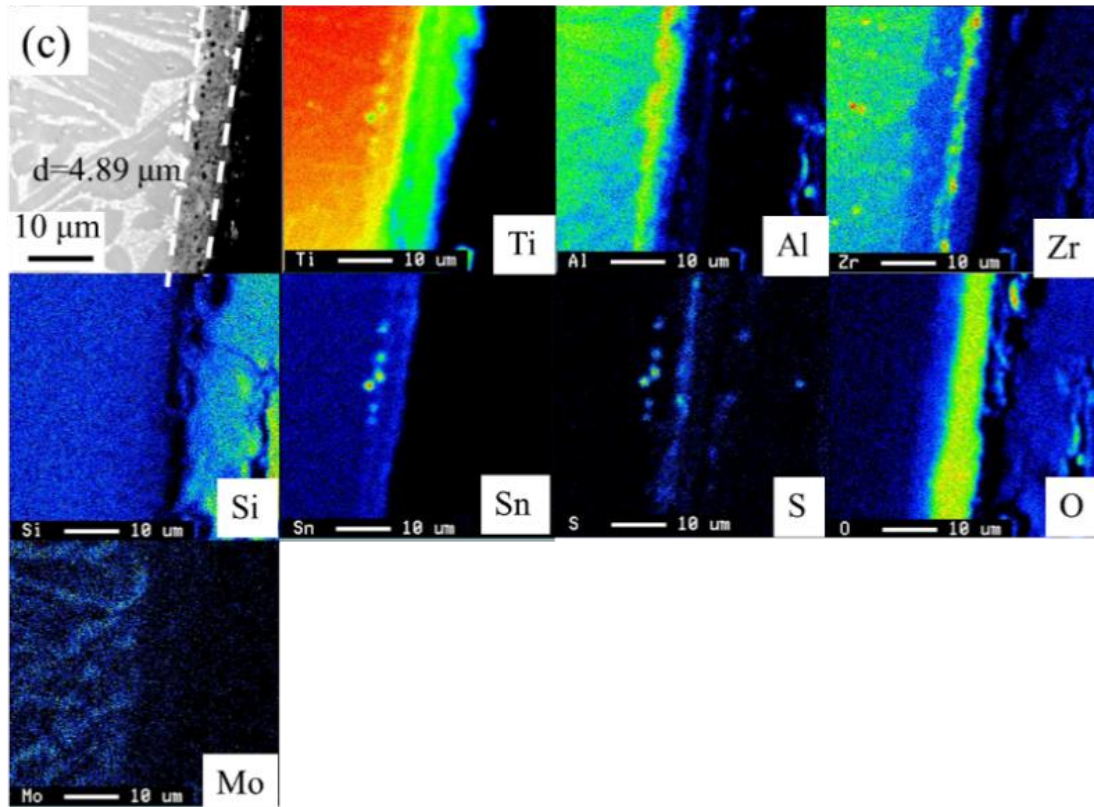


Fig. 4-20 Compositional images of (a) Ti-6Al-2Sn-5Zr-1Mo-0.3Si, (b) Ti-6Al-3Sn-9Zr-1Cu-0.2Si and (c) Ti-6Al-2.75Sn-4Zr-0.4Mo-0.45Si near- α alloys in solution treated condition, and EPMA mappings showing the distribution of Ti, Zr, Al, Si, Sn, O, S, Mo, and Cu, respectively.

The cross section of experimental near- α titanium alloys showed the thickness of corrosion layers and the elements distribution in alloys after hot salt corrosion test continuously for 28.8 ks. These results also showed highly consistent with their weight loss during the hot salt corrosion test. However, even the elements distribution and the corrosion positions of specimens were known by compositional images and EPMA mappings, the detailed mechanism of the possible reactions and corrosion procedures were still not very clearly described with the present results. The explanation of the reactions and corrosion processes in mechanism is important and meaningful.

4.4.4 The mechanism of hot salt corrosion test of titanium alloys

The mechanism of the reactions and corrosion procedures were described in Fig. 4-21. The Gibbs function of $\Delta G = \Delta H - T\Delta S$ was used to evaluate whether the reactions can be carried out spontaneously. The $\Delta G < 0$ is known as the sign of a chemical reaction can take place spontaneously. According to the Gibbs free energy results of titanium and additional alloying elements to the Oxygen (O_2) in the hot salt corrosion test temperature of 923 K, the titanium (Ti), aluminum (Al) and zirconium (Zr) can react with O_2 . In the initial oxidation state, TiO_2 form and grow along their optimal growth direction. A titanium oxide layer rapidly forms on the surface of the alloys.²⁸⁾

For the Ti oxides, there are monoxide TiO and dioxide TiO_2 , however, the calculation results of affinity energy show that the TiO formed by Ti and O_2 is approximately -28.27 eV, and that of Al_2O_3 formed by Al and oxygen is approximately -30.00 eV. It is known that the affinity energy of Al_2O_3 and TiO is very similar. However, TiO is an extremely unstable oxide and possesses anion vacancy. And further calculation shows that the affinity energy of TiO_2 formed by Ti and oxygen is -54.99 eV. Therefore, in practice TiO_2 is usually found rather than TiO since the monoxide is rapidly oxidized to the dioxide.²⁹⁾ The illustrative schematic of the corrosion productions for specimens were showed in Fig. 4-21 (a). The corrosion reactions occurred on the different positions of the surface of specimen. The acidic-fluxing mode was widely known as a salt corrosion behavior, and this corrosion behavior was also observed in the present paper. In the last stage, the reactions between the refractory oxides and molten sulphate according to Eq. (4-5), the deposition of corrosion productions and ionizations of Ti^{4+}

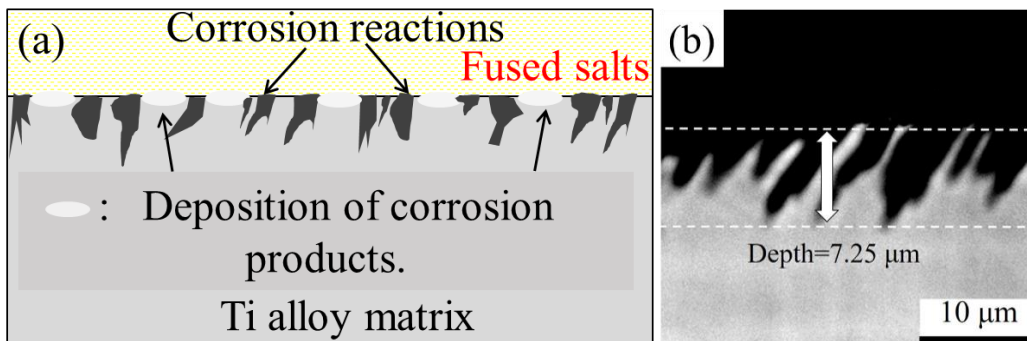
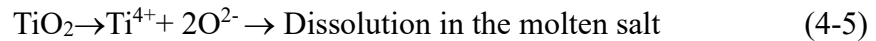


Fig. 4-21 Illustrative schematic of (a) showing corrosion process for specimens and (b) the corrosion surface morphology after hot salt corrosion test.

and O^{2-} led to the different corrosion rate in the corrosion surface of specimen.



The severe corrosion occurred in the position with little or no protect local part, and the subsequent corrosion diffusion toward the inter of matrix. The mild corrosion may be happened in the sites with a few ZrO_2 and Al_2O_3 , where chlorine ions will not collide easily with titanium oxide. The slight corrosion behaviors will be carried out in the sites coated with the solid corrosion products or refractory oxides. The final corrosion surface morphology after hot salt corrosion test were shown in Fig. 4-21 (b), a specimen of Ti-5Al-2.5Sn α -Ti alloy with the highest amount of weight loss during the hot salt corrosion test. The zigzag surface in micro was attributed to the different corrosion rate as mentioned above.

4.5 Summary

(1) New experimental α and near- α titanium alloys with hcp cluster structure were successfully proposed on the basis of electron parameters (Bo_t and Md_t). Three α -Ti alloys showed mono α phase which was consistent with their locations in the Bo_t - Md_t diagram. Moreover, three α -Ti alloys with grain size 600 μm and the near- α titanium alloys with grain size 500 μm and homogeneous microstructures were obtained by the effect of CCLM in the present research.

(2) The designed alloy Ti-5Al-4Zr-3.6Sn with optimized composition showed the highest σ_{UTS} value of 801 MPa and ϵ_f value of approximately 16% among three α -Ti alloys. These were consistent with the microstructural and mechanical properties prediction contour lines in the Bo_t - Md_t diagram. The tensile tests of three α -Ti alloys were also carried out in solution treated condition. The σ_{UTS} and ϵ_f values were shown on Ti-5Al-4Zr-3.6Sn alloy: 970 MPa and 13%, Ti-6Al-1.7Sn-1.3Zr alloy: 888 MPa and 10% and Ti-5Al-2.5Sn: 664 MPa and 17% in solution treated condition, respectively. All three α -Ti alloys showed improvement in tensile strength in solution treated condition compared with those of three α -Ti alloys in as-cast condition. For the α -Ti alloys to be applied in ambient temperature, the solution treatment might be an effective method to improve their tensile strength. In addition, the designed alloy Ti-5Al-4Zr-3.6Sn which is an alternative material for the commercial Ti-5Al-2.5Sn has also been proved in as-cast condition, according to its improved tensile property and corrosion resistance ability.

(3) The designed near- α titanium alloy Ti-6Al-4Zr-2Sn-2Mo-0.3Si with σ_{UTS} value of 989 MPa and ϵ_f of 11.6% in as-cast condition, and 1118 MPa and 3.4% in solution treated condition. The modified near- α titanium alloy Ti-6Al-9Zr-3Sn-1Cu-0.2Si with σ_{UTS} value of 993 MPa and ϵ_f of 13.5% in as-cast condition. While a higher σ_{UTS} value of 1354 MPa with ϵ_f of 2.3% in solution treated condition. The reference alloy showed σ_{UTS} value of 991 MPa, ϵ_f value of 12.7% in as-cast condition and σ_{UTS} value of 1238 MPa, ϵ_f value of 3.1% after solution treated treatment. The objective values were almost achieved by three alloys in as-cast condition, which showed highly consistent with the

contour lines of σ_{UTS} values. For the near- α Ti alloys, the as-cast application might be possible as an effective method as cost save measures. The solution treatment improved the σ_{UTS} values of near- α titanium alloys, but their ε_f values drastically decreased as a trade-off.

(4) The hot salt corrosion test after 43.2 ks showed the ratio of weight loss of near- α titanium alloys were less than those of α titanium alloys in respective as-cast and solution treated conditions. The higher corrosion resistance ability and mechanical properties of near- α titanium alloys indicated they are more suitable for high temperature applications. The reaction between α -Ti alloys and fused salts were happened on the contact surface of specimens. The acidic-fluxing corrosion process for specimens and the formation of corrosion surface morphology were illustrated in detailed. In addition, the dissolution of Ti oxide and corrosion products in the molten salt were discussed in the present study.

References:

- 1) C. Leyens, M. Peters. Wiley-Vch Verlag GmbH and Co. KgaA. (2003) 1–30.
- 2) I.V. Gorynin: Mater. Sci. Eng. A. **263** (1999) 112–116.
- 3) M. Peters, J. Kumpfert, C.H. Ward and C. Leyens: Adv. Eng. Mater. **5** (2003) 419–427.
- 4) K. Tajima, M. Hironaka, K.K. Chen, Y. Nagatsu, H. Kakigawa and Y. Kozono: Dent. Mater. J. **27–2** (2008) 258–265.
- 5) E.O. Ezugwu and Z.M. Wang: J. Mater. Proc. Technol. **68** (1997) 262–274.
- 6) A. Ghisi and S. Mariani: Int. J. Fract. **146** (2007) 61–77.
- 7) P. Laheurte, F. Prima, A. Eberhardt, T. Gloriant, M. Wary and E. Patoor: J. Mech. Behav. Biomed. **3** (2010) 565–573.
- 8) M. Morinaga: Mater. Trans. **57** (2016) 213–26.
- 9) Y. Liu, K. Matsugi, Z F. Xu and Y.B. Choi. (2018) Hiroshima university.
- 10) C. Veiga, J.P. Davim and A.J.R. Loureiro: Rev. Adv. Mater. Sci. **32** (2012) 133–148.
- 11) A. Zhecheva, W. Sha, S. Malinov and A. Long: Surf. Coat. Tech. **200** (2005) 2192–2207.
- 12) C.P. Liang and H.R. Gong: Int. Hydrogen. Energ. **35** (2010) 3812–3816.
- 13) W.J. Joost, S. Ankem and M.M. Kuklja: Acta. Mater. **105** (2016) 44–51.
- 14) K. Matsugi, T. Kashiwagi, Y. B. Choi and G. Sasaki: Mater. Trans. **52** (2011) 2189–2196.
- 15) K. Matsugi, H. Kishimoto, D. Yamakawa, Z.F. Xu and Y.B. Choi: Mater. Trans. **56** (2015) 1747–1755.
- 16) M. Morinaga, N. Yukawa, T. Maya, K. Sone and H. Adachi: Proc. 6th World Conf. TMS. (1988) 1601–1606.
- 17) M. Abdel-Hady, K. Hinoshita and Masahiko Morinaga: Scripta. Mater. **55** (2006) 477–480.
- 18) D. Kuroda, M. Niinomi, M. Morinaga, Y. Kato and T. Yashiro: Mater. Sci. Eng. A. **243** (1998) 244–249.
- 19) X.L. Ma, K. Matsugi, Z.F. Xu, Y.B. Choi, R. Matsuzaki, J. Hu, X.G. Liu and H.

- Huang: Mater. Trans. 60 (2019) 2426–2434.
- 20) A. Morita, H. Fukui, H. Tadano, S. Hayashi, J. Hasegawa and M. Niinomi: Mater. Sci. Eng. A. **280** (2000) 208–213.
 - 21) H.C. Watson and E.B. Watson: Phys. Earth. Planet. In. **139** (2003) 65–75.
 - 22) K. Matsugi, T. Endo, Y.B. Choi and G. Sasaki: Mater. Trans. **51** (2010) 740–748.
 - 23) E. Takeda, K. Matsugi, Z F. Xu and Y.B. Choi. (2012) Hiroshima university.
 - 24) X.J. Jiang, Y.K. Zhou and Z.H. Feng: Mater. Sci. Eng. A. **639** (2015) 407–411.
 - 25) P. Laheurte, F. Prima and A. Eberhardt: JMBBM. **3** (2010) 565–573.
 - 26) I.J. Polmear: Design. Patent. Act. (1988) 83–421.
 - 27) J.R. Myers, H.B. Bomberger and F.H. Froes: J. Metal. (1984) 50–60.
 - 28) J.J. Dai, J.Y. Zhu, C.Z. Chen and F. Weng: J. Alloy. Compd. **685** (2016) 784–798.
 - 29) G.L. Liu and Y. Li: Acta. Phys. Sin. **61-17** (2012) 1–5.

Conclusions

The as-cast application possibility of α , near- α and β titanium alloys were discussed in this research. These titanium alloys were proposed by using mainly ubiquitous elements, in the diagram consisting of bond order (Bo) and d-orbital energy level (Md). For the β titanium alloys, three alloys were proposed in the predicted regions showing the slip, twin and martensite dominant deformation behaviors in wide range β -Ti alloys area in the Bo_t - Md_t diagram, respectively. Their properties were compared in both as-cast and solution treated conditions. The object was to develop β -type titanium alloys with ultimate tensile strength value of 1000 MPa and fracture strain value of 10% in as-cast condition without the post-treatments after cold crucible levitation melting, as energy consumption and cost saving measures. The candidate area for the proposal of as-cast applicable titanium alloys with comparable mechanical properties and lower cost than those of practical applied commercial Ti alloys were confirmed in the present research, as shown in the Fig. 5-1.

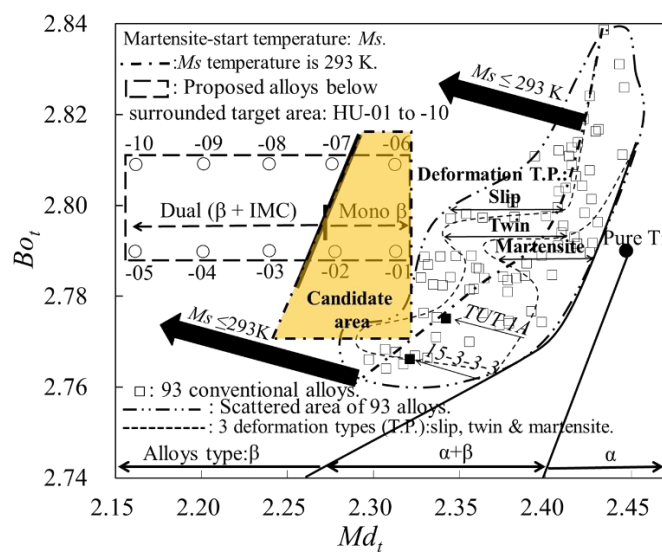


Fig. 5-1 Candidate area for proposing of as-cast applicable Ti alloys in the Bo_t - Md_t diagram.

It was found that as-cast application possibility of Ti-5.5Cr-5.4Mn-5.1Zr-2.8Fe alloy could not be refused in the view of tension behaviors. In addition, ten β -type titanium alloys for as-cast applications were proposed by using mainly ubiquitous elements in the area greatly differ from conventional alloys in the Bo_t - Md_t diagram. HU-01 Ti-5.2Cr-5.5Mn-5.5Zr-2.2Fe, HU-02 Ti-11Cr-6Mn-4.5Zr-0.5Al and HU-06 Ti-13Zr-6Mn-6Cr-5V alloys with a β mono phase achieved objective values of mechanical properties in as-cast condition, which led to development of alternative materials to the conventional β -type titanium alloys, since they reduced energy consumption and 25~35% production costs by omitting complex post processing procedures. Moreover, the phase boundary between the mono β phase and dual β plus intermetallic compound phases were predicted for the first time, according to the ten proposed β -type titanium alloys in newly expanded compositional area of the Bo_t - Md_t diagram. For the α and near- α titanium alloys, which were widely used for building materials on the ocean and high-temperature applications in aircraft engines. The design of new alloys with improved corrosion resistance ability and mechanical properties were carried out by using the Bo_t - Md_t diagram. The influence of Bo_t values on the corrosion resistance ability and the dependability of prediction of σ_{UTS} values on the basis of the contour lines in the Bo_t - Md_t diagram were evaluated in this section. The results showed their mechanical properties could be further improved by the solution treatment, which means their applications is difficult to obtain both mechanical properties and economic benefits at the same time. In this case, they are thought not good candidate titanium alloys for as-cast applications. The detail conclusions of this thesis are summarized as follows:

1. Ti-5.5Cr-5.4Mn-5.1Zr-2.8Fe alloy located in the slip DT showed mono β phase and the highest segregation degree of solute elements in experimental alloys. In contrast, Ti-4.5Cr-2.5Mn-1.1Al and Ti-10.8Mo-2.3Sn-1.0Al alloys located in the twin and martensite DTs showed the β phase and precipitated α'' martensite, respectively, regardless of heat treatment conditions. Ti-5.5Cr-5.4Mn-5.1Zr-2.8Fe alloy showing highest β phase stability with the lowest Md_t among three β -Ti alloys, had the slip behavior in the stress-strain curves showing a classical elasto-plastic behavior, and led to the high $\sigma_{0.2}$ more than 950 MPa, high σ_{UTS} more than 1000 MPa and ϵ_f more than

8 %, regardless of the heat treatments. The Vickers hardness values were 320 and 240 in as-cast Ti-5.5Cr-5.4Mn-5.1Zr-2.8Fe and Ti-10.8Mo-2.3Sn-1.0Al specimens, respectively. Their solution treated specimens showed 3-5 % lower Hv values, compared with as-cast ones. Their hardness properties were similar to tensile behaviors. It was found that as-cast application possibility of Ti-5.5Cr-5.4Mn-5.1Zr-2.8Fe alloy could not be refused in the view of tension behaviors. Promising alloys for as-cast applications could be proposed accurately in short periods using the Bo_t - Md_t diagram which showed high level in the prediction of classification in alloys by DT.

2. The ten newly proposed alloys which were produced by the CCLM technique as the single manufacturing process, and their microstructures were approximately controlled to the same level in both as-cast and after solution treated conditions. The distribution of equiaxed and columnar grains in ingot were evaluated by the rectangle blocks and the cutting positions for tensile specimens were chosen in the upper part of ingot with equiaxed grains. The line among the HU-02, HU-03, HU-06 and HU-07 alloys indicating the phase boundary between the mono β phase and dual β plus intermetallic compound phases, were successfully identified in the newly expanded area of Bo_t - Md_t diagram for the first time. The existence of brittle intermetallic compounds in proposed alloys caused their serious deterioration in tensile properties. The HU-01, HU-02 and HU-06 alloys, with mono β phase, showed the satisfaction in objective values of mechanical properties even in as-cast condition, which led to development of alternative materials to the conventional β -Ti alloys, since they reduced energy consumption and production costs by omitting complex post-treatments. For the alloys with same Bo_t value of either 2.79 or 2.81, the Vickers hardness values increased with decreasing Md_t values by the effect of solid solution hardening and the existence of hard intermetallic compounds. There were similar hardness values in both as-cast and solution treated specimens. The prediction of the phase boundary between the mono β phase and dual β plus intermetallic compound phases could be proposed in the newly expanded area large differing from compositional positions of conventional β alloys, indicating the possible area in the Bo_t - Md_t diagram to develop β -Ti for as-cast applications.

3. The α and near- α titanium alloys with improved mechanical properties were successfully proposed in as-cast condition, according to the prediction of σ_{UTS} values, on the basis of the contour lines in the Bo_t-Md_t diagram. For the α type titanium alloys, this is the first time to propose the contour lines in the Bo_t-Md_t diagram calculated under the hcp cluster model. The designed alloy Ti-5Al-4Zr-3.6Sn with σ_{UTS} value of 801MPa and ϵ_f value of approximately 16% showed consistent with the prediction results of the contour lines in the Bo_t-Md_t diagram. The designed alloy Ti-5Al-4Zr-3.6Sn which is an alternative material for the practical commercial Ti-5Al-2.5Sn (σ_{UTS} :730MPa, ϵ_f :15%) has also been proved in the present research, according to its improved tensile property and corrosion resistance ability. Previously, it is believed that the stable α phase in room temperature almost have no response to the heat treatments, with no phase transition after the heat treatment. However, all three α -Ti alloys showed improvement in tensile strength in solution treated condition compared with those of three α -Ti alloys in as-cast condition. The σ_{UTS} and ϵ_f values were shown on Ti-5Al-4Zr-3.6Sn alloy: 970 MPa and 13%, Ti-6Al-1.7Sn-1.3Zr alloy: 888 MPa and 10% and Ti-5Al-2.5Sn: 664 MPa and 17% in solution treated condition, respectively. The segregation behavior was thought as the major reason for this phenomenon. For the α -Ti alloys, the solution treatment can improve their tensile strength with increased cost. For the near- α titanium alloys, the designed near- α titanium alloy Ti-6Al-4Zr-2Sn-2Mo-0.3Si with σ_{UTS} value of 989 MPa and ϵ_f of 11.6% in as-cast condition, and 1118 MPa and 3.4% in solution treated condition. The modified near- α titanium alloy Ti-6Al-9Zr-3Sn-1Cu-0.2Si with σ_{UTS} value of 993 MPa and ϵ_f of 13.5% in as-cast condition. While a higher σ_{UTS} value of 1354 MPa with ϵ_f of 2.3% in solution treated condition. The reference alloy showed σ_{UTS} value of 991 MPa, ϵ_f value of 12.7% in as-cast condition and σ_{UTS} value of 1238 MPa, ϵ_f value of 3.1% after solution treated treatment. The objective values were almost achieved by three alloys in as-cast condition, which showed highly consistent with the prediction contour lines which were obtained by summarized the near- α titanium alloys in the Bo_t-Md_t diagram under the hcp cluster model. The influence of Bo_t values on the corrosion resistance of near- α titanium alloys showed that higher Bo_t values corresponded to higher corrosion resistance ability, which is agreement with previous reports. The hot salt corrosion test after 43.2 ks showed the ratio of weight loss of near-

α titanium alloys were less than those of α titanium alloys in respective as-cast and solution treated conditions. The higher corrosion resistance ability and mechanical properties of near- α titanium alloys indicated they are more suitable for high temperature applications. The reaction between α -Ti alloys and fused salts were happened on the contact surface of specimens. The acidic-fluxing corrosion process for specimens and the formation of corrosion surface morphology were illustrated in detailed. In addition, the dissolution of Ti oxide and corrosion products in the molten salt were discussed in the present study.

Acknowledgements

I would like to express my sincere gratitude to Professor Kazuhiro Matsugi for his great guidance and insight throughout this study. He gave me full support not only on my research, but also on my life and career, which has played an important role in both my professional and future development. I am also greatly indebted to Assistant Professor Yongbum Choi and Assistant Professor Zhefeng Xu. They gave me so much positive help on the research, the accumulation of the knowledge and my life, and I have learnt so much from them. In addition, I would like to express my heartfelt thanks to Associate Professor Kenjiro Sugio and Associate Professor Huang Hao, Yanshan University, for their technical advice and experimental assistance. I would like to acknowledge the helpful comments and suggestions from Professor Gen Sasaki, Associate Professor Ryuutarou Hino and Professor Jinku Yu, Yanshan University.

I would like to thank Mr. Ye Liu, Mr. Ryohei Matsuzaki, Mr. Zifeng Lin and Mr. Taisei Inoshita for their considerable assistance and help in my experiments. Moreover, I would also like to thank all the past and present members of Property Control of Materials Laboratory, in Department of Mechanical Physical Engineering, Hiroshima University, for their enthusiastic help to both of my life and study.

Then, my thanks would go to my beloved family for their loving considerations and great confidence in me all through these years. I also owe my sincere gratitude to my friends who gave me their help and time in helping me work out my problems during the difficult course of the thesis.

Published papers in regard to this thesis

1. **X. L. Ma**, K. Matsugi*, Z. F. Xu*, Y. B. Choi, R. Matsuzaki, J. Hu, X. G. Liu and H. Huang. Applicability of as-cast on β type titanium alloys proposed in the compositional region with different tensile deformation types. *Materials transactions*. **60** (2019) 2426–2434. (Chapter 2)

2. **X. L. Ma**, K. Matsugi*, Z. F. Xu*, Y. B. Choi, R. Matsuzaki, Z. F. Lin, X. G. Liu and H. Huang. Possibility of as-cast applications on proposed β -type titanium alloys in the newly expanded area of $Bor-Mdi$ diagram. *Materials transactions*. **61** (2020) in press. (Chapter 3)

3. 許哲峰*, 松木一弘, 松崎諒平, 崔龍範, 馬喜龍, 滑り変形挙動を有する持続社会実現型 β 型Ti合金の設計と特性評価, 日本鑄造工学会中国四国支部会報誌 こしき **No.40** (2017) 32–34. (Chapter 3)

4. **X. L. Ma**, K. Matsugi*, Z. F. Xu*, Y. B. Choi, Y. Liu, J. Hu, X. G. Liu and H. Huang. Optimization of both composition and manufacturing process for α -type titanium alloys and their characterizations. The Tenth Pacific Rim International Conference on Advanced Materials and Processing (PRICM 10th), The Chinese Society for Metals (CSM), (2019) 572–579. (Chapter 4)

5. **X. L. Ma**, K. Matsugi*, Z. F. Xu*, Y. B. Choi, Y. Liu, J. Hu, X. G. Liu and H. Huang. Cold crucible levitation melting of near- α titanium alloys and their characterizations. 日本鑄造工学会中国四国支部会報誌 こしき **No.41** (2018) 37–41. (Chapter 4)

Presentations

1. **Xilong Ma**, Kazuhiro Matsugi, Zhefeng Xu, Yongbum Choi, Ye Liu, Ryohei Matsuzaki and Zifeng Lin. Propose of titanium alloys using the Bo_T-Md_i diagram, and their as-cast applicability. 鑄物第24委員会, 鑄造プロセス分科会第23回会議, 2019年12月20日, 近畿大学東京センター大会議室.

2. 馬喜龍、松木一弘、許哲峰、崔龍範、劉燁、劉鑫剛、黃浩. α 型チタン合金の組成と製造プロセスの両最適化と特性評価, 日本鑄造工学会, 第174回全国講演大会, 2019年9月28-29日, 福岡国際会議場.

3. **Xilong Ma**, Kazuhiro Matsugi, Zhefeng Xu, Yongbum Choi, Ye Liu, Jie Hu, Xingang Liu and Hao Huang. Optimization of both composition and manufacturing process for α -type titanium alloys and their characterizations. The Tenth Pacific Rim International Conference; August 18-22, 2019, Xi'an, China.

4. 馬喜龍、松木一弘、許哲峰、崔龍範. 鑄放使用可能なNear- α 型チタン合金の設計と特性評価. 2019年2月23日. 広島大学, 産学地域連携センター.

5. **Xilong Ma**, Kazuhiro Matsugi, Zhefeng Xu, Yongbum Choi, Ryohei Matsuzaki, Jie Hu, Xingang Liu and Hao Huang. Possibility of as-cast applications on β -type titanium alloys for energy-saving measures. The 7th Japan-Korea Conference for Young Foundry Engineers, October 13-15, 2018, Ishikawa Industrial Promotion Center (IIPC), Kanazawa, Ishikawa-Pref., Japan.

6. **Xilong Ma**, Kazuhiro Matsugi, Zhefeng Xu, Yongbum Choi, Ye Liu, Jie Hu, Xingang Liu and Hao Huang. Design of α type titanium alloys and their characterizations. 第10回軽金属学会, 中国四国支部, 2018年7月28日, 広島工業大学.

7. 馬喜龍、松木一弘、劉燁、松崎諒平、崔龍範、許哲峰、黃浩、劉鑫剛. Design of α -type titanium alloys and their characterizations. 日本金属学会・日本鉄鋼協会・中国四国支部 第37回・若手フォーラム—中国四国支部・チタン・チタン合金研究最前線 (2)—, 2017年11月17日, 愛媛大学.